MEASUREMENT OF EVAPOTRANSPIRATION WITH COMBINED REFLECTIVE AND THERMAL INFRARED RADIANCE OBSERVATIONS

Final Report Submitted To:

The National Aeronautics
And Space Administration,
Washington, D.C.

Grant No. NAG 5-911
1/87 - 8/93

Allen S. Hope
Principal Investigator

Department of Geography
San Diego State University
San Diego, CA 92182

1993

ACKNOWLEDGEMENTS

The research summarized in this report was based on data collected at the FIFE study site in 1987 and 1989 by a large number of investigators from other institutions, along with their technical staff and graduate students. This generous contribution and the considerable assistance given by the staff of the FIFE Information System (FIS) under the leadership of Dr. Donald Strebel, is gratefully acknowledged. I am indebted to Dr. Forrest Hall and Dr. Piers Sellers for the support, scientific guidance and inspiration they provided throughout the project.

This study was part of a collaborative research effort with Dr. Samual Goward at the University of Maryland. The regular meetings and discussions with Dr. Goward significantly influenced many of the ideas and investigations summarized in this report. I very much appreciate Dr. Goward's significant contribution to my scientific development over the past decade.

The results summarized in this report have been drawn from a number of published and unpublished studies conducted in collaboration with co-investigators or graduate students. The contributions made by the following collaborators is acknowledged (primary chapters in parentheses):

Andrew Abouna	(6)	Eugene Peck	(Appendix 1)
Tom McDowell	(2, 3, 4)	Sally Westmoreland	(Appendix 2)
Frederick Mertz	(Appendix 2)	Douglas Stow	(Appendix 2)

TABLE OF CONTENTS

LIST OF TABLES

LIST OF FIGURES

1. INTRODUCTION

1.1 Background

A negative and linear relationship between surface temperature (T_S) and a spectral vegetation index (SVI) has been observed using data collected over a variety of landscape types and with different sensors (Gurney et al. 1983; Goward et al. 1985; Hope et al. 1986; Whitehead et al. 1986; Goward and Hope 1989; Nemani and Running 1989; Carlson et al. 1990; Price 1990; Hope 1992). Changes in the characteristics of the relationship between T_S and a SVI (e.g., slope of the regression line) were hypothesized to be indicative of variations in latent heat flux (LE) (Hope, Petzold et al. 1986). The possibility of using the T_S-SVI relationship to predict LE was investigated as part of the First International Satellite Land Surface Climatology Project (ISLSCP) Field Experiment (FIFE). Results from this project are summarized in the following chapters.

A theoretical basis for the T_S-SVI investigation was provided by Hope (1986) who used an integrated energy balance-spectral reflectance model to demonstrate that variations in soil moisture, and hence LE fluxes, may affect the slope of the linear least squares regression of T_S on the normalized difference vegetation index (NDVI). Goward and Hope (1986) extended this concept in designing a research strategy to investigate whether the characteristics of the T_S-NDVI regression were indicative of variations in LE over the FIFE study site (Konza prairie).

1.2 Hypothesized Relationship Between LE, T_S and SVI

The hypothesized relationship between LE, T_S and a SVI was presented by Goward and Hope (1986) and Goward and Hope (1989) and is illustrated in Figure 1.1.

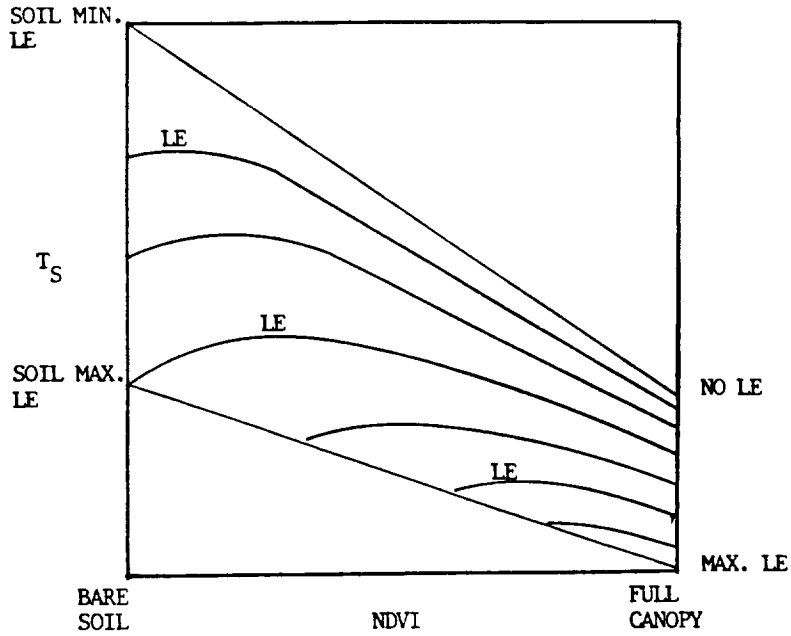

Figure 1.1: Proposed relationship between remotely sensed spectral vegetation indices and surface temperature. Hypothesized lines of equal LE flux are indicated (Goward and Hope 1986).

Remotely sensed surface temperatures will vary as a function of vegetation canopy cover, even in the absence of LE because the thermal inertia of the vegetated interface is lower than that of the substrate. Transpiring vegetation further reduces T_S because of the energy used for LE. Vegetation also reduces ground heat flux (G) and, as Kustas (1989) has shown, SVIs can be used to predict G. A fundamental assumption in Figure 1 is that the SVI is an indicator of fractional vegetation cover, an assumption substantiated by Huete et al. (1985). The area averaged LE

illustrated in Figure 1.1 were thus considered to be related to the SVI and T_S by way of the relative contributions of evaporation from bare soil and vegetation under different soil moisture conditions. Since T_S is also affected by meteorological conditions and differences in surface roughness, variations in these conditions can also affect the nature of the T_S-SVI relationship. A more realistic representation of the relationships given in Figure 1.1 may thus include surface temperatures "normalized" for these variations.

1.3 Objectives and Approach

The broad goal of the research summarized in this report was "To facilitate the evaluation of regional evapotranspiration (ET) through the combined use of solar reflective and thermal infrared radiance observations" (Goward and Hope 1986, p. 5). The specific objectives stated by Goward and Hope (1986) were to:

1) Investigate the nature of the relationship between T_S and the NDVI and develop an understanding of this relationship in terms of energy exchange processes, particularly LE.

2) Develop procedures to estimate large area LE using combined T_S and NDVI observations obtained from AVHRR data.

3) Determine whether measurements derived from satellite observations relate directly to measurements made at the surface or from aircraft platforms.

Both empirical and modeling studies were used to develop an understanding of the T_S-NDVI relationship. Most of the modeling was based on the Tergra model (Soer 1977) as originally proposed by Goward

(1986). This model, and modified versions developed in this project, simulates the flows of water and energy in the soil-plant-atmosphere system using meteorological, soil and vegetation inputs. Model outputs are the diurnal course of soil moisture, T_S, LE and the other individual components of the surface energy balance. This model was originally selected for the study since:

1) The model was developed specifically for application to grassland situations and was thus considered to be suitable for the Konza prairie.

2) Tergra had been tested previously by numerous investigators and had generally been shown to be an accurate simulator of LE and T_S (Huygen and Reiniger 1977; Soer 1980; Hope, Petzold et al. 1986).

3) The simple model structure can be readily modified and the data needs are not excessive.

4) Tergra had been interfaced with a canopy reflectance model (SAIL) by Hope (1988) which provided for the combined simulation of T_S and the NDVI if necessary.

The general sequence of research activities followed in this project was to:

1) Conduct a series of empirical studies to determine how the T_S-NDVI relationship changes with different sensors/platforms, variations in land cover/use and treatment, terrain, soil moisture and surface energy balance. This component of the study examined the relationship at local and regional scales.

2) Use the Tergra model and modified versions of this model to integrate SVI and T_S observations into the modeling of LE at point locations within the FIFE study area.

3) Model spatial patterns of LE using data from the AVHHR system (T_s and the NDVI) and the modified Tergra model developed in 2).

The study was regarded as part of the integrative science activities of FIFE and so every attempt was made to incorporate findings from other FIFE investigations. Also, the project utilized data from a wide range of remote sensing systems (non-imaging radiometers held by hand or mounted on a helicopter, the NS001 data collected by the C-130 aircraft, Thematic Mapper (TM) and NOAA 9 and 10 satellite data (AVHRR)). As the project evolved, the need for information on the spatial patterns of soil moisture became apparent and the scope of the project was increased to include a component of soil moisture mapping in collaboration with E. Peck of the Hydex Corporation (Vienna, VA). This research is described in Appendix 1. Collaborative research with Photon Engineering (San Diego, CA) was also initiated later in the project with the goal of implementing and testing an easy to use, state-of-the-art atmospheric correction routine. This collaboration was under the direction of F. Mertz and the research is described in Appendix 2.

2. THE T_S-NDVI RELATIONSHIP: SENSOR SYSTEMS AND ATMOSPHERIC EFFECTS

2.1 Background

Data collected during the FIFE were valuable for determining how the T_S-NDVI relationship varied because of differences in data collection systems (differences in spectral and spatial resolution) and atmospheric conditions. These variations needed to be understood and quantified if the relationship was to be used to predict LE. An initial study was designed to investigate how sensor/platform and atmospheric conditions could affect the T_S-NDVI relationship. The relationship was compared using data collected with a Barnes modular multiband radiometer (MMR), NS001 Thematic Mapper simulator and NOAA Advanced Very High Resolution Radiometer (AVHRR). These data were all collected on a single date, June 6, 1987.

2.2 Data Sources and Processing

The MMR data were collected using the NASA H-1 (Huey) helicopter flown at 230 m agl. The 1∞ field-of-view of the MMR had a ground resolution of approximately 4 m. The data were collected between 1141 and 1251 CDT or 1609 and 1643 CDT. Approximately 30 observations were made over each flux measurement station (within a 5 minute period). Reflectances were calculated by ratioing the observed reflected spectral radiances to radiances collected over a calibration sheet (details are contained in the FIFE Information System - FIS). Arithmetic means from

the 30 observations were used to determine the NDVI and T_S at each flux station.

The NS001 instrument was mounted on a NASA C-130 aircraft flown at approximately 4,800 m agl, giving a ground resolution of approximately 12 m at nadir. Only data from flight lines parallel to the solar plane were used in the study. An 80 x 80 box of pixels around each flux station was extracted from the NS001 imagery. Two adjacent flight lines covered all of the flux stations used in this study and the maximum view (scan) angle for any station was 30∞. Seventeen flux stations were located using the latitude-longitude geocoding provided by the FIS. Sub-images were rectified to be oriented north-south. The NS001 thermal counts were converted to apparent surface temperatures using the procedure and constants provided by the FIS. This technique does not account for atmospheric attenuation of thermal radiances. The station characteristics and NS001 view angle for each station are given in Table 2.1.

The AVHRR image was acquired by the NOAA 9 Polar Orbiter satellite at 1636 CDT over the FIFE site on June 6, 1987. The view angle was 34.9° which resulted in a ground resolution of 1.34 km. Pixels corresponding to the FIFE site were extracted from the full scene after geometric rectification. Apparent T_S was calculated for both AVHRR thermal bands using the equations provided in the NOAA Polar Orbiter User's Guide (Kidwell 1986). These two temperatures were then used to obtain a "corrected" T_S using the split window technique described by Price (1984). Emissivity over the FIFE study site was taken to be 1.0.

Table 2.1: Flux station characteristics and NS001 view angle for June 6, 1987.

Station	Characteristics*	View Angle (Deg.)
02	UB	8.4
06	UM	1.1
08	BM	22.0
10	BB	23.9
12	US	15.4
14	UM	11.4
18	BT	25.7
20	BM	14.6
22	BM	29.9
24	UM	21.7
28	BM	30.0
34	BM	25.4
36	UM	18.4
38	UM	18.4
40	BS	22.4
42	BS	17.3
44	BT	0.3

* The first letter represents unburned (U) or burned (B) and the second letter represents valley bottom (B), moderate slope (M), steep slope (S) or plateau top (T).

2.3 Atmospheric Corrections of Reflected Radiances

Red and near infrared MMR reflectances (obtained using a reference target calibration procedure) provided by the FIS were taken to be standard ("correct") values. The NS001 and AVHRR data were, however, not corrected for atmospheric scattering of the reflected radiation. The improved dark object subtraction technique (Chavez 1988) was selected as a means for removing the effects of atmospheric scattering from the

NS001 and AVHRR red and near infrared observations.

The dark object subtraction technique is based on the assumption that completely shadowed pixels should have radiances close to zero in the visible bandwidths, with values above zero being attributed to contributions from atmospheric scattering. Traditional dark object subtraction techniques require an examination of the histogram of each band to determine the "take-off point", or the point of separation between shadowed and illuminated pixels (Chavez 1988). This radiance value becomes a "haze correction" value for the band and is then subtracted from the radiance values for all pixels. The improved technique incorporates two factors: the wavelength dependency of atmospheric scattering and the relative radiometric sensitivities of the sensor's channels (Chavez 1988).

The improved technique requires the user to assess the overall atmospheric conditions at the time of the scene acquisition, selecting from: very clear, clear, moderate, hazy and very hazy. The amount of atmospheric scattering in each of the sensors channels varies depending on the designation of atmospheric condition (clear - approaches Rayleigh scattering; very hazy - approaches Mie scattering). Based on this wavelength dependency, Chavez (1988) developed a set of equations for calculating the amount of scattering for the visible and near infrared bands of a sensor. Equations are specific to the designated atmospheric condition.

The next step in the improved technique requires histogram analysis of one of the visible channels to determine the haze correction value for the selected band. Haze corrections in the other bands are then calculated using the scattering model appropriate to the general atmospheric conditions. The calculated haze values are adjusted ("normalized") for the

gains and offsets of each band. Thus, the haze values are scaled to the appropriate digital number (DN) range for each band. Finally, the normalized haze values are subtracted from the brightness values for all pixels.

The darkest object subtraction technique is unsuited to AVHRR data because the large pixels almost certainly preclude the possibility of obtaining completely dark/shadowed areas in the instantaneous field-of-view (IFOV). However, the technique was applied to these data to make a "relative" correction for the effects of atmospheric scattering. The red band was used for the histogram analysis step for the AVHRR data (the only visible band) while the blue band was selected for the analysis of the NS001 data since it had the most distinct division between apparently shaded and unshaded pixels in the histogram.

2.4 Results and Discussion

Helicopter MMR data were available for nine flux stations on June 6, 1987 and were used to determine station T_s and NDVI reference values (assumed to be true). NS001 data were analyzed for the same nine stations by first extracting a window of 80 x 80 pixels centered on the station and then calculating the mean T_s and NDVI values for each station. Since it is not possible to precisely locate AVHRR pixels over each flux station, 16 random pixels were selected for the comparison with MMR and NS001 observations. The scatter plots of T_s versus the NDVI for each sensor with no correction for atmospheric scattering is given in Figure 2.1.

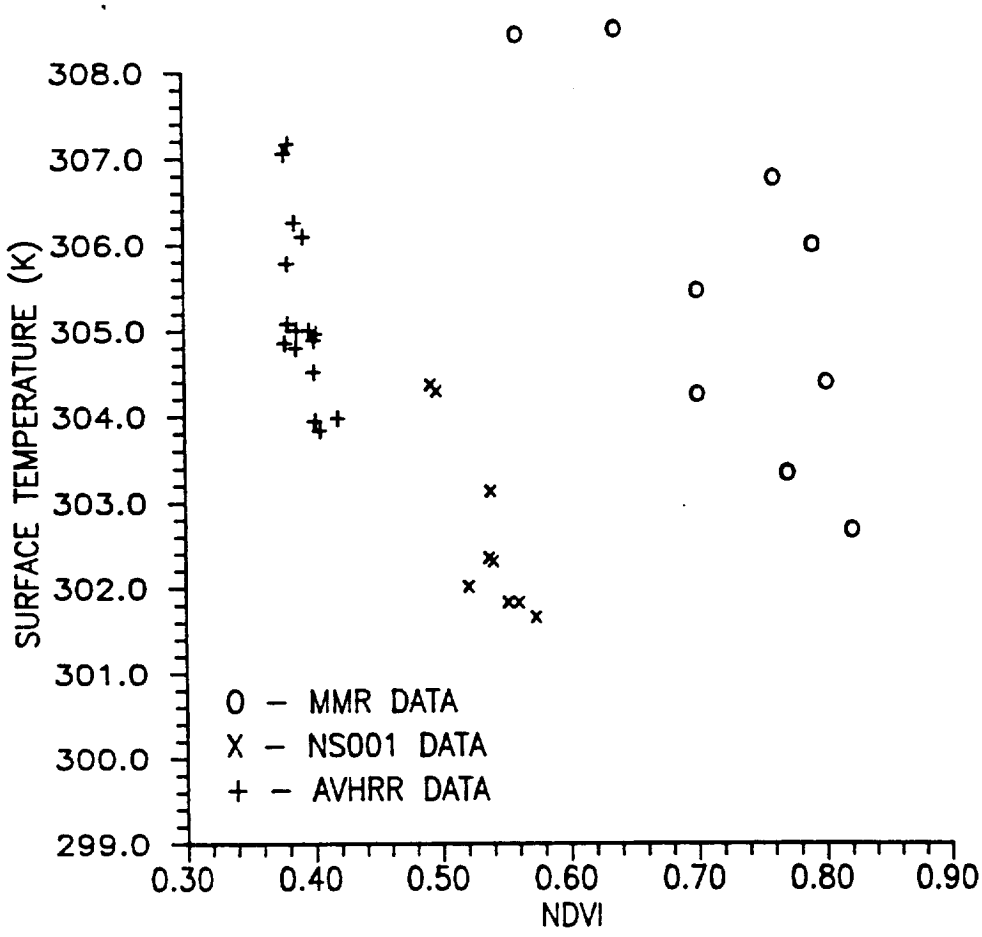

Figure 2.1: Surface temperature versus NDVI scatterplots for MMR, NS001 and AVHRR observations - no haze corrections.

While the negative and linear relationship between T_s and the NDVI was observed using data collected by the three different sensors, it is apparent from Figure 2.1 that:

1) The MMR data exhibited the largest range in T_s values.

2) NDVI values decreased with height of the sensor above the Earth's surface.

When the haze corrections are applied to the red and near infrared data,

the NS001 and AVHRR scatter plots align with the MMR points (Figure 2.2). This is verified by the summary statistics given in Table 2.2 where the range in mean NDVIs for the three sensors is reduced substantially after the correction is applied.

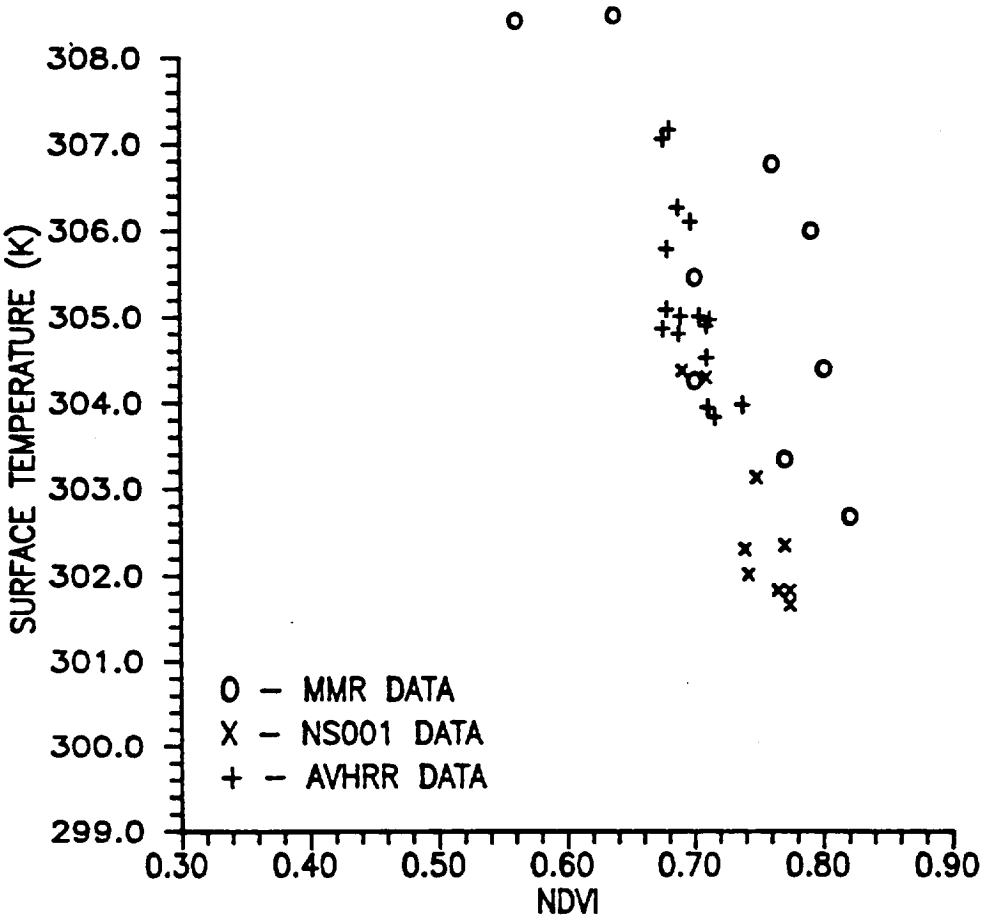

Figure 2.2: Surface temperature versus NDVI scatterplots for MMR, NS001 and AVHRR observations - haze corrected.

Table 2.2 NDVI and surface temperature means and coefficients of variation for observations made by three sensors.

	MMR	NS001	AVHRR
Mean NDVI (No Haze Correction)	.726	.534	.392
Mean NDVI (Haze Corrected)	---	.745	.696
Mean Surface Temperature (K)	304.7	302.2	304.4
Coefficient of Variation: NDVI (No Haze)	.118	.051	.031
Coefficient of Variation: NDVI (Haze Corrected)	---	.040	.026
Coefficient of Variation: Surface Temperature	.006	.003	.003

Although the scatterplots reveal sensor differences in observed T_s over the FIFE site, the mean values given in Table 2.2 differ by little more than 2.0 °C which is commonly regarded as the resolution of satellite thermal sensors. The averaging of surface temperature in the large AVHRR pixels or the 80 x 80 pixel windows of NS001 is also likely to have minimized the range in observed T_s values, with these large pixel values approaching the local/regional mean T_s value.

Theoretical modeling studies have demonstrated that the slope of the T_s-NDVI relationship is likely to change consistently with changes in

soil moisture and the associated changes in LE (Hope, Goward et al. 1988). Consequently, variations in the regression slopes which may have been caused by factors other than the surface energy balance were addressed early in this project (e.g., sensor characteristics, atmospheric effects, spatial resolution). The slopes of the T_S-NDVI regressions for the MMR, NS001 and AVHRR data on June 6 were not significantly different from one another (using the Scheffe F-test described by Roscoe (1975)) after corrections had been made for atmospheric haze. A summary of the results from regressing T_S on the NDVI for each sensor and for haze corrected data is given in Table 2.3.

Table 2.3: Scheffe F-test scores for comparison of T_S-NDVI regression slopes (Critical F value at 99% level = 3.54).

Sensor 1	vs	2	Slope F-score
MMR		NS001	1.58
MMR		AVHRR	2.02
NS001		AVHRR	0.54

2.5 Conclusion

Simple atmospheric corrections such as the split window technique and the improved darkest object subtraction technique were found to be valuable for making initial corrections to the data used in preliminary T_S-NDVI investigations. The differences in the variance in the observations

made using different sensors appeared to be largely a function of the different ground resolution of these sensors. Mean NDVI and T_s values for the FIFE site were similar when the simple atmospheric corrections were made to the data. The value of simple radiometric corrections was also demonstrated in the FIFE project by Hall (1991). The relative radiometric correction of TM data made by Hall (1991) was used in the modelling of canopy minimum conductance later in this study (cf. Chapter 5).

3. FACTORS AFFECTING THE T_S-NDVI RELATIONSHIP: LOCAL SCALE

3.1 Introduction

Analyses of the T_S-NDVI relationship were made at two general spatial scales. The initial focus was on the fluxes observed at the individual flux measurement stations with MMR or NS001 spectral radiances being used to determine the T_S-NDVI relationship for the areas surrounding each flux tower (i.e., local scale observations). Since the ultimate goal was to evaluate regional LE fluxes using AVHRR data and the T_S-NDVI relationship, this was the second scale of analysis (cf. Chapter 4).

Factors affecting the local scale T_S-NDVI relationship (individual flux stations) were studied using data collected in 1987. The following four empirical sub-studies were conducted using NS001 data and are summarized in the remainder of this chapter:

1) *Window size and regression characteristics.* This initial investigation was designed to determine whether the size of the area (window of pixels) selected around each flux tower would affect the station-to-station differences in T_S-NDVI regression characteristics. Fluxes at the towers were assumed to have most of their fetch within an upwind distance of 500 m, so 80 x 80 pixels was the maximum window size considered. Regressions based on data from these 80 x 80 pixel windows as well as 40 x 40 and 20 x 20 pixel windows were compared.

2) *T_S-NDVI regression slope, soil moisture and LE.* A station-to-station comparison was made of the regression slopes on a single day when soil moisture was considered to be adequate for unstressed transpiration. It was hypothesized that similar T_S-NDVI regression slopes would be observed at all stations under these conditions. A further test of this hypothesis was made under varying soil moisture conditions. The regression slopes from selected stations were determined using data representing three dates when soil moisture conditions and LE varied. Differences in the regression slopes were then related to station differences in soil moisture and LE.

3. *T_S-NDVI regression slope, burn treatments and other landscape controls.* The results from the second analysis indicated that differences in soil moisture and LE may not be the primary or only controls over the T_S-NDVI regression slope at local scales. Also, T_S and the NDVI have been shown in previous studies to be affected by burn treatment and other landscape features such as slope and aspect (Schmugge et al. 1987), so these variables were tested as possible determinants of the regression slope.

4. *Analysis of regression residuals.* The final empirical study was designed to provide further insight into landscape control over the T_S-NDVI regression characteristics. The spatial arrangement of regression residuals was examined as well as the relationship between the residuals and terrain induced variations in incident solar radiation.

3.2 Window Size

The NS001 data for this analysis were collected on June 6, 1987 (see Section 2.2) and the red and near infrared radiances were haze

corrected (see Section 2.3). The difference in T_S-NDVI regression characteristics (r^2 and slope) obtained from analyses using the three window sizes were examined for statistical significance using the Scheffe F-test. A summary of these results is given in Table 3.1.

From Table 3.1 it is apparent that variations in window size can lead to significant differences in the slope of the T_S-NDVI regression line. Apparently, landscape changes over short distances (< 250 m) influenced the regression characteristics. Given this intra-station variability in the regression slope, it was suspected that station-to-station variability would also be observed due to differences in landscape conditions across the FIFE site.

3.3 T_S-NDVI Regression Slope, Soil Moisture and LE

3.3.1 Specific objectives

As mentioned previously, it has been hypothesized that the slope and the intercept of the T_S-NDVI regression will vary with changes in soil moisture content and the corresponding change in LE fluxes if all other environmental variables are assumed to be constant. Therefore, it may be expected that there would be minimal spatial variability in these regression characteristics when the vegetation within the FIFE area was not water stressed. The first specific objective of this study was to investigate this hypothesis using data collected on June 6, 1987.

The second objective of this study was intended to indicate whether changes in the regression characteristics could be associated with the observed differences in soil moisture or LE fluxes. The variability in

Table 3.1: Significance of Scheffe F-scores for T_s-NDVI regression slope differences using three window sizes. (NS = not significant; * = significant at 95% level; ** = significant at 99% level).

Station	Window sizes compared	r^2	Slope
02	20X20 VS 40X40	NS	*
	20X20 VS 80X80	NS	**
	40X40 VS 80X80	NS	*
06	20X20 VS 40X40	**	**
	20X20 VS 80X80	**	**
	40X40 VS 80X80	*	NS
08	20X20 VS 40X40	NS	NS
	20X20 VS 80X80	NS	**
	40X40 VS 80X80	**	**
10	20X20 VS 40X40	**	*
	20X20 VS 80X80	NS	**
	40X40 VS 80X80	**	**
12	20X20 VS 40X40	NS	NS
	20X20 VS 80X80	**	**
	40X40 VS 80X80	**	**
14	20X20 VS 40X40	**	**
	20X20 VS 80X80	**	**
	40X40 VS 80X80	NS	NS
18	20X20 VS 40X40	**	**
	20X20 VS 80X80	**	**
	40X40 VS 80X80	**	NS
20	20X20 VS 40X40	NS	*
	20X20 VS 80X80	NS	NS
	40X40 VS 80X80	NS	**
22	20X20 VS 40X40	NS	**
	20X20 VS 80X80	*	**
	40X40 VS 80X80	**	**

Station	Window sizes compared	r^2	Slope
24	20X20 VS 40X40	**	NS
	20X20 VS 80X80	**	**
	40X40 VS 80X80	**	**
28	20X20 VS 40X40	**	NS
	20X20 VS 80X80	**	NS
	40X40 VS 80X80	NS	NS
34	20X20 VS 40X40	**	NS
	20X20 VS 80X80	**	NS
	40X40 VS 80X80	NS	NS
36	20X20 VS 40X40	**	**
	20X20 VS 80X80	*	**
	40X40 VS 80X80	NS	**
38	20X20 VS 40X40	**	**
	20X20 VS 80X80	**	**
	40X40 VS 80X80	NS	*
40	20X20 VS 40X40	NS	NS
	20X20 VS 80X80	NS	*
	40X40 VS 80X80	NS	**
42	20X20 VS 40X40	NS	NS
	20X20 VS 80X80	*	*
	40X40 VS 80X80	NS	**
44	20X20 VS 40X40	NS	**
	20X20 VS 80X80	NS	**
	40X40 VS 80X80	**	**

NS = Not Significant. * = Significant at 95% Level.

** = Significant at 99% Level.

T_s-NDVI regression characteristics at four selected flux measurement stations within the FIFE study area were examined on three days with different soil moisture conditions (June 6, June 28 and August 17, 1987). Mean volumetric soil moisture contents measured at each station on the three test dates are given in Table 3.2.

Table 3.2: Volumetric soil moisture content (%) at 25 mm depth at four test sites on three dates

	Station Number			
Date	8	36	38	42
6/6	20.6	20.6	18.3	21.3
6/28	43.3	39.7	38.0	40.3
8/17	28.9	21.8	26.9	30.1

3.3.2 Methodology

The analyses used 80 x 80 windows of NS001 data centered on each flux tower within the FIFE study site. The original 6,400 pixels obtained for each station were resampled by selecting every fourth pixel. This resampling was intended to minimize spatial autocorrelation in the data to be used in the regression analyses. T_S-NDVI regressions were determined for 17 flux stations on June 6 and four stations (8, 36, 38 and 42) on the remaining two days.

LE fluxes were obtained for the four selected flux stations from the FIS for the 30 minute period at the time of the overflights on each of the three study days. Total daily LE fluxes were also extracted from the data base for these stations but were found to vary systematically with the 30 minute average values and were generally not considered in the analyses. The four stations were selected so that scan angle differences from day to day and station to station would be minimized.

3.3.3 Analytical procedures

The Scheffe F-test was used to determine whether the T_S - NDVI regression slopes on June 6, 1987 were significantly different from one another. This is a conservative test which is insensitive to departures from normality (Roscoe 1975). The T_S - NDVI scattergrams were examined to identify possible non-linear trends in the relationships. Soil moisture content measured (gravimetrically) at depths of 25 mm and 75 mm on June 6, June 28 and August 17, 1987 was plotted against the T_S - NDVI regression slopes of stations 8, 36, 38 and 42. The 25 mm depth was assumed to represent surface soil moisture while the 75 mm depth was taken to be representative of soil moisture in the rooting zone of the dominant grasses. The dependence of the T_S - NDVI regression slope on soil moisture was evaluated by way of linear least squares regression and the coefficient of determination.

3.3.4 Results and discussion

Spatial variability of T_S-NDVI relationships

The results from the regression of T_S on NDVI for each station are summarized in Table 3.3. The r^2 values were all significantly different from zero at the 99 percent confidence level (n = 1600) and ranged from 0.353 for station 8 to 0.885 for station 24.

Table 3.3: Slope, intercept, standard error (SE) and coefficient of determination (r^2) for the regression of T_s on NDVI for each station (n = 1600) (Hope and McDowell 1992).

STATION	SLOPE	INTERCEPT	SE (K)	r^2
02	-14.866	312.7	0.997	0.704
06	-16.943	314.4	0.751	0.640
08	-12.656	311.1	1.181	0.353
10	-16.615	314.5	1.245	0.634
12	-15.529	313.5	1.115	0.491
14	-16.070	313.5	1.041	0.580
18	-15.549	313.3	0.864	0.737
20	-17.496	316.0	1.709	0.784
22	-18.502	316.1	0.958	0.668
24	-18.729	316.5	1.554	0.885
28	-19.812	317.2	1.219	0.770
34	-15.775	314.0	1.311	0.741
36	-19.642	317.6	2.460	0.769
38	-15.287	312.3	1.953	0.733
40	-22.057	318.6	1.152	0.783
42	-23.174	319.7	1.093	0.790
44	-23.968	320.5	1.336	0.626

An examination of the T_s-NDVI scatter plots revealed that all the relationships were linear which was consistent with the results obtained for other regions by Gurney et al. (1983), Goward et al (1985) and Nemani and Running (1989). Three examples of the T_s - NDVI scatterplots are given in Figure 3.1. Slopes of the regression lines were variable, ranging from -12.7 to -24.0 and most of these slopes were significantly different from one another at the 95 percent confidence level (Table 3.4).

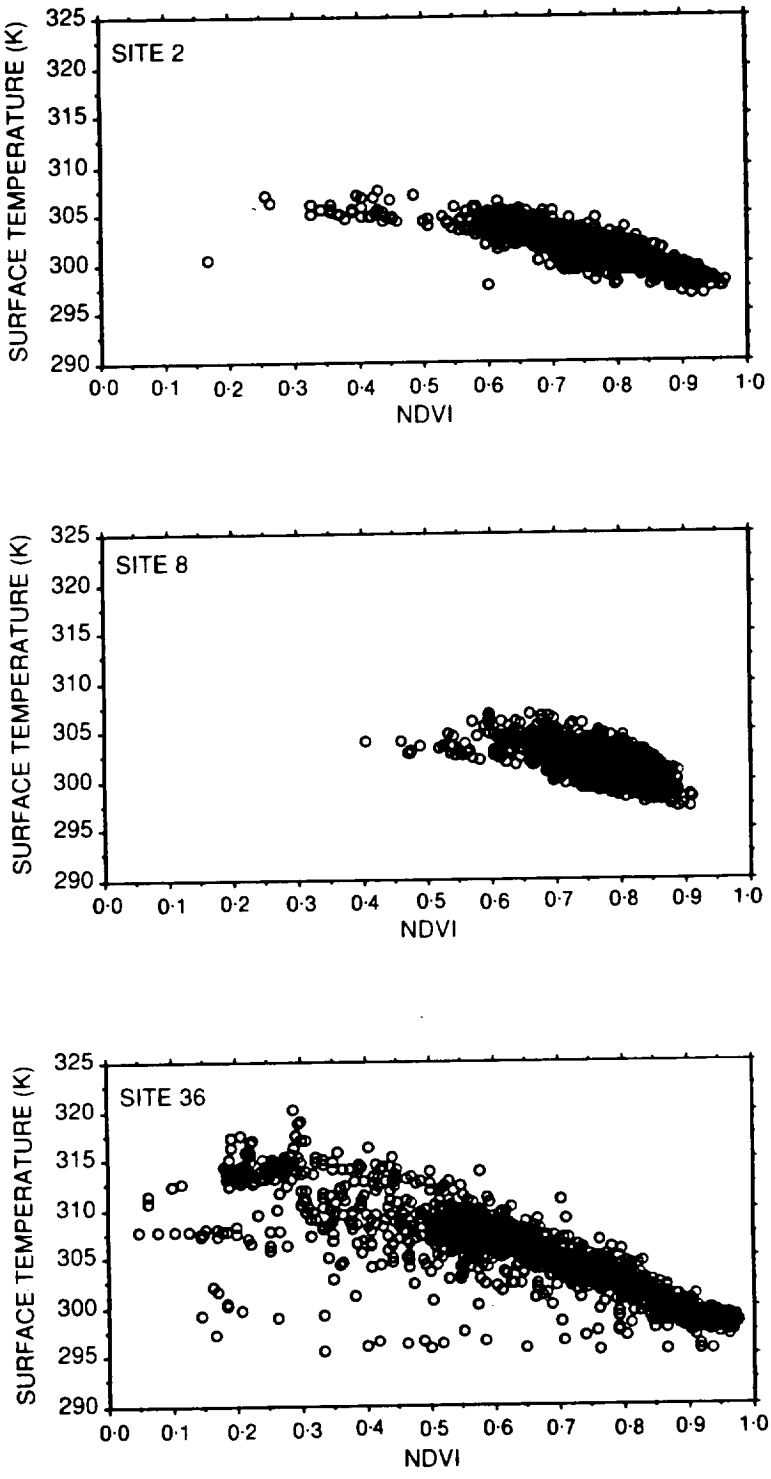

Figure 3.1: Examples of the T_S-NDVI scatterplots from stations 2, 8 and 36 (Hope and McDowell 1992).

Table 3.4: Sites with T_S-NDVI regression slopes that were not significantly different from each other (•) (Hope and McDowell 1992).

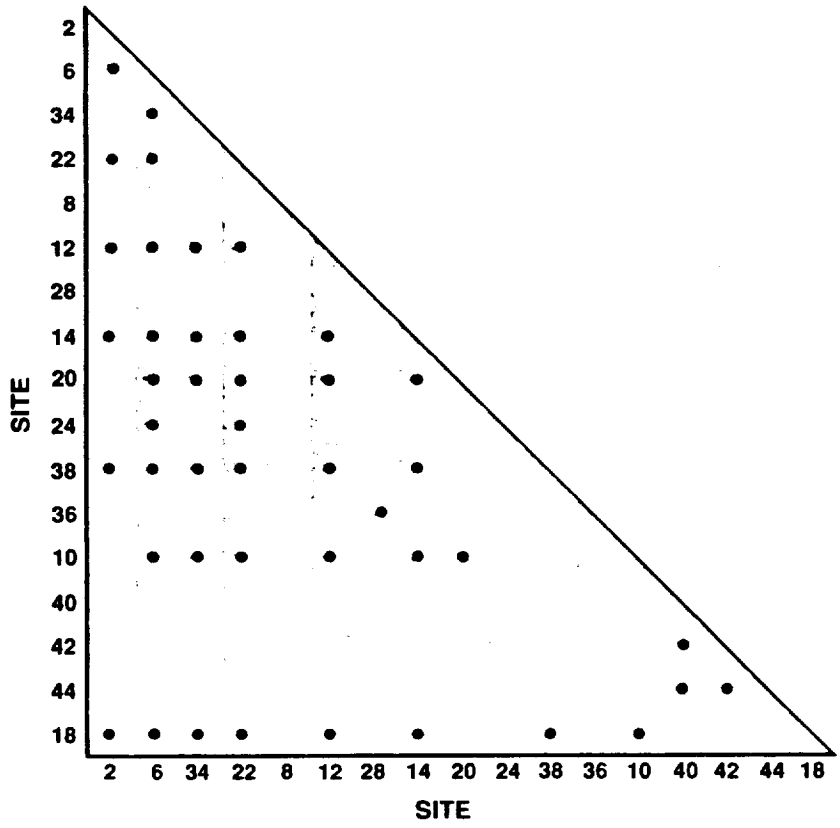

Sites with similar regression slopes generally were not spatially clustered, although there was a tendency for sites in the natural Konza area in the north-west to have similar slopes (sites 2, 6, 10, 12, 14 and 18).

The best fit linear least squares regression lines for each station are plotted in Figure 3.2.

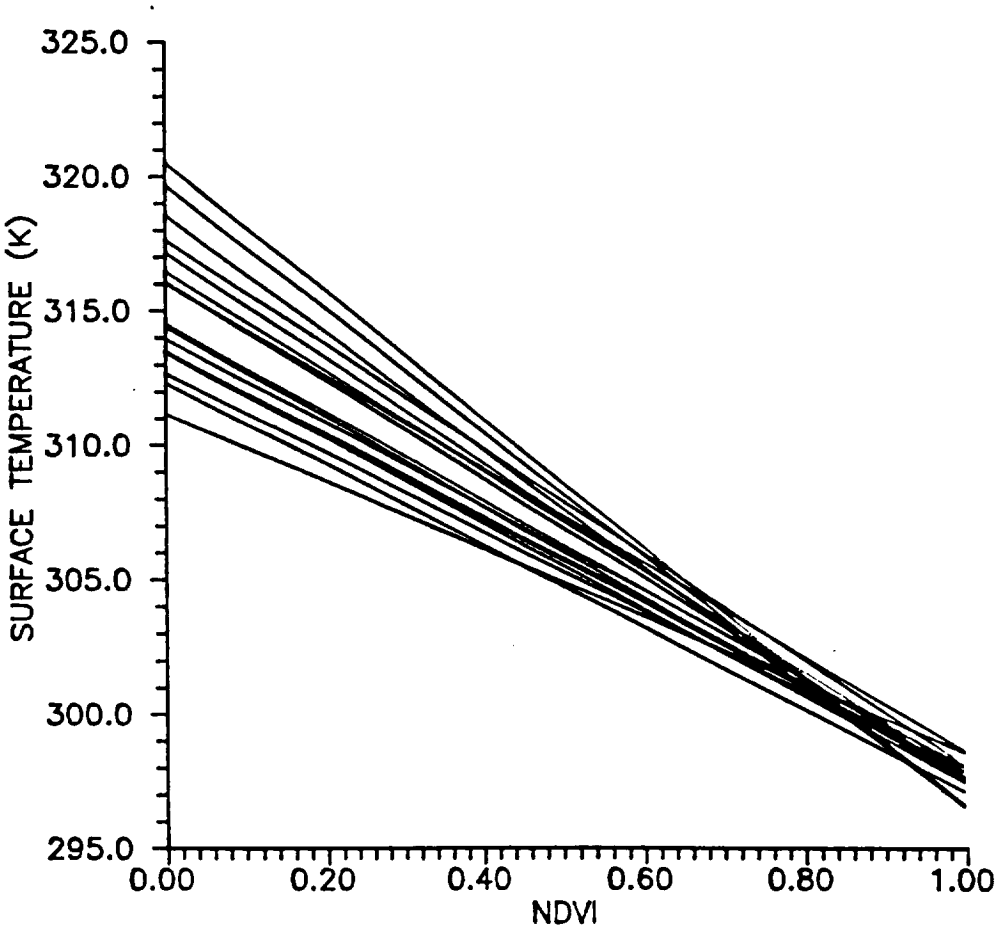

Figure 3.2: Linear least squares regression lines for 17 sub-scenes (Hope and McDowell 1990).

The regression lines all converged as the NDVI approached a value of 0.8. Nemani and Running (1989) observed a similar phenomenon and found that the T_S - NDVI regressions calculated for two different dates over a conifer forest had different slopes but converged as the NDVI approached the maximum observed value. When the regression equations for each station were solved for NDVI = 0.8, the calculated temperatures had a range of less than 1.8 K compared to the regression intercepts that had a range of 9.3 K. This finding may be explained in terms of the different thermal

responses of bare soil and vegetation. It is likely that surface heating of the bare or partially exposed soils was more variable than that of well vegetated surfaces on June 6 since antecedent precipitation was adequate to ensure that the vegetation was not stressed in any part of the study area. The small observed differences in the canopy temperatures at large NDVI values could be attributed to variations in T_S being caused by factors such as spatially variable meteorological conditions, physiological and architectural differences in the plants causing differences in canopy and/or aerodynamic resistance and variations in the terrain resulting in station-to-station differences in insolation. Large differences in bare soil temperatures may, in contrast, have arisen from variations in surface soil moisture and shading. Although soil moisture in the rooting zone of the vegetation is unlikely to have limited transpirational rates, the last rainfall prior to June 6 was on June 3 which allowed for differential surface drying of exposed and partially exposed soils. Consequently, the latent heat fluxes of bare soils would have been less than the potential rate in many exposed areas at the time of data acquisition resulting in elevated surface temperatures.

The results presented above have implications for using the T_S-NDVI relationship for evaluating station-to-station differences in vegetation stress or variations in LE fluxes. The T_S-NDVI relationship is more likely to be diagnostic of plant water stress at larger NDVI values. For unstressed conditions, it may be expected that the regression lines at the upper NDVI limit would have similar values of T_S, as was demonstrated in this study. Dissimilar values are likely to occur under conditions of variable stress when stomatal closure would restrict transpiration and induce canopy heating. Furthermore, if a time series of the T_S-NDVI

relationship is to be examined for a particular region, then temporal differences in heat fluxes associated with stressed and unstressed conditions of the vegetation may also be reflected in changes in the relationship at larger NDVI values. Hope et al. (1986) concluded from a theoretical study of the T_S-NDVI relationship that the regression lines at the upper range of the NDVI would be displaced towards larger T_S values as stress in the canopy increased. For given meteorological conditions, the surface of bare soils would tend to attain a stable maximum surface temperature once soil moisture had been depleted. Consequently, spatial variability in plant available moisture (i.e., in the rooting zone) would not be reflected in the T_S of pixels dominated by bare soil (i.e., small NDVI). An increase in vegetation moisture stress would cause the T_S of pixels with large NDVI values to increase and the T_S - NDVI regression slope to have a reduced gradient.

Since the spatially variable heating of bare soil was considered to be a possible cause of the T_S-NDVI regression slopes diverging as the NDVI approached zero, the analyses outlined above were repeated for a data set which only included pixels with NDVI's greater than or equal to 0.6. It was assumed that all the pixels in this restricted data set were completely covered by vegetation. However, the exclusion of bare soil and mixed soil/vegetation pixels resulted in similar findings to those obtained for the unrestricted data set. Differences in the soil background temperature may still have affected the observed thermal emissions in this data set or mechanisms other than the differential heating of bare soil and vegetation (e.g., the consequences of differences in management treatment and terrain) could be responsible for the convergent-divergent nature of the regression slopes.

Research presented by Hope (1986) suggested that a change in slope would be associated with variations in LE fluxes while Nemani and Running (1989) attributed the change in slope over deciduous forests to differences in canopy resistance and therefore by inference, changes in LE fluxes. However, attempts to relate the regression slopes of these 80 x 80 pixel sub scenes to LE measured at the corresponding flux stations were not successful. It should be noted that these fluxes were fairly consistent from station to station on June 6 (variability generally less than 10 percent of the mean). Furthermore, the T_S-NDVI regressions were based on data collected from a square area with the flux station in the center and no attention was given to the fetch associated with the fluxes.

Since the variations in the regression slopes could not be related to variations in LE fluxes, it may be argued that the variability in surface characteristics (fractional vegetation cover, terrain etc.) that were not affecting LE fluxes on this day, were influencing the T_S-NDVI relationship. It should also be noted that variations in view angle of the sensor had no systematic relationship with the regression slope. The maximum difference in the T_S-NDVI relationship observed at the smaller NDVI values (Figure 3.2) indicates that greater variability in T_S values occurs when the vegetation cover is not complete and there are contributions to the thermal response from both bare soil and vegetation. Following this line of reasoning, it may then be concluded that fractional vegetation cover was the major determinant of the differences in the regression slopes on June 6. The FIFE study area had received precipitation on June 2 and some variable drying of the surface soils could have been expected on June 6. This variable drying of bare soil may thus have accounted for the greater range of T_S values associated with partial vegetation cover

conditions (i.e., lower NDVI's) since soil moisture in the rooting zone of the vegetation was likely to have been adequate for plant potential transpirational rates. Station to station differences in area averaged canopy resistance, atmospheric conditions or topography may also have contributed to the observed differences in the regression characteristics.

Temporal comparison of T_S-NDVI relationship

A comparison of the T_S-NDVI relationship (regression slope) observed on three dates at four stations was made to determine whether the temporal changes in soil moisture conditions and LE fluxes were related to the T_S-NDVI regression slope. No direct relationship between these regression characteristics and LE fluxes at the time of the overflight (or total for the day) could be established ($r^2 < 0.039$). However, when ground heat flux (G) is subtracted from LE flux, the regression slope has a significant (95 percent confidence level) linear relationship with this variable. The relationship between the T_S-NDVI regression slope and LE-G is presented in Figure 3.3.

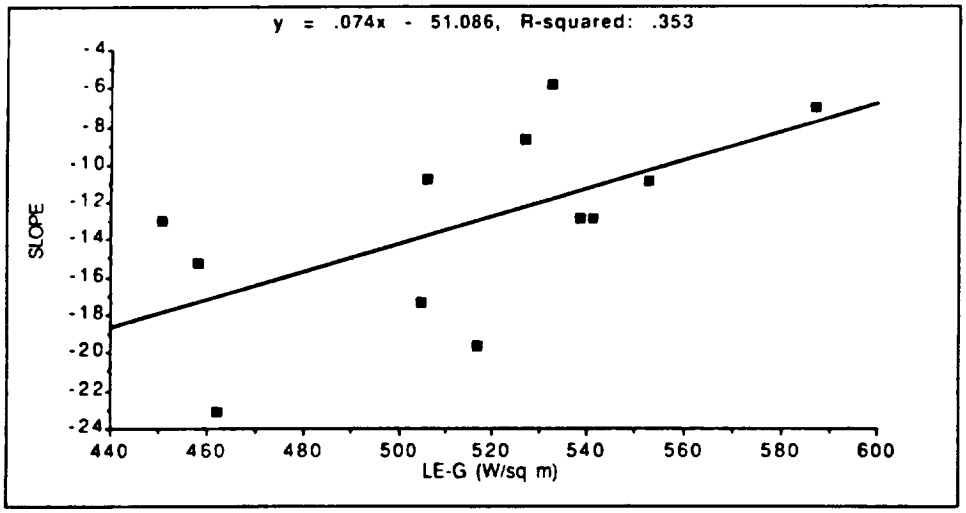

Figure 3.3: Relationship between T_S-NDVI regression slopes and LE-G.

The results presented in Figure 3.3 reveal substantial scatter about the linear least squares regression line. These results are, however, consistent with the previous reasoning that the T_S-NDVI relationship appears to be controlled to a large extent by the fractional vegetation cover. As the regression slope approaches zero the LE fluxes increase, a situation that would be expected if bare soil surfaces were wet with their LE fluxes and T_S values approaching those of well vegetated surfaces with plant potential transpirational rates. Differences in the LE flux and T_S of the contrasting surfaces under these wet conditions were likely to arise due to variations in the turbulent transfer of heat fluxes associated with the differences in surface roughness or wind speeds.

Further evidence of the interplay between fractional vegetation cover and surface soil moisture affecting the regression characteristics of the T_S-NDVI relationship may be found in comparing the scatterplots from day-to-day. The scatter of points for each station on each day except June 28 followed a well defined linear pattern. However, two of the four stations had notably different scatters on June 28 (stations 36 and 38). Once NDVI values were below 0.6 the decrease in T_S with further reductions in NDVI were minimal. Since there was rainfall on the morning of this day prior to the data acquisition, it could be expected that the surface soils were wet and evaporation from these surfaces nearly matched atmospheric demand. Consequently, the surface resistance to LE fluxes at NDVI values less than 0.6 matched those of the areas with NDVI at or slightly above 0.6. An example of this observed difference in the scatter plots is given for station 36 in Figure 3.4.

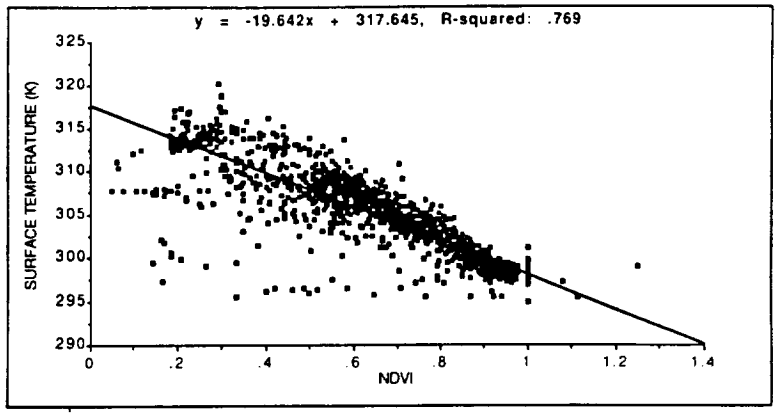

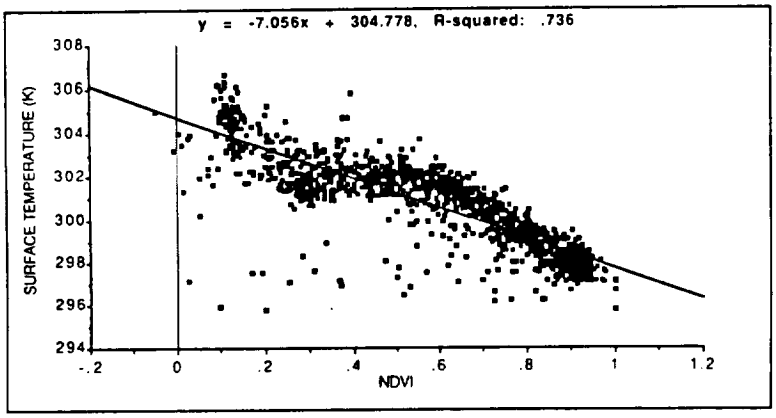

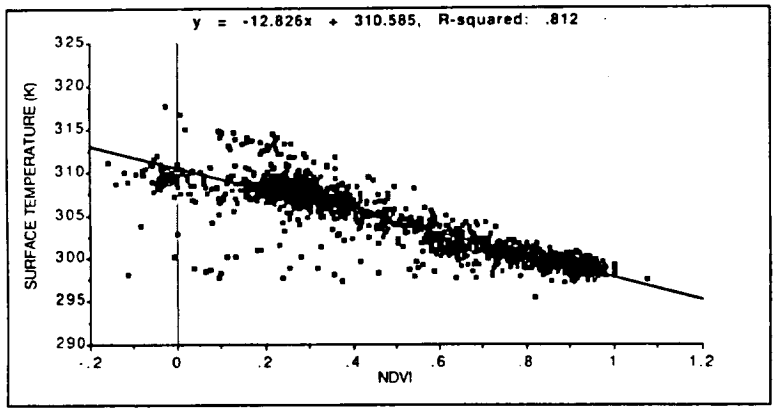

Figure 3.4: Relationship between T_S and the NDVI for station 36 on three days of data acquisition, a) June 6, b) June 28 and c) August 17.

The small group of 'warm' pixels at NDVI = 0.12 in Figure 3.4 could be associated with exposed rock surfaces that may have dried prior to the overflight. Each of the three scatterplots in Figure 3.4 has a number of points plotting at the minimum T_S value across a range of NDVI values. This lower T_S limit appears to coincide with the ambient air temperature. It would be expected that the T_S value for the maximum NDVI would approach air temperature while shadowed pixels (low NDVI) would also assume this value.

A relationship between the T_S-NDVI regression slope and soil moisture content was apparent regardless of the depth of soil moisture measurement (25 mm or 75 mm). Soil moisture measured at 25 mm depth had a slightly better relationship with the regression slope than values obtained from a depth of 75 mm (Figure 3.5) These results also support the contention that fractional vegetation cover and surface soil moisture content are major determinants of the T_S-NDVI relationship. Soil moisture content at 25 mm is likely to have been a better indicator of surface soil moisture content than the measurements made at 75 mm.

The dependence of the T_S-NDVI regression slope on soil moisture content was investigated further by entering the net radiation, sensible heat flux (H), ground heat flux (G) and LE measured at each station into a forward stepwise regression along with soil moisture measured at the 25 mm depth as independent variables and the T_S-NDVI regression slope as the dependent variable. The r^2 increased from 0.507 to 0.733 when G entered the equation to predict the T_S-NDVI regression slope. None of the other variables entered the equation when a threshold of four was designated for the partial F-ratio used in variable selection. Since LE-G was shownto have a better association with the regression slopes,

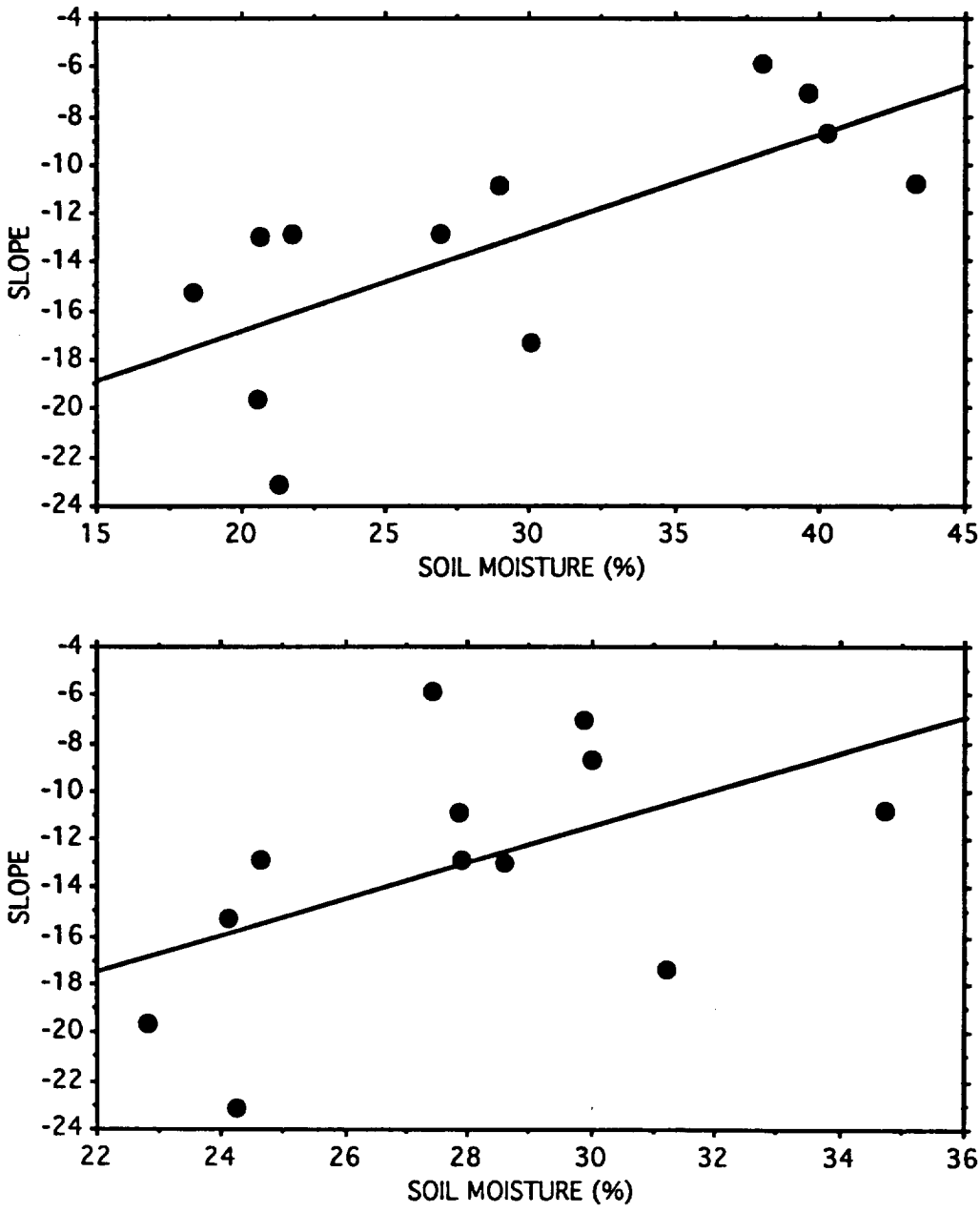

Figure 3.5: Relationship between T_S-NDVI regression slope and soil moisture measured at depths of a) 25 mm and b) 75 mm.

it is apparent that the variability in the regression characteristics is somehow partially affected by variations in G. This result is not unexpected since both the NDVI and T_S may be related to G. As vegetation cover and the corresponding NDVI change, so it may be expected that the amount of energy entering the soil would also change (i.e., less G with greater vegetation cover). Kustas (1989) has demonstrated that the fraction of net radiation partitioned to ground heat flux decreases with an increase in a spectral vegetation index. Surface temperature is also likely to relate to the thermal gradient between the soil surface and the substrate. Furthermore, it may be anticipated that soil moisture content and G would be related due to the dependence of thermal conductivity on soil moisture content. There was, however, no observed relationship between G and soil moisture content (r^2 = 0.006) for the data used in this study.

3.3.5 Conclusion

The study of the T_S-NDVI relationship reported in this section was conducted using a limited data set but the results provided a basis for determining the directions of future research. The most notable finding was that the interplay between fractional vegetation cover and surface soil moisture conditions was a major determinant of the slope or intercept of the regression of T_S on NDVI. With further research, the relationship may provide the basis for partitioning total evaporative fluxes of an area into the contributions from the bare soil and vegetation components. The results also indicated that the T_S-NDVI relationship was affected by variations in ground heat flux. Although this is generally a

minor component of the surface energy balance, there are conditions under which G may be as important as the LE or H and therefore can not be ignored.

3.4 Burn Treatments and Other Landscape Controls

3.4.1 Background

The spectral reflectance and surface temperature properties of Kansas tallgrass prairie have been shown independently to be affected by burning (Asrar et al. 1986; Schmugge, Kanemasu et al. 1987; Asrar et al. 1988; Asrar et al. 1989). Since parts of the FIFE site were burnt prior to the growing season and data acquisition for FIFE in 1987, it was necessary to determine the effects of burn treatments on the T_S-NDVI relationship.

Burning of grass canopies has generally caused a reduction in red reflectance and an increase in near infrared reflectance when compared to the reflectances of unburnt areas (Asrar et al. 1986 and Asrar et al. 1989). These differences also lead to differences in the SVI's of burnt and unburnt areas as has been demonstrated by Schmugge et al. (1987), the former treatment being associated with larger SVI values. Hulbert (1969) and Knapp (1984) concluded that burning causes an increase in the growth of tall grasses while Weiser et al. (1986) found that this management practice altered the vegetation species composition. These consequences of burning are likely causes for the observed differences in the spectral reflectance properties of burnt and unburnt prairie grasses.

In a comparison of the energy budget of burnt and unburnt grasses of the Konza prairie in Kansas, Schmugge et al. (1987) and Asrar et al. (1988) have found that burnt areas had cooler afternoon surface temperatures than the unburnt areas when soil moisture did not limit transpirational rates. Using NS001 scanner data collected using a C130 aircraft, Schmugge et al. (1987) reported that the T_s of unburnt areas was 3 to 4 °C warmer than those of the burnt areas at 2:00 p.m. LST. Asrar et al. (1988) examined the diurnal changes in radiative surface temperatures and found that the two treatments had distinctly different diurnal patterns. These authors reported that when soil moisture did not limit transpirational rates, the unburnt areas were warmer than the burnt areas after midday. An opposite trend was observed when soil moisture was limiting. Asrar et al. (1988) concluded that the differences in the energy balance and T_s associated with the two treatments were primarily due to the presence (unburnt) or absence (burnt) of a layer of senescent vegetation at the soil surface.

Schmugge et al. (1987) examined how the T_s and NDVI of burnt areas of the Konza prairie differed from those of unburnt areas. In this investigation, T_s was plotted against the NDVI. These authors found a strong linear relationship (R^2 = 0.80) to exist between T_s and the NDVI of the grassland which is consistent with other results presented in this report. Although both the NDVI and T_s of burnt and unburnt areas were different, the management treatment did not appear to affect the relationship between the two variables with the data points plotting on the same regression line (Figure 3.6). This observation is, however, based on a single data set.

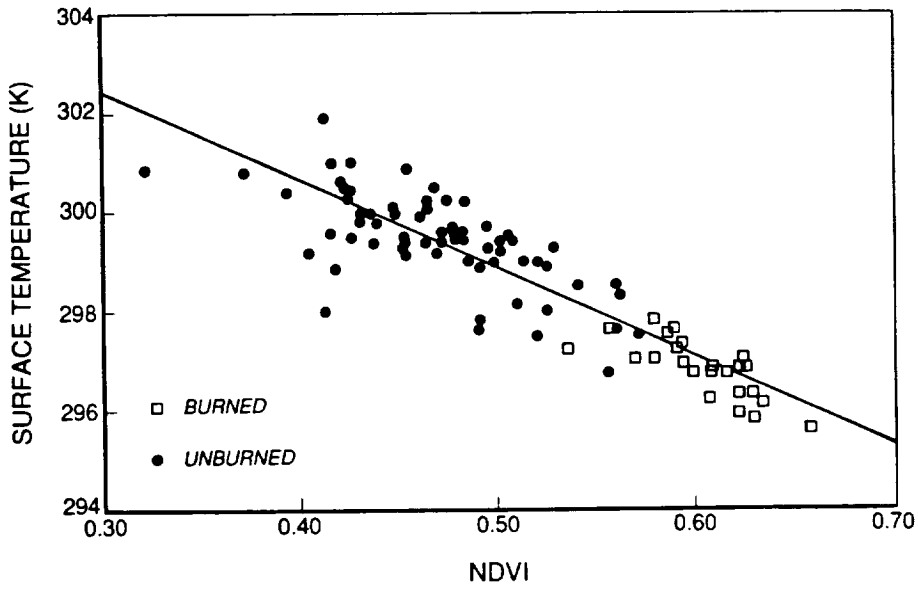

Figure 3.6: Scatterplot of T_S versus NDVI for burnt and unburnt areas of the Konza prairie (Schmugge et al. 1987)

The study presented in this section was designed as an extension of the research described by Schmugge et al. (1987) and had the broad aim of determining whether the T_S - NDVI relationship was consistent across the FIFE study area regardless of management treatment and topographic variability. The focus of the study was on the T_S-NDVI regression slope (SL) since, as stated previously, it was hypothesized that variations in the slope are diagnostic of differences in LE fluxes or surface parameters affecting these fluxes.

3.4.2 Specific objectives

Based on the findings of Schmugge et al. (1987), it was hypothesized that SL would be similar from location-to-location within the FIFE study area regardless of management treatment (burnt versus unburnt). The primary goal of this investigation was to determine the extent to which burn treatments contributed to the variability in the T_S-NDVI regression slope (SL).

Terrain variability (slope and aspect) across the FIFE study area has been shown to cause differences in surface irradiation (Dubayah et al. 1989). Because solar radiation is the primary source of energy for surface heating, differences in irradiation could be expected to contribute to the spatial variability in T_S. Topographically induced variations in illumination affect the spectral response, and hence, NDVI of surfaces (Holben and Justice 1980). If terrain affects both T_S and the NDVI it could be expected to also affect SL. Consequently, it was a goal of the study to establish whether variations in terrain needed to be considered in relating SL to differences in management treatment.

Although forests (generally along riparian zones) and agricultural lands are only a small fraction of the FIFE study area, these land-uses have contrasting physical characteristics to those of the prairie grasslands. Differences in canopy structure, leaf optical and orientation properties, phytomass, shadowing and the proportion of exposed bare soil could be expected to result in distinct reflectance and thermal emission properties of forest and agricultural lands. The final goal was, therefore, to determine whether these minor land-use components contributed to the observed variance in SL values across the FIFE study area.

3.4.3 Methodology

The 80 x 80 pixel sub-scenes centered on the flux towers were also used in this investigation (see section 3.1). The FIFE Information System (FIS) provided a geographic information system (GIS) which included data layers representing the burnt and unburnt areas. These two treatments were subdivided according to the terrain slope categories of valley bottom, hill top, moderate slopes (3 - 6 percent), and steep slopes(> 6 percent). The steep slope category was also divided into three aspect classes (north, south and east and west combined). Some sub-scenes included small areas of agricultural or forested lands that were also identified in the GIS. The GIS had a resolution of 30 m and was used to determine the proportions of each burn-terrain category in the 80 x 80 pixel sub-scenes. The selected sub-scenes represented a wide range of proportions of burnt and unburnt areas and terrain categories, these station characteristics being given in Table 3.5.

An initial step in evaluating landscape control over the T_S-NDVI relationship was to use cluster analysis to group station sub-scenes on the basis of their terrain slope, aspect, landcover and management treatment (Table 3.5). Two distance measures were used in the cluster analysis, namely, squared Euclidean distance and the 'group average' method described by Ludwig and Reynolds (1988). The former procedure was considered appropriate since all measures were in percentages and thus contributed proportionately to the distance measure.

Table 3.5: Percentage of each sub-scene categorized as burnt grass, agricultural land, forest, steep slopes (> 6%), moderate slopes (3-6%), hill tops and valley bottoms (Hope and McDowell 1992).

STATION	TREATMENT/LANDUSE				SLOPE		
	BURNT	AGRIC.	FOREST	STEEP	MOD.	TOP	BOT.
2	0.00	0.00	10.84	10.10	25.53	0.18	53.35
6	0.00	0.00	3.40	24.62	31.86	14.69	25.44
8	29.94	0.00	0.80	19.58	33.67	24.91	21.04
10	75.23	0.00	0.80	17.16	36.09	16.65	29.29
12	24.24	0.00	4.98	29.47	32.24	17.63	15.67
14	0.00	0.00	6.45	40.00	23.51	12.49	17.55
18	94.23	0.29	0.29	7.38	20.23	62.75	9.06
20	43.42	8.32	4.40	17.55	29.80	16.41	23.51
22	21.12	0.00	7.38	17.39	37.10	16.73	21.41
24	35.50	17.82	6.65	23.53	22.72	3.29	26.00
28	23.52	1.90	7.01	26.59	21.91	12.27	30.31
34	4.60	4.09	6.87	25.57	31.63	11.10	20.74
36	41.63	12.08	26.69	12.90	20.08	0.16	28.08
38	21.71	16.73	3.59	13.14	26.94	0.81	38.77
40	98.69	0.00	0.00	27.25	32.36	14.68	25.72
42	92.66	0.00	0.98	29.80	28.41	5.88	34.93
44	96.32	0.00	7.44	21.85	24.70	26.35	19.65

The group average method was selected because the chord distance measure used in the algorithm is more reliable than the Euclidean measure when zero data are present (Ludwig and Reynolds 1988). The 17 study stations were grouped into six clusters based on their slope-cover-treatment characteristics (Figure 3.7). The results were similar regardless of the clustering algorithm used. A large increase in similarity distance coefficients occurred between stages 11 and 12, so additional clustering would force the merger of two dissimilar groups.

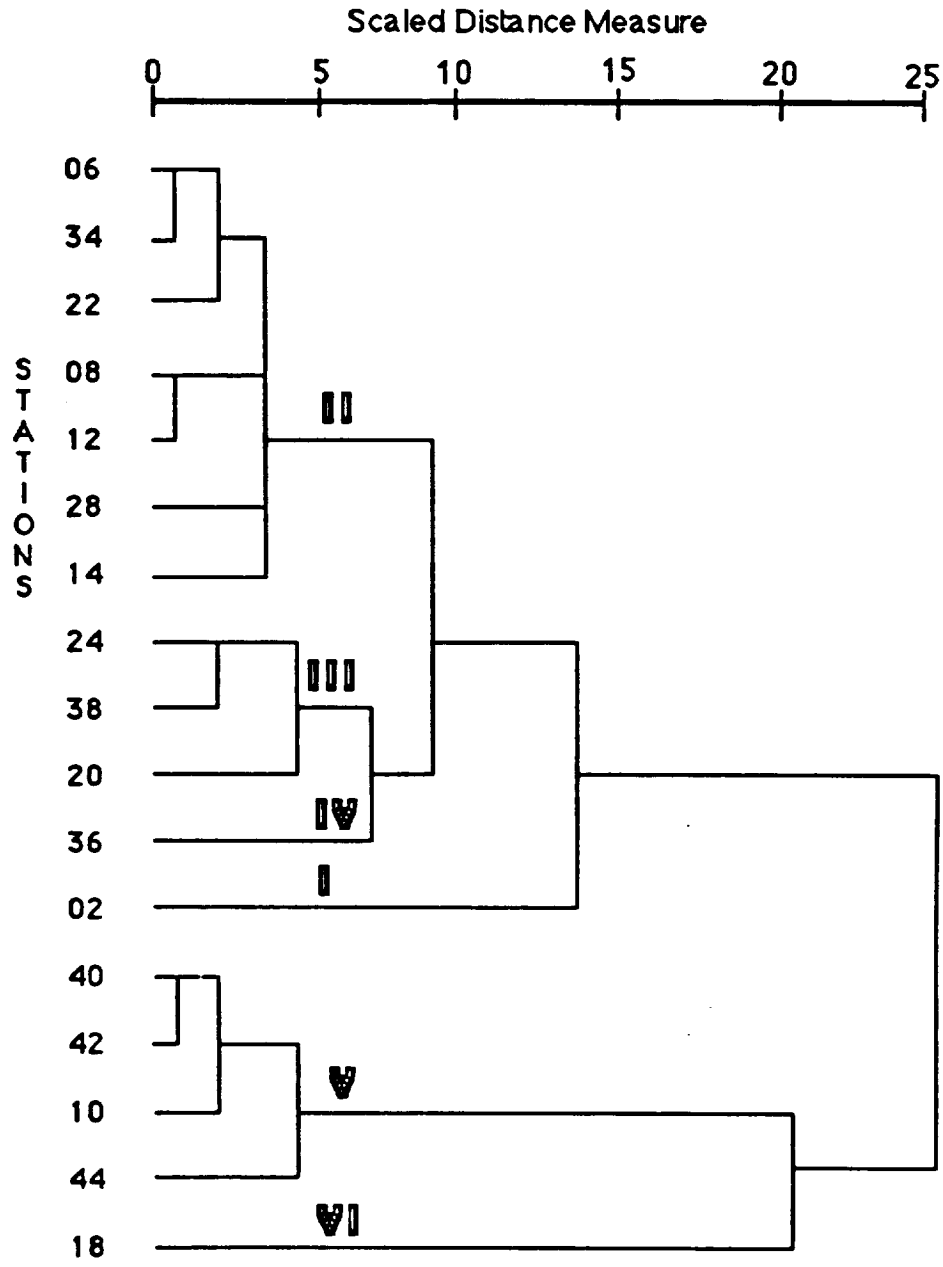

Figure 3.7: Dendrogram illustrating clustering of flux stations on the basis of slope-cover-treatment. Six clusters identified at distance 4.7 are indicated by Roman numerals.

Three of the clusters (I,V and VI) include only one station each. Station 2 (cluster I) is exclusively unburnt land and has mainly moderate slopes and bottomlands while station 18 (cluster V) is an upland area characterized by burnt grasslands. Reducing the number of clusters to three did not result in the two individual stations combining with the larger burnt and unburnt clusters. Cluster II grouped stations that are mainly unburnt grasslands with steep slopes, cluster III stations are also predominantly unburnt grasslands but on moderate slopes while the stations in group IV are characterized by a high percent of burnt grassland (> 75) on moderate slopes and bottomlands.

The mean T_s and NDVI, and SL from the 17 sites were regressed on eight independent burn-terrain variables. These independent variables were defined according to a hierarchy based on treatment, terrain slope and aspect (Figure 3.8).

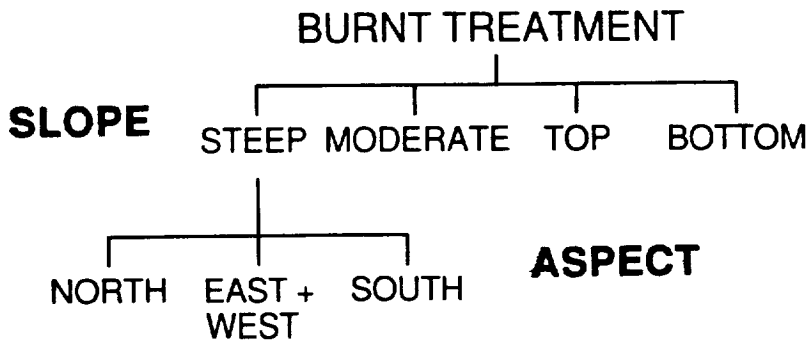

Figure 3.8: Hierarchy of burn-terrain independent variables (Hope and McDowell 1992).

The data for the independent variables were extracted from the FIFE GIS. The coefficient of determination from each regression was tested using Student's t-test to determine whether the value was significantly different from zero.

In order to determine whether the small proportions of agricultural or forest lands within each sub-scene would account for variability in SL, these quantities were included along with the management treatment and physiographic variables as the independent variables in a stepwise regression analysis. The independent variables were entered into a forward stepwise linear regression procedure which included the elimination of unnecessary variables (Feldman et al. 1987).

3.4.4 Results and discussion

Management treatment and terrain variability

Based on the studies conducted by Asrar et al. (1986), Schmugge et al. (1987) and Asrar et al. (1989), the mean NDVI and mean T_s of the sites used in this study would be expected to covary with the proportion of burnt area in each sub-scene. Results from regressing these mean values on the burn-terrain independent variables did not support these published findings (Table 3.6). The mean NDVI had an insignificant relationship ($p > 0.05$) with each of the independent variables except for the proportion of burnt prairie on steep north facing slopes (B.ST.N). This relationship was not substantial as indicated by the small r^2 value (0.268).

Table 3.6: Coefficient of determination for the regression of the mean NDVI (NDVI), mean T_S (T_S) and SL on the percent of total burnt grassland (B.TOTAL), burnt grassland on hill tops (B.T), moderate slopes (B.M), steep slopes (B.ST), steep north facing slopes (B.ST.N), steep south facing slopes (B.ST.S) and steep east and west facing slopes (B.ST.EW) (Hope and McDowell 1992).

	NDVI	T_S	SL
B.TOTAL	0.006	0.098	**0.369**
B.T	0.102	0.054	0.006
B.BT	0.059	0.183	**0.447**
B.M	0.013	0.155	**0.378**
B.ST	0.136	**0.382**	**0.698**
B.ST.N	0.268	**0.595**	**0.536**
B.ST.S	0.066	0.226	**0.627**
B.ST.EW	0.073	0.222	**0.472**

Significant at 95% confidence level
Significant at 99% confidence level
(n = 1600)

Similar results were obtained for the mean T_S, although B.ST.N accounted for more variance in the mean T_S than in the mean NDVI (r^2 = 0.595). Furthermore, 38.2 percent of the variance in the mean T_S was associated with the variable B.ST, representing the proportion of burnt prairie on all steep slopes (Table 3.6). The representation of terrain (categorical format and spatial resolution) in the GIS did not appear to quantify the expected effects of terrain differences on the mean T_S or NDVI of the sub-scenes. No significant r^2 values were obtained when the mean NDVI and T_S were regressed on the proportions of the sites falling into each of the terrain slope categories if no distinction was made between burnt and unburnt management treatments.

While the mean NDVI and T_S were largely independent of the variables representing different burn-terrain units, SL had a statistically significant relationship with seven out of the eight independent variables. The proportion of burnt prairie on steep slopes regardless of aspect (B.ST) was a major determinant of the regression slope with 69.8 percent of the variance in SL being attributable to this variable. An increase in the proportion of burnt area within a sub-scene caused a reduction in SL (i.e., a steeper regression slope) as is evident from the relationships illustrated in Figure 3.9.

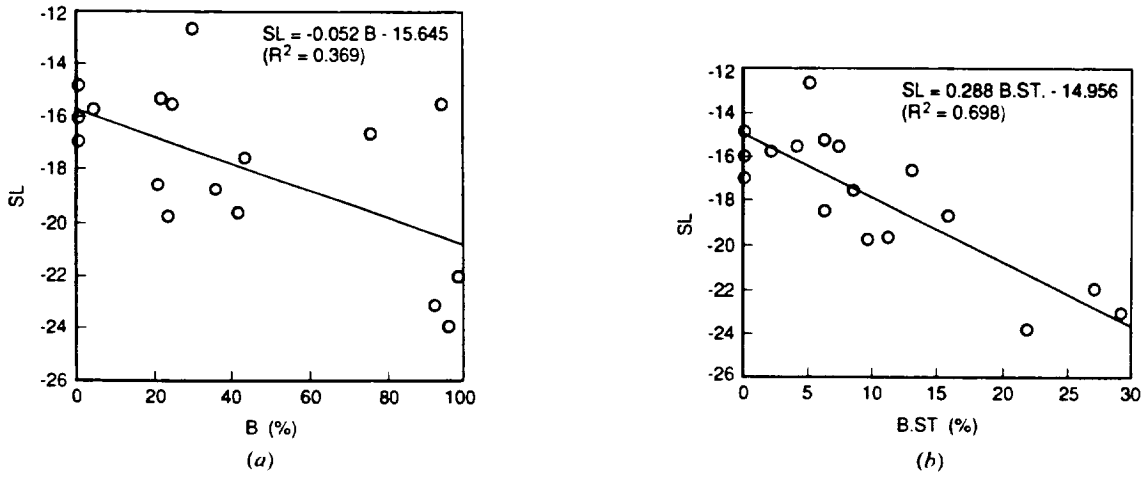

Figure 3.9: Scatterplots of the T_S-NDVI regression slope (SL) versus the area of each sub-scene (a) burnt on all slopes (B) and (b) burnt on steep slopes (B.ST) (Hope and McDowell 1992).

When SL was regressed on the terrain slope proportions that had been determined without the burnt/unburnt stratification, only the steep south facing class had a statistically significant relationship with SL (r^2 = 0.452).

Agricultural and forested areas

The final goal of this investigation was to determine whether the small proportions of forest and agricultural lands in the sub-scenes contributed to the observed variance in SL. Since it was suggested earlier in this paper that surface soil moisture may have been a factor affecting the convergent-divergent nature of the T_s - NDVI regression slopes, a measure of soil moisture was included as an additional independent variable in this stepwise regression analysis. Average soil moisture content measured at a depth of 25 mm was obtained from the FIFE data base. The averages were based on soil moisture measured gravimetrically at approximately 10 locations around each flux measurement station.

Seven independent variables were included in the stepwise linear regression analysis with SL as the dependent variable, namely; the proportions of forest (F) and agricultural lands (A); burnt prairie on steep slopes (B.ST), moderate slopes (B.M), hill tops (B.T) and valley bottoms (B.BT) and the volumetric fraction of soil moisture measured at 25 mm depth (SM_{25}). The equations resulting from each step were as follows:

$$SL = -14.956 - 0.288\ B.ST \qquad r^2 = 0.678 \qquad (3.1)$$

$$SL = -8.393 - 0.335\ B.ST - 0.264\ SM_{25} \qquad r^2 = 0.781 \qquad (3.2)$$

$$SL = -6.503 - 0.358\ B.ST - 0.297\ SM_{25} - 0.154\ F \qquad r^2 = 0.872 \qquad (3.3)$$

The regression model given in Equation 3.3 indicates that a large amount of the variance in SL across the FIFE study site on June 6 was due to variations in three independent variables representing management

treatment-terrain, soil moisture and land-use. Although soil moisture was measured at a central location within each sub-scene area, it was clear from the results given above that this variable contributed to observed variance in SL. As expected, the proportion of burnt area on steep slopes (B.ST) was responsible for most of the variance in SL while the inclusion of SM_{25} in the regression equation caused the r^2 to increase from 0.678 to 0.781. It is possible that an even larger proportion of the variance in SL could be associated with surface soil moisture if a spatial estimate of this variable could be made (e.g., from microwave imagery).

Since the variability in SL was not reduced when the data set was restricted to pixels with NDVI > 0.6, the analysis was repeated using SL from the restricted data set as the dependent variable ($SL_{0.6}$). In the first step B.ST produced an r^2 of 0.672 which was comparable to the first step in the original analysis. The second and final step included the proportion of forested area (F) as a variable in the regression equation, resulting in a final r^2 of 0.787. Soil moisture did not enter the equation, making no contribution to the explained variance in $SL_{0.6}$. While this result is consistent with the hypothesis outlined earlier that surface soil moisture variations in pixels with sparse vegetation cover give rise to the convergent-divergent nature of the T_s-NDVI regression slopes in the FIFE study area, surface soil moisture can not be discounted from having an effect on the SL of well vegetated areas until a more spatially explicit quantification of this independent variable is included in a similar analysis.

Of the two contrasting land-use types included in the regression analysis, only the proportion of forested area contributed significantly to the observed variance in SL (for both restricted and unrestricted data

sets). However, the failure of agricultural land-use to be a significant variable in the regression equation may be due to the inadequate distribution of data values for this variable with ten of the observations having values of zero.

3.4.5 Conclusions

Station-to-station variability in SL was shown to be related to the proportion of burnt area on steep slopes, soil moisture content near the surface and the proportion of forested area. The effect of burning on the SL contrasted to the results presented by Schmugge et al. (1987) in which the relationship between T_S and the NDVI for the same area did not appear to be affected by burn treatments. While a number of previous studies had indicated that the T_S and NDVI of burnt and unburnt prairie areas would differ, this study failed to confirm this finding using NS001 aircraft data and data from the FIFE GIS.

Although it was not an original goal of the study to examine the effect of surface soil moisture variability on the SL, the results of the initial analyses pointed to the possible relationship between these two variables. It was suggested that the convergent-divergent nature of the regression lines was caused by bare or partially exposed soils having a range of surface soil moisture contents that resulted in a wide range of thermal responses. In contrast, where vegetation was dense and the LE fluxes and T_S were largely controlled by soil moisture in the rooting zone, T_S values were similar because soil moisture did not limit transpirational rates. Further examinations of the T_S - NDVI relationship under varying soil moisture conditions are needed to test this hypothesis.

Since management treatment, terrain and small areas of contrasting land-use (forested areas) were significant determinants of SL, future research directed at using SL as an aid to estimating LE fluxes will need to consider stratifying the T_S and NDVI data on the basis of these physical characteristics. Furthermore, the need to develop an understanding of the role of surface soil moisture on the NDVI, T_S and SL was identified. The ability to determine spatial patterns of surface soil moisture was also considered to be critical to this endeavor and collaborative research in this field is described in Appendix 1.

3.5 Regression Residuals

Results from the preceding studies pointed to the importance of considering differences in land cover type and terrain in evaluating the T_S-NDVI relationship in the context of the surface enrgy balance. Residuals from the regression of T_S on NDVI using the NS001 data were examined to:

1) Determine whether the spatial pattern of residuals conformed to land cover types by exhibiting an organized spatial pattern that resembled fields/land units within the FIFE site. This spatial organization would be expected if the T_S and/or the NDVI were dependent on cover type and the least squares regression line was representative of a heterogeneous area.

2) Determine whether the observed dependence of the T_S-NDVI regression slope, SL, on terrain slope and aspect was largely due to differences in solar illumination.

3.5.1 Spatial pattern of T_S residuals

Residuals from the regressions for stations 8, 10 and 12 were mapped using gray tones to represent the magnitude of over and under prediction of T_S. Each of these residual maps revealed distinct spatial coherence in the pattern of over and under prediction, an example being given in Figure 3.10 for station 8.

Besides land cover type, the spatially coherent pattern of residuals also appeared to be influenced by soil moisture and surface water distributions. The linear strip of overpredicted T_S values indicated by "A" in Figure 3.10 is a stream while the linear feature indicated by "B" is a small depression or non-perrenial tributary of the steam. High levels of soil moisture or surface water are likely to have reduced T_S in these areas. The underpredicted T_S values in the field designated by "C" and overpredicted values in the field designated by "D" can be ascribed to differences in burn history. Field "C" was categorized as "unburnt" in the FIS GIS, while field "D" had been previously burnt.

This residual analysis supports the findings summarized in Section 3.4, namely, that burn history, land cover type and soil moisture status are important determinants of the slope of the T_S-NDVI least squares regression line.

Figure 3.10: Image of residuals from the regression of T_S on NDVI for station 8. Dark shades represents underpredicted T_S and light shades represent overpredicted T_S.

3.5.2 Relationship between T_S residuals and solar radiation

Since solar radiation is the major forcing variable for T_S and slope and aspect were found to be significant variables affecting SL (Section 3.4), it was hypothesized that there would be a significant relationship between T_S-NDVI regression residuals and incident solar radiation. In order to test this hypothesis it was necessary to construct a terrain-based radiation model to calculate the incident solar radiation for each NS001 pixel.

A two part FORTRAN program was developed to calculate terrain induced variations in the amount of incident solar radiation across the FIFE site. The first part of the program (KONTAB) included an ephemeris algorithm described by Wilson (1980) and the geometric calculations were based on equations given by Kondratyev (1969). Atmospheric optical depth was calculated using a procedure described by Sirkov (1971). Solar irradiance was determined for a horizontal surface and then adjusted for variations in slope and aspect. The output from KONTAB was a look-up table of solar radiation values for combinations of slope and aspect. Solar radiation observed at a FIFE measurement station was used to calibrate the model for a horizontal surface.

The second part of the radiation program (RAD2) was a raster-based GIS module that interfaced KONTAB with co-registered slope and aspect information obtained from a digital terrain model of the FIFE site. RAD2 produced an output image and file of radiation values for each pixel. The digital terrain data were originally at 30 m resolution and thus had to be resampled to correspond to the ground resolution of the NS001 sensor.

Stations 2, 6, 8, 10 and 12 were selected for this investigation to represent a range of T_S-NDVI regression characteristics. The r^2 values for stations 8 and 12 were the two lowest values (0.35 and 0.49 respectively). The other stations were selected to represent different treatments (burnt/unburnt), land cover variability and topographic position. The 80 x 80 sub-scenes around stations 2 and 6 contained 100% unburnt area while station 10 had 75% burnt area. Over 20% of the pixels for station 6 and 12 were categorized as "steep" slopes and over 30% of the pixels for stations 6, 8, 10, 12 and 31 were classified as "moderate" slopes. Stations 2 and 10 were flat plateau locations.

The regression of solar radiation (at the time of aircraft overflight) on the T_S residuals accounted for less than 2% of the variance in the residuals. Misregistration of the NS001 and terrain data may have contributed to this lack of association so the analysis was repeated using spatially degraded data (8 x 8 pixel averages). The r^2 values ranged between 0.3 and 0.13 indicating that misregistration may have had some effect on the original results. However, a more likely explanation for the poor relationship between T_S residuals and solar radiation is that the thermal inertia of the surface is ignored by considering instantaneous radiation values. Thermal properties of the surface and the integrated effects of different radiation loads may have been reflected in the regression equations for SL that included slope, aspect and cover type as significant predictor variables (cf. Section 3.4.4).

4. REGIONAL ANALYSES OF THE T_S-NDVI RELATIONSHIP

4.1 Introduction

Most of the research conducted at SDSU as part of this project focussed on analyses of local scale data (helicopter, NS001, Thematic Mapper, flux tower observations). The University of Maryland (Dr. S. Goward) took the lead in analyzing regional scale observations (AVHRR). Integration of the studies did, however, require that both institutions conduct analyses at both scales. Furthermore, the stated goal (Chapter 1) of ultimately applying the proposed methodology to regional LE flux estimation also required that the question of scaling be addressed throughout the study.

The results summarized in this chapter are from two AVHRR-based studies that were conducted during the early phases of the project. The first study was an extension of the research using NS001 data (local scale) that had demonstrated the dependence of the T_S-NDVI relationship on land-cover type (Chapter 3). The second study reports on the findings from an earlier study (Goward and Hope 1989) that examined the T_S-NDVI relationship over a number of days in 1987 and investigated whether the relationship was indicative of CO_2 fluxes over the FIFE site.

4.2 T_S-NDVI Relationship for Different Land-Cover Types

This sub-study was conducted to determine whether different land-cover types affected the T_S-NDVI relationships obtained using AVHRR data. An AVHRR image acquired on June 6, 1987 over central Kansas was

selected for the study. The split window technique (Price 1984) was used to estimate surface temperature for selected sub-scenes. The sub-scenes were chosen to represent the following land-cover classes:

1) Fallow/bare soil.
2) Range/short grassland.
3) Range/medium grassland.
4) Short agricultural crops.
5) Medium agricultural crops.
6) Mixed agriculture.
7) Forest and suburban.
8) Tallgrass prairie.
9) Water/shoreline.

These categories were established from a classified Landsat MSS image.

Scatterplots of T_S versus NDVI for selected sub-scenes are given in Figure 4.1. Consistent with the results obtained using local-scale observations (Chapter 3), the regression slopes of the sub-scenes were dissimilar for the various land-cover types. The presence of water/shoreline in a subscene reversed the direction of the regression slope. It was also apparent from these results that the scatterplots using the AVHRR data exhibited substantial scatter. Scatterplots for the different land-cover types were also centered on substantially different mean T_S and NDVI values. A plot of the mean T_S against the mean NDVI for each class is given in Figure 4.2.

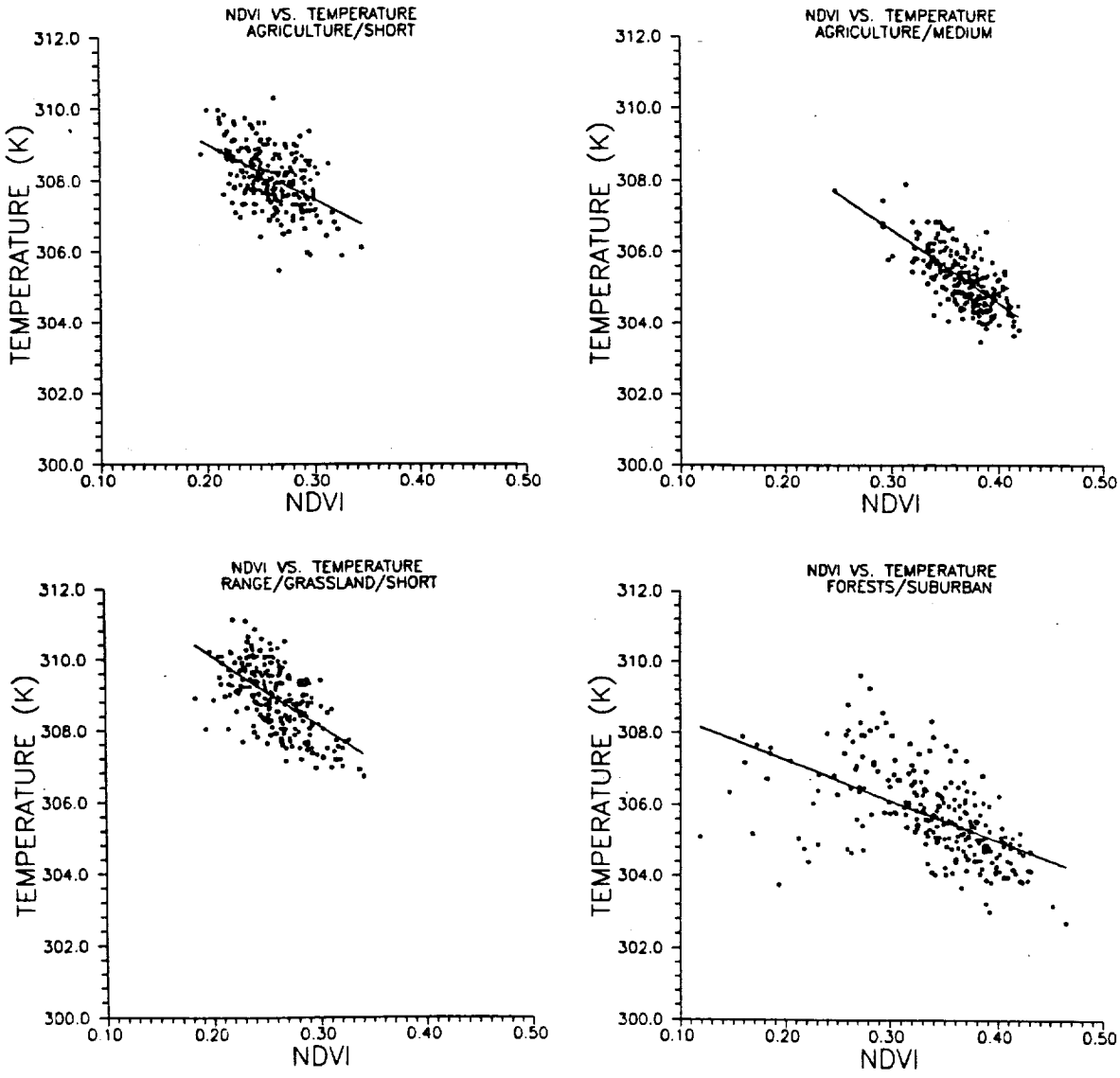

Figure 4.1: Scatterplots of T_S versus NDVI using AVHRR data for selected land-cover types in Kansas

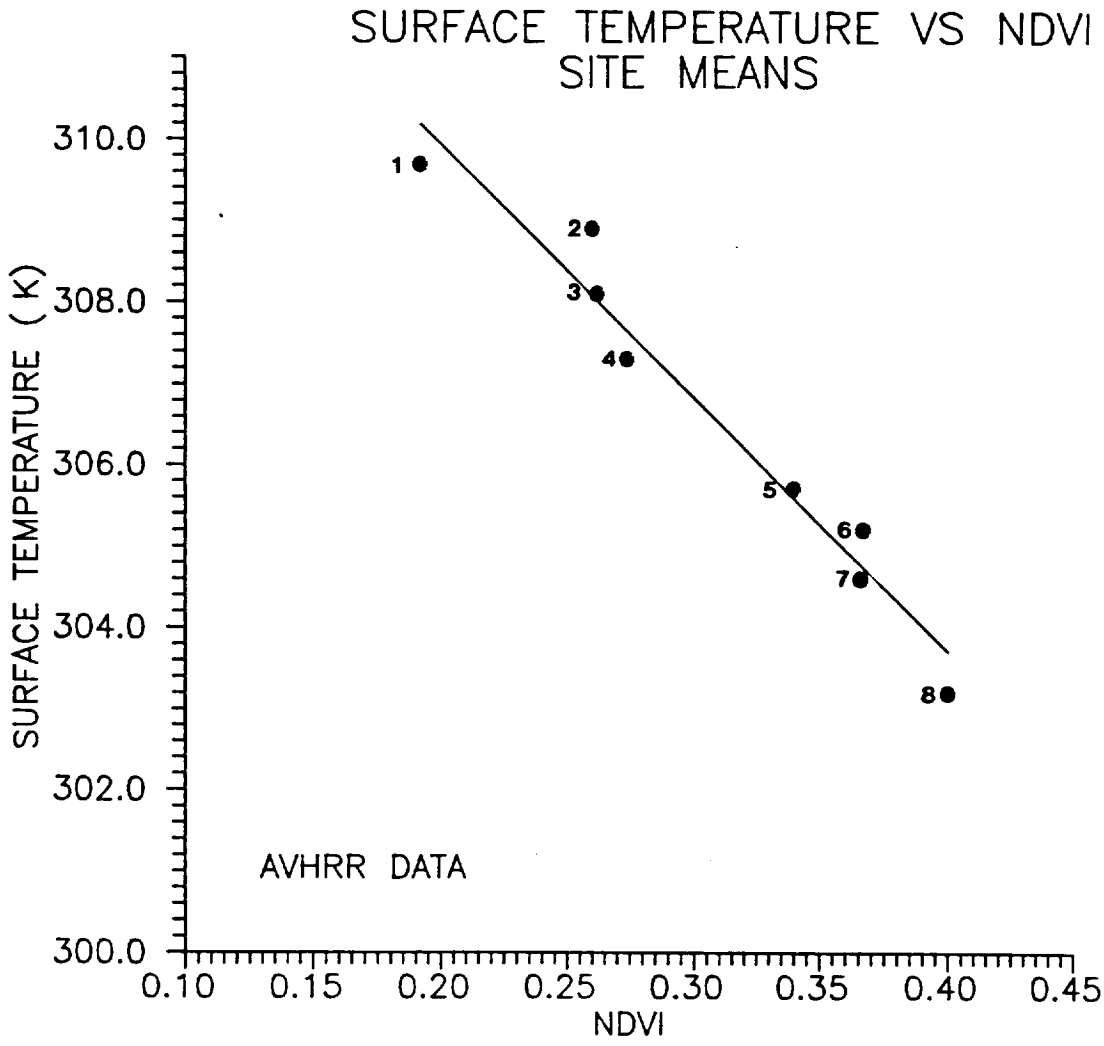

Figure 4.2: AVHRR mean T_S and NDVI for different land-cover types over Kansas (1 - fallow/bare soil; 2 - short grassland; 3 - Medium grassland; 4 - short crops; 5 - forest and suburban; 6 - medium crops; 7 - mixed agriculture; 8 - tall grass prairie).

At the regional scale, the mean T_S for each class had a close association with the corresponding mean NDVI (Figure 4.2). The arrangement of the points appears to follow consistently the relative amount of fractional vegetation cover that could be expected in each class.

4.3 Analysis of T_S-NDVI Time Series[1]

4.3.1 Objective

Between July 9, 1987 (day 190) and August 4, 1987 (day 216) little rainfall occurred at the FIFE site. This produced a deficiency in soil moisture that caused an observed rapid decrease in canopy conductance of CO_2 exchange with the atmosphere. If the T_S-NDVI relation is diagnostic of surface flux conditions, particularly as related to surface Bowen ratios, then changes in this relation should be observed during this major dry-down event in the FIFE region. To evaluate T_S-NDVI hypothesis, all "clear-sky" observations on the FIFE region collected by the NOAA-9 AVHRR afternoon overpass, between July 15, 1987 (196) and the August 15, 1987 (227) were examined. The afternoon view was selected to maximize thermal contrast and minimize the effects of terrain on the observed spectral radiance fluxes.

4.3.2 AVHRR data processing

NOAA-9 and NOAA-10 AVHRR local area coverage observations were acquired daily by the FIFE Information Systems (FIS) at the NASA Goddard Space Flight Center. A 256 by 256 pixel sample of these data, centered on the FIFE site, were extracted by FIS staff. Locational and radiometric calibration information were appended to each acquisition by the FIS team. These data were subjected to further processing and analysis in the

[1] Section extracted from Goward and Hope (1989) and included for completeness of this Report.

remote sensing research facilities in the Geography Departments at the University of Maryland and San Diego State University.

The first step in producing a common data set for the FIFE region was to geographically register all of the AVHRR data. Preliminary inspection of the FIS-sampled data showed that a region of approximately 1^{o} latitude (111 km) by 2^{o} longitude (174 km) is consistently available in the FIFE AVHRR data set. This region was defined as the FIFE region. Because this is a relatively small portion of the globe, a mapping projection of linear latitude and longitude, with the central axis oriented north-south, was selected. The NOAA-9 satellite orbit is inclined 12^{o} from the polar axis of the Earth which results in the pixels being rotated 12^{o} with respect to the map base.

At nadir, the nominal ground resolution of the AVHRR sensor is 1.1 km (it actually varies slightly between spectral bands). In order to produce daily observations, the AVHRR scans over 50^{o} off-nadir, which, when convoluted with Earth curvature, produces off-nadir views in excess of 60^{o}. As off-nadir view increases the ground resolution of the sensor decreases and the pixel shape becomes trapezoidal. At the view angle of 50^{o} the effective ground resolution decreases to 2.8 km along scan and 1.8 km across scan. At nadir a nominal array of 110 by 170 AVHRR pixels covers the FIFE region. This decreases to a 61 by 64 pixel array at 50^{o} off-nadir. To preserve, as much as possible, the radiometric integrity of the original sensor data, these arrays were mapped into a 1224 by 784 array of display rasters. To reduce the computational complexity of the mapping, pixels were assumed to be rectangles, with the sides of the rectangle oriented to the central axis of the projection. Because of the 12^{o} orbital inclination, this introduced a small error in the geographic

precision of pixel boundaries and caused a small overlap between adjacent pixels in the mapped array. Precise location of pixel boundaries in the mapped data array was not computed because the expense of the computation exceeds the accuracy gain. The AVHRR sensor over-samples in the along-scan direction precision and therefore precise determination of pixel edge location is not possible (Kidwell 1986). The overlap was treated by selecting the lower of the two overlapped radiances in the solar reflective bands and higher observed radiance in the thermal infrared bands. This approach was taken because averaging of the data would produce a gradient in the observations not observed by the sensor. The low-high criteria is aimed at selecting the less cloud-contaminated observations.

Cloud identification was carried out to locate clear views of surface conditions. The procedures were based on previous research (Saunders and Kriebel 1988). Dense, low-level cumulus and stratus cover are easily located by analysis of the visible band histogram. Surface reflected radiance forms a strong mode of low reflected radiance. Clouds create an extended tail on the high reflected radiance side of this histogram. By selecting a threshold value on the high side of the primary mode all low-level clouds were isolated. Location of sub-pixel clouds and cirrus is more difficult and had not been successfully accomplished at the time of this study. Early efforts to employ the procedures proposed by Saunders and Kriebel (1988) for cirrus clouds were not successful.

Calibration information provided by the FIS staff were applied to the individual spectral bands to convert the digital numbers to at-satellite observed radiance. In general, this is a linear equation with offset and gain terms. The offset term was determined from the space views that

the sensor collects during each scan. The gain was derived from the preflight bench calibration, although current FIFE research suggests that the gain characteristics of the sensor have varied since launch. The TIR sensor data were further treated for nonlinearity following NOAA procedures (Kidwell 1986).

Attenuation of spectral radiance between the surface and the satellite in the visible and near-infrared spectral bands was not addressed in this analysis. The variability this introduces, particularly as a function of view angle is significant. At first order the computation of an index, such as the normalized difference vegetation index (NDVI), adjusts for day-to-day variations in overall radiant flux. However, the differential effects of scattering, that predominate in the visible band, and water vapor absorptance, which dominate in the near infrared band, introduce a bias in the NDVI which is a strong function of view angle. Unfortunately, this bias is convoluted with varying pixel size (area averaging) and anisotropy in surface exitance which makes simple empirical normalization of this effect rather difficult.

Accounting for atmospheric attenuation in the thermal infrared was somewhat easier. The split-window technique of Price (1984) was adopted for this study. This technique is premised on the surface being a "black-body" emitter. Fortunately the FIFE investigators conducted an extensive survey of surface emissivity at the Konza and found that this region has an emissivity close to one (Pallaconi 1988). The Price (1984) approach was therefore considered to be applicable to derivation of surface temperature form the NOAA-9 AVHRR data from the FIFE region.

4.3.3 Results and discussion

Based on the criteria that cloud cover over the FIFE region was less than fifty percent, 12 of the 32 days processed in this analysis were found to have acceptable observing conditions. Cloud cover during these twelve days varied, based on a visual assessment, between 0% and 35% (Figure 4.3).

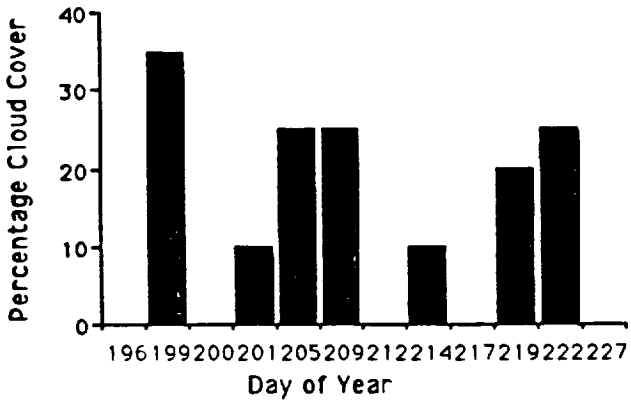

Figure 4.3: Visually assessed percentage cloud cover in AVHRR observations (Goward and Hope 1989).

After the data were co-registered and radiometrically processed a uniformally spaced, 10 by 20 (200) sample of the NDVI and T_S measurements were extracted from the data. If cloud was present at the sample location, the measurements from that location were excluded from the sample. The expected strong relation between NDVI and T_S was consistently observed on every day (Figure 4.4).

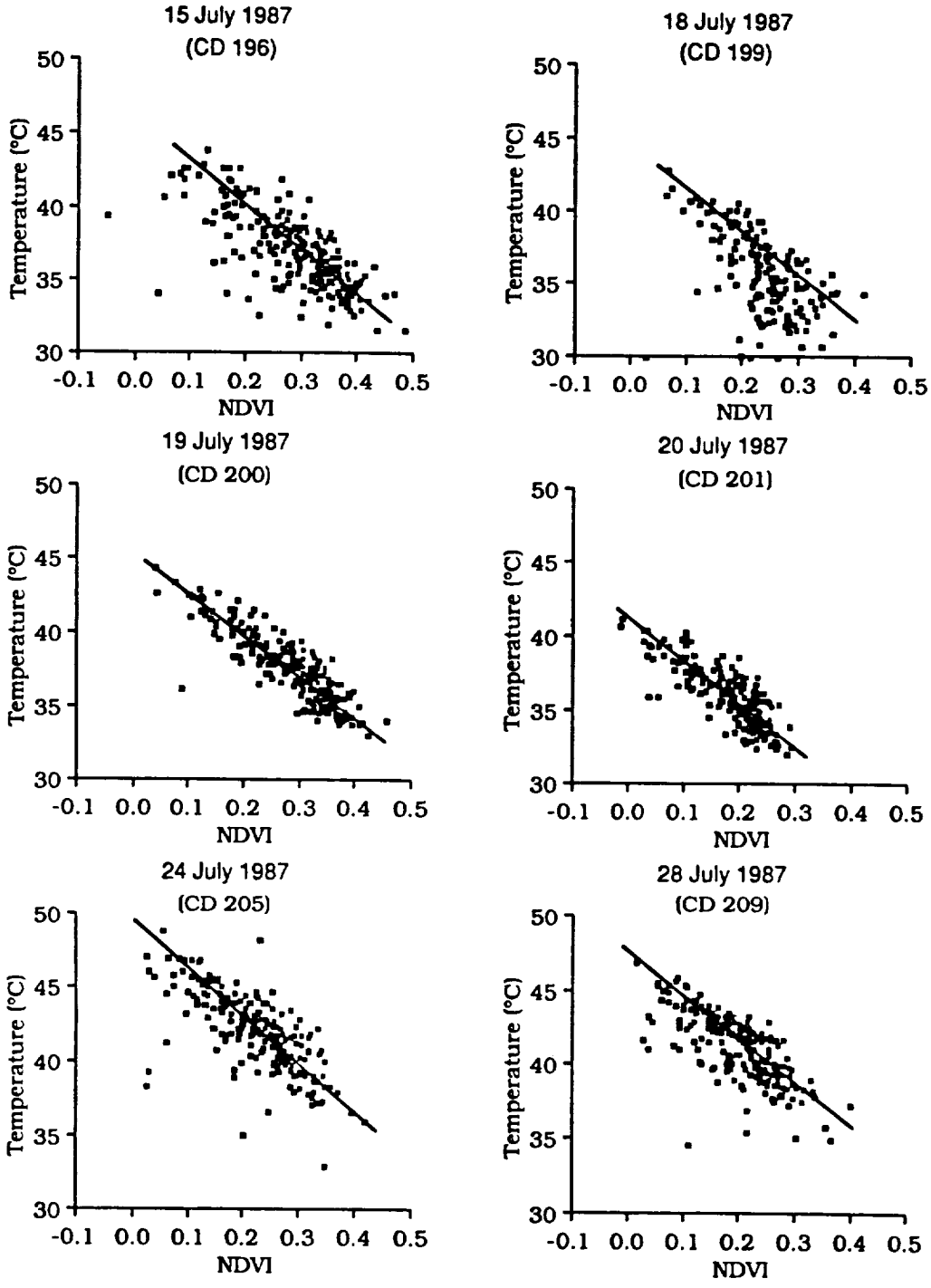
15 July 1987
(CD 196)
18 July 1987
(CD 199)
19 July 1987
(CD 200)
20 July 1987
(CD 201)
24 July 1987
(CD 205)
28 July 1987
(CD 209)
Temperature (°C)
NDVI
50
45
40
35
30
-0.1
0.0
0.1
0.2
0.3
0.4
0.5

Figure 4.4 .....

Figure 4.4 .....

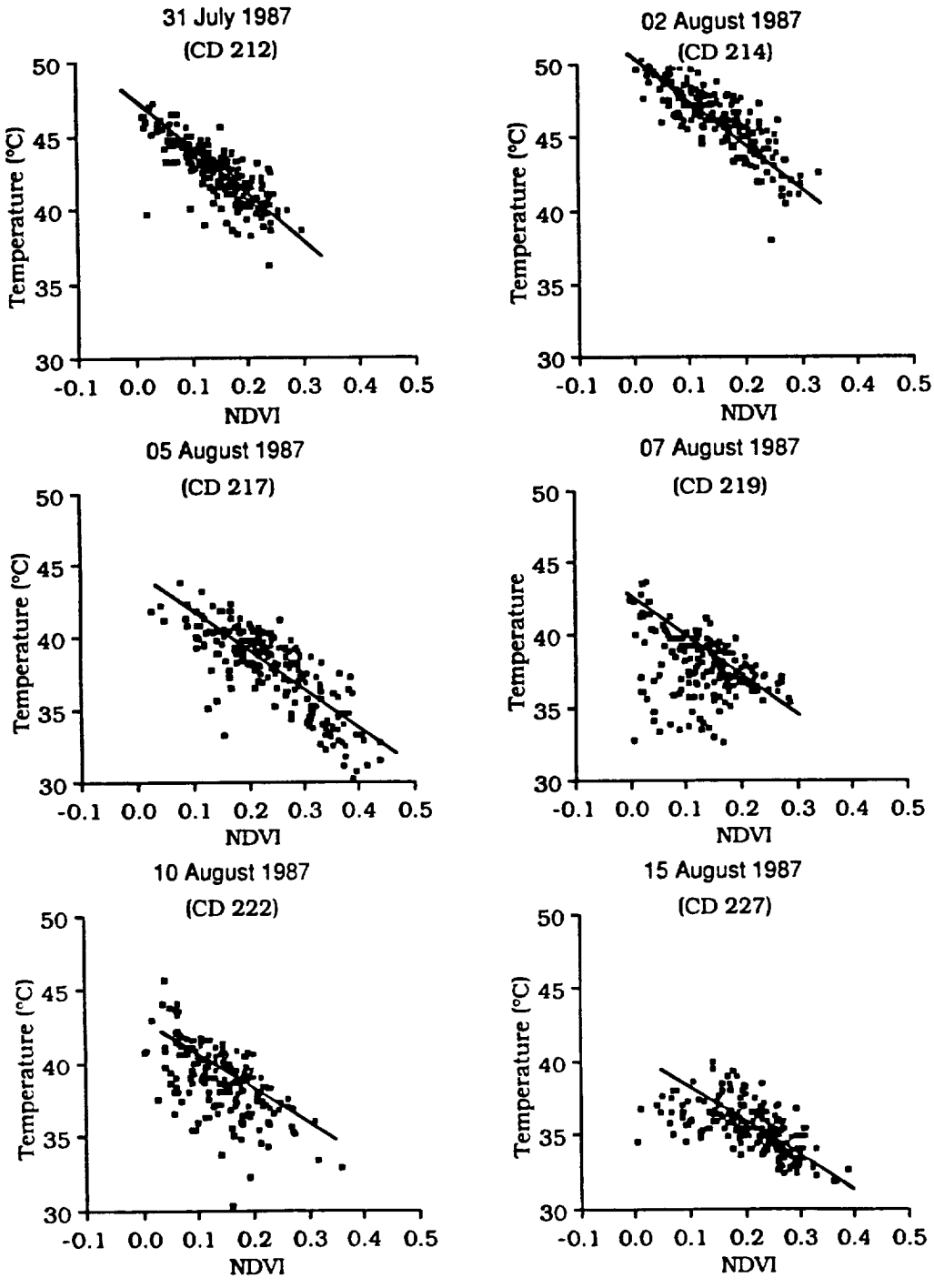

Figure 4.4: Observed relation between the T_s and NDVI on 12 selected dates in 1987 (Goward and Hope 1989).

The satellite-observed NDVI values typically ranged between 0.0 and 0.4 across the entire region whereas the helicopter-measured NDVI for the FIFE site varied between 0.3 and 0.8 (see Chapter 2). The range and magnitude of NDVI values from the FIFE region also appeared to vary with view angle as would be expected (see Figure 4.5 for view zenith angles).

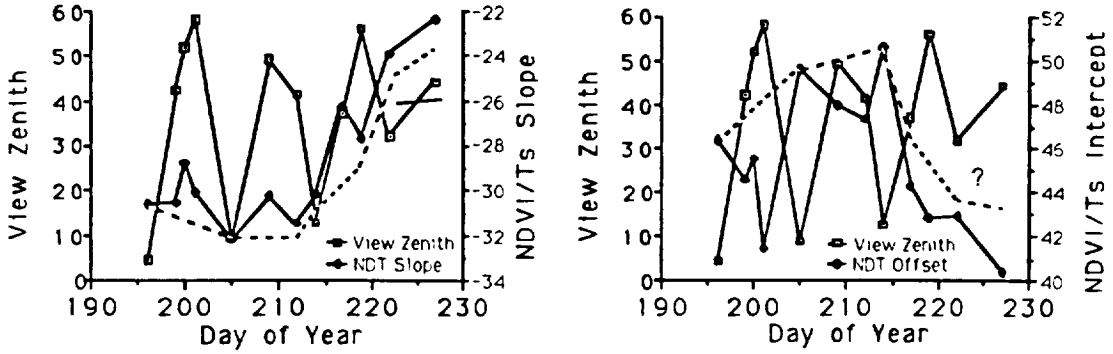

Figure 4.5: Slope and intercept of T_S-NDVI relationship compared to sensor view zenith angle. Dashed line is the variation in the relationship that was expected after atmospheric attenuation and other factors were removed (Goward and Hope 1989).

The observed patterns in the NDVI values clearly illustrated the need to account for atmospheric attenuation when using satellite data to extract surface features. The range of surface temperatures (30°C to 50°C) appears to be close to observed ground temperatures at the FIFE site.

The T_S-NDVI plots display increased scatter on cloudy days (199, 205, 209, 219, and 222) which suggests that the cloud screening approach used here was only partially successful. The increased scatter on these days appeared to be the result of including pixels that are either partially cloud covered or obscured with cirrus.

Because of residual clouds, a statistical fit of the central axis of the T_S-NDVI relationship was not possible. As an alternative, a visual "best-fit" line was located on each plot. Note that particularly on days 199, 209, 219 and 222, this line is plotted in the upper portion of the distribution. This was done based on the notion that cloud contamination will reduce both the NDVI and T_S and therefore the clear view pixels are located in the highest portion of the plot.

The slope and intercept of the observed T_S-NDVI relationship were compared to the sensor view zenith (Figure 4.5) to isolate variations in the relationship which may have been diagnostic of changes in ground conditions from changes that occurred as a result of variable view zenith. The variability in the T_S-NDVI relationship that were introduced by variations in view zenith is clearly illustrated in Figure 4.5.

On three days (196, 205 and 214) during the dry down cycle the NOAA-9 AVHRR collected near-nadir ($<10^o$ view zenith) afternoon observations of the FIFE region. The variation in the T_S-NDVI relationship observed on these days appeared to co-vary with surface moisture conditions. The intercept of the T_S-NDVI increased from 46 ^oC to 50 ^oC between July 15 (196) and August 2 (214). The slope first increased (196 to 205) from 30.5 ^oC/NDVI to -32 ^oC/NDVI and then decreased (205 to 214) to -30.0 ^oC/NDVI. Both intercept and slope decreased substantially following day 205, although no additional near-nadir views were available in this 32 day period to confirm the magnitude of the decrease. A dashed line, connecting days 196 and 214 and visually extrapolated passed that point, was constructed as a first estimate of the "expected" variation of this relation that will be found in atmospherically adjusted data. This first look at the AVHRR observations, taken during a major dry-down cycle

at the Konza Prairie, suggested that the Ts-NDVI relation is diagnostic of surface Bowen ration conditions.

4.3.4 Conclusions

The dry-down of the FIFE region which occurred between July 9, 1987 and August 4, 1987 was observed in the T_S-NDVI relationship as an overall heating of the land surface. Following rainfall, the relationship recorded a cooling of the surface. The observed change in the slope of the relation was less dramatic but may have been related to variable surface resistance to evaporation over this time period.

5. LOCAL SCALE MODELING OF LE FLUXES AND T_S

5.1 Introduction

The early phases of this research project were characterized by empirical studies which attempted to establish links between the T_S-NDVI relationship and surface characteristics (e.g., soil moisture) and fluxes. As the project matured, more attention was directed at investigating the T_S-NDVI relationship with the aid of a soil-plant-atmosphere (SPA) model. As mentioned in Chapter 1, the Tergra model (Soer 1977) was considered appropriate for the modeling tasks but required modification to include a SVI. The model was used initially to determine the sensitivity of the T_S-NDVI relationship to variations in station characteristics such as soil moisture, insolation and vegetation height. However, as the empirical studies progressed the project underwent a philosophical shift and the simulation modeling took on a more central role

The preceding empirical studies revealed the difficulty of relating the T_S-NDVI regression slope to LE because land cover type and anthropogenic treatment of the vegetation were first order factors affecting the regression characteristics. This finding was not restricted to the local scale analyses but was also observed using a regional data set (AVHRR). The approach of using combined T_S and SVI data to predict LE directly was reevaluated in the light of these results and findings from other FIFE investigations. Consequently, integrating the SVI and T_S observations into the SPA model (Tergra) and estimating the heat fluxes using this model became the focus of the investigation. Other investigators were also moving in this direction and similar approaches

were adopted by Price (1990), and to a lesser extent Nemani (1989) to include SVIs and T_S in LE simulation models. Price (1990) used the T_S-NDVI scatterplot to determine fractional vegetation cover components (bare soil and vegetation) to help in the calibration of an energy balance model. Nemani (1989) used a T_S-SVI relationship based on AVHRR data to determine canopy resistance in a SPA model.

Modifications to the Tergra model described in this chapter provided a means for simulating the T_S-NDVI relationship under a variety of conditions. The modifications to Tergra drew on the findings of other FIFE investigators and were intended to fully exploit all appropriate data collected during the FIFE field seasons.

5.2 The Original Tergra Model and Applications

Models that simulate the flows of water and energy through the soil-plant-atmosphere (SPA) system are generally complex, requiring numerous parameters or data inputs. However, these physically based models have been useful in helping to understand the functioning of the SPA system and have also been used to interpret remotely sensed observations affected by the surface energy budget (Soer 1977; Carlson et al. 1981; Choudhury and Idso 1985; Choudhury et al. 1986; Hope et al. 1988; Nemani and Running 1989).

The Tergra model, which was developed by Soer (1977), is a steady state resistance model structured so that the soil, plant, stomatal, and atmospheric resistances are in series. Under defined meteorological regimes and an initial soil moisture condition, the Tergra model simulates the daily course of actual transpiration, net radiation, sensible heat flux,

ground heat flux, canopy temperature and soil moisture. Tergra has been tested extensively in Europe by authors such as Soer (1977), Nieuwenhuis and Klaasen (1978) and Nieuwenhuis et al. (1985), who found the model to be a good predictor of latent heat fluxes from grasslands when transpiration is the the dominant source of evaporative fluxes. Since the Tergra model also simulates canopy temperature, the model has been used in conjunction with remotely sensed surface temperature to determine spatial distributions of LE and soil moisture (Soer 1980)

The original Tergra model (Tergra-1) was developed specifically for use on grasslands and is described in detail by Soer (1977, 1980 #143). The arrangement of the soil, plant, canopy and atmospheric resistances for water and heat transport through the SPA system is illustrated in Figure 5.1. Boundary conditions are the soil temperature and moisture pressure at a reference level, energy balance at the crop surface, and temperature and vapor pressure at a reference level in the atmosphere. Besides the plant and soil parameters, the basic input data are air temperature, vapor pressure, and wind speed (all measured at a reference level in the atmosphere), and the incident solar radiation or net radiation.

The use of Tergra-1 in this project was limited because the model could not relate T_S to the NDVI. However, it was used to support some of the empirical analyses that investigated the effect of terrain and solar radiation differences on T_S. Figure 5.2 illustrates the difference between T_S of a horizontal grassland surface and that of a number of different slopes and aspects. The differences are plotted against changes in canopy height which, during this initial investigation, were assumed to be synonymous with differences in the NDVI.

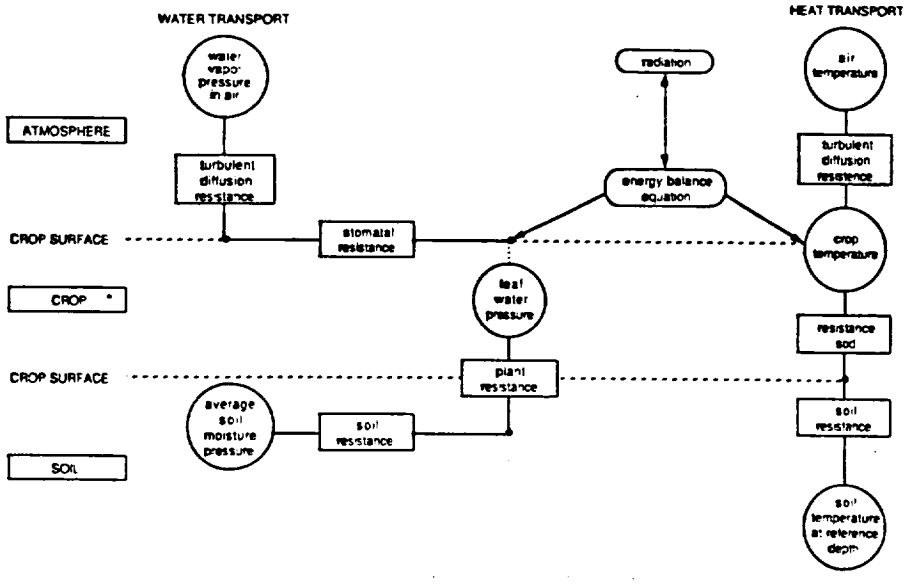

Figure 5.1: Arrangement of soil, plant and atmospheric resistances in the Tergra model (Soer 1977).

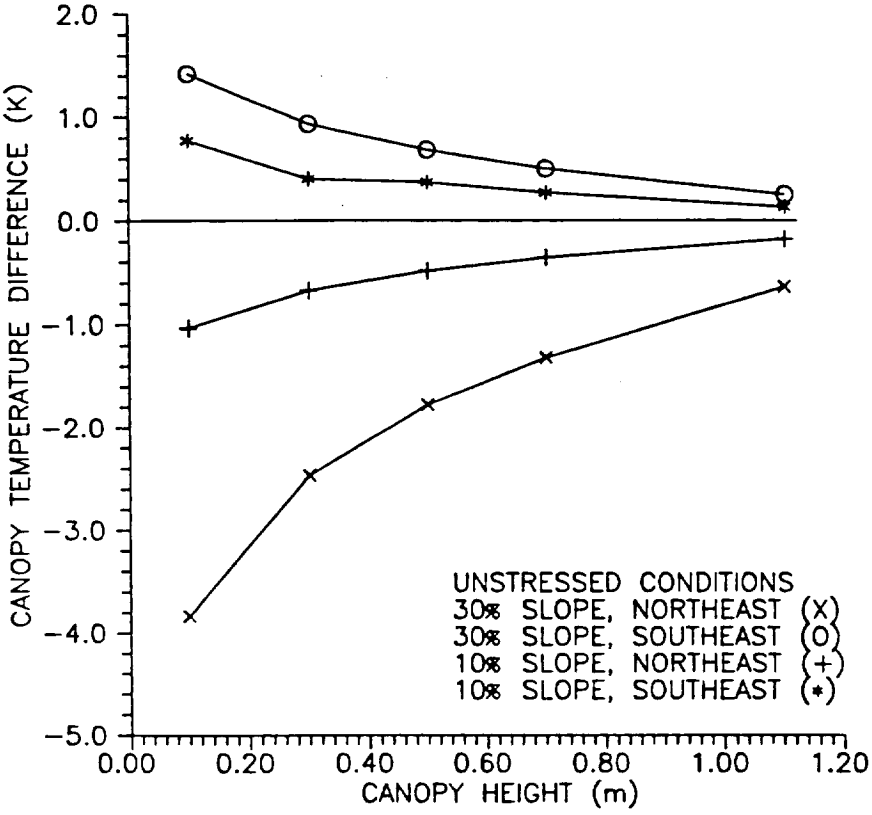

Figure 5.2: Difference between simulated grass canopy temperature on a horizontal surface and simulated values on four slope-aspect combinations. Simulations were conducted for a range of canopy heights.

The simulation results in Figure 5.2 were obtained using meteorological and soil moisture inputs for June 6, 1987 at 1545 CDT (time of the NS001 overflight). Since most of the slopes in the FIFE site are less than 10% and canopy heights generally ranged between 30 and 60 cm, differences in T_S due to terrain variability could not be expected to exceed 1.5 K over most of the area. This is probably less than the measurement error of the NS001 sensor. It should be noted, however, that Tergra does not account for soil background temperature and these differences could have been considerably larger than the canopy temperature differences.

5.3 A Modified Tergra Model

5.3.1 Background

In its original form, the Tergra model is not well suited to simulating LE over the Konza prairie owing to the empirical expressions used in the model to estimate canopy resistance. The research presented in this section reports on a number of modifications made to the canopy resistance component of the Tergra model. The accuracy of the modified model for predicting LE over the Konza prairie was evaluated using data from the FIFE.

5.3.2 The modified Tergra model (Tergra-2)

The canopy resistance component of Tergra-1 is based on the following expression for stomatal resistance (r_s) given by

Shawcroft (1973),

$$r_s = f(\Psi_L) + \frac{a}{K + b}, \qquad (5.1)$$

where a and b are empirical constants, K is the incoming solar radiation and Ψ_L is the leaf water potential of the canopy. Leaf water potential is calculated in the model. Based on observations made by Rijtema (1965), Soer (1977) concluded that leaf water potential had no effect on r_s when it was greater than -0.7 MPa. Two separate equations are presented by Soer (1977) to calculate r_s, one expression is used when Ψ_L is between -0.7 and -5 MPa and another when Ψ_L is equal to -5 MPa. The simulation of leaf water potential in Tergra-1 is thus bounded between -0.7 and -5 MPa. To account for variations in photosynthetically active vegetation and to convert r_s to canopy resistance (r_c), Soer (1977) arbitrarily assumed r_c to be inversely proportional to the square root of the height of the vegetation.

As stated previously, the empirical and arbitrary features of the canopy resistance formulation in Tergra-1 may result in significant errors in the simulation of LE when the vegetation canopy differs from that described by Soer (1977). Many of the grasses of the Konza prairie have evolved stomatal behavior to withstand periods of drought, and the mix of transpiring C_3 and C_4 plants varies both temporally and spatially (Reichman 1987). Barnes and Harrison (1982) have shown that there is a substantial difference in the relationship between stomatal conductance and leaf water potential of C_3 and C_4 grasses in a Nebraska prairie. While Soer (1977) and other investigators such as Choudhury and Idso (1985)

considered leaf water potential to be the primary factor that would increase the resistance of adequately illuminated stomata, Sellers et al. (1990) concluded that atmospheric vapor pressure deficit was a more important stress factor affecting the canopy resistance of Konza prairie vegetation. The most significant weakness of the canopy resistance component of Tergra-1 pertains to the "arbitrary" relationship between r_c and vegetation height. Although it is recognized that r_c will vary in relation to the amount of green vegetation at the surface, empirical relationships between remotely sensed indices of green vegetation amount and r_c would be preferable to this arbitrary approach.

To make the Tergra model more suitable for LE simulations over the Konza prairie, the canopy resistance component of the model was modified as follows:

(1) Minimum canopy resistance (r_{cm}), which is the resistance of the canopy when environmental factors do not induce stomatal closure, was calculated using a relationship between this resistance, a spectral vegetation index, and incident photosynthetically active radiation (K_{par}) (Sellers, Heiser et al. 1990).

(2) The closure of stomata in response to leaf water potential stress and the subsequent conversion of r_{cm} to r_c was based on a stress index described by Fisher et al. (1981).

(3) The relationship between r_c and leaf water potential was defined separately for C_3 and C_4 plants so that the modeled fluxes could be weighted according to the observed C_3:C_4 ratio.

(4) Vapor pressure deficit was included as an additional environmental factor that could increase canopy resistance (Sellers, Heiser et al. 1990).

Studies conducted by authors such as Sellers (1985), Hope et al.

(1986; 1988), and Hall et al. (1990) have demonstrated, both theoretically and empirically, that there is a well-defined relationship between r_{cm} and spectral vegetation indices that combine remotely sensed red and infrared radiances. Sellers et al. (1990) used data collected as part of the FIFE to determine the unstressed canopy conductance ($1/r_{cm}$) at individual flux measurement sites. They found unstressed canopy conductance (g^*_c) to be linearly related to K_{par}, and the derivative of g^*_c with respect to K_{par} (dg^*_c/dK_{par}) was considered to be the slowly varying vegetation-dependent quantity that should be related to spectral vegetation indices. Sellers et al. (1990) examined the relationship between this derivative and the simple ratio (SR) spectral vegetation index (near-infrared radiance/red radiance) calculated from Thematic Mapper data. The relationship was found to be linear, and the intercept of the linear least squares regression line was close to zero. Therefore, if K_{par} and SR are known, g^*_c can be determined from this relationship. The calculation of r_{cm} in the modified model (Tergra-2) uses this approach, substituting the normalized difference vegetation index (NDVI) for the SR. The relationship between these indices is then given by

$$NDVI = (SR - 1)/(SR + 1) . \qquad (5.2)$$

The conversion of r_{cm} to r_c in Tergra-2 follows the approach presented by Jarvis (1976) and employed by Choudhury and Idso (1985), Hope et al. (1986), and others. Dimensionless stress factors (S) are calculated to describe the effects of leaf water potential and vapor pressure deficit on stomatal opening. These stress factors can range from close to zero (maximum effect on stomatal closure) to unity (no effect on stomatal

closure), and r_c is obtained from

$$r_c = r_{cm}/S \ . \qquad (5.3)$$

The extent of the interactions between stress factors is uncertain (Jarvis 1976). Feedbacks between leaf water potential and atmospheric vapor pressure deficit could not be represented in the model, which was structured to only include the most restricting factor in the calculation of r_c.

The relationship between stomatal conductance and leaf water potential of well illuminated leaves of prairie grasses (C_3 and C_4) has been presented by Barnes and Harrison (1982) and Polley et al. (1992). Fisher et al. (1981) and Choudhury and Idso (1985) have demonstrated that the relationship between these two variables may be described by the following expression:

$$1/r_c = \frac{d_1}{1 + (\Psi_L/d_2)^{d_3}} \ , \qquad (5.4)$$

where d_1, d_2 and, d_3 are model parameters. By scaling the conductances to the maximum observed value, d_1 in (5.4) becomes 1.0 and the dimensionless stress factor for leaf water potential (S_l) is obtained from

$$S_l = \frac{1}{1 + (\Psi_L/d_2)^{d_3}} \ . \qquad (5.5)$$

The dimensionless stress factor for vapor pressure deficit given by Sellers et al. (1990) for the Konza prairie is of the form

$$S_v = 1 - d_4 \, VPD \quad , \qquad (5.6)$$

where S_v is the vapor pressure deficit stress factor, d_4 is a model parameter and VPD is the vapor pressure deficit between the vapor pressure of the atmosphere and the saturated vapor pressure at T_s.

5.3.3. Experimental goals and methodology

The experimental goal of this study was to simulate LE fluxes at four FIFE flux measurement sites using Tergra-2 and then to evaluate the simulation accuracy of the model. For comparative purposes, LE was also modeled using Terga-1. The four selected experimental sites represented different topographical positions and management treatments (burnt versus unburnt). The models simulated LE over three periods having a range of soil moisture conditions. Each simulation period started at least 3 days after a rainfall event so that evaporation from soil surfaces would be minimized. The sites used in this experiment, their soil series and soil depth, topographical position and management treatment they represented during FIFE 1987 and FIFE 1989 are summarized in Tables 5.1 and 5.2. The three test periods and the corresponding initial soil water potential at each of the sites are listed in Table 5.3.

Table 5.1: Characteristics of the four experimental flux measurement stations in 1987.

	Station			
	02 (1916-BRS)	08 (3129-BRK)	36 (2655-BRL)	44 (2043-BRL)
Soil series	Dwight	Tulley	Dwight	Tulley
Soil depth, cm	30	14	19	25
Position/aspect	B	E	NE	T
Treatment	Bt	Bt	Ut	Bt

All slopes were moderate (3° - 8°). B=Bottomland, T=Ridgetop, E=East, N=North, NE=North-East, Bt=Burnt,Ut=Unburnt.

Table 5.2: Characteristics of the four experimental flux measurement sites in 1989.

	Station			
	902 (1916-BRK)	908 (2330-BRK)	936 (2655-BRL)	944 (1942-BRL)
Soil series	Dwight	Tulley	Dwight	Tulley
Soil depth, cm	30	14	19	21
Position/aspect	N	E	E	T
Treatment	Bt	Bt	Ut	Ut

All slopes were moderate (3° to 8°). B=Bottomland, T=Ridgetop, E=East, N=North, NE=North-East, Bt=Burnt,Ut=Unburnt

Table 5.3: Simulation periods, NDVI, mean canopy height, ratio of C_3 to C_4 plants and initial soil water potential at 10 cm depth for each station

Station	Period	NDVI	Mean Canopy height (cm)	C_3:C_4	Soil Water Potential (kPa)
02 (1916-BRS)	June 4 - 6, 1987	0.435	34.3	0.77:0.23	-130
08 (3129-BRK)	June 4 - 6, 1987	0.667	37.8	0.22:0.78	-53
36 (2655-BRL)	June 4 - 6, 1987	0.544	26.5	0.57:0.43	-83
44 (2043-BRL)	June 4 - 6, 1987	0.606	38.2	0.73:0.27	-137
02 (1916-BRS)	Aug. 15 - 17, 1987	0.437	31.0	0.52:0.48	-80
08 (3129-BRK)	Aug. 15 - 17, 1987	0.534	38.2	0.18:0.82	-30
36 (2655-BRL)	Aug. 15 - 17, 1987	0.280	27.6	0.64:0.36	-67
44 (2043-BRL)	Aug. 15 - 17, 1987	0.442	47.6	0.47:0.53	-89
902 (1916-BRK)	Aug. 3 - 4, 1989	0.362	25.0	0.52:0.48	-1016
908 (2330-BRK)	Aug. 3 - 4, 1989	0.663	45.0	0.18:0.82	-794
936 (2655-BRL)	Aug. 4, 1989	0.317	22.0	0.64:0.36	-94
944 (1942-BRL)	8/4/89	0.267	7.0	0.47:0.53	-698

Most of the data used in this experiment were obtained from the FIFE Information System (FIS). Meteorological input data (incident shortwave radiation, net radiation, air temperature, vapor pressure and wind speed), and the observed LE were available as 30-min averages so the models were set to simulate LE for this time interval. Net radiation can be either a model input or simulated in a subroutine of Tergra. Since the accuracy

of this sub-component of the model can be tested independently, the models were executed with net radiation as an input.

The relationship between dg^*_c/dK_{par} and a spectral vegetation index given by Sellers et al. (1990) had limited utility for this study since these investigators used Thematic Mapper data to derive the spectral vegetation index. Owing to the lack of temporal coverage provided by the Thematic Mapper platform, the relationship between the derivatives calculated by Sellers et al. (1990) and the NDVI was redetermined using red and near-infrared radiance data collected with a Barnes modular multiband radiometer (MMR) mounted on a helicopter. These helicopter data were collected at an altitude of approximately 200 m and the relationship between dg^*_c/dK_{par} and the helicopter NDVI is given in Figure 5.3.

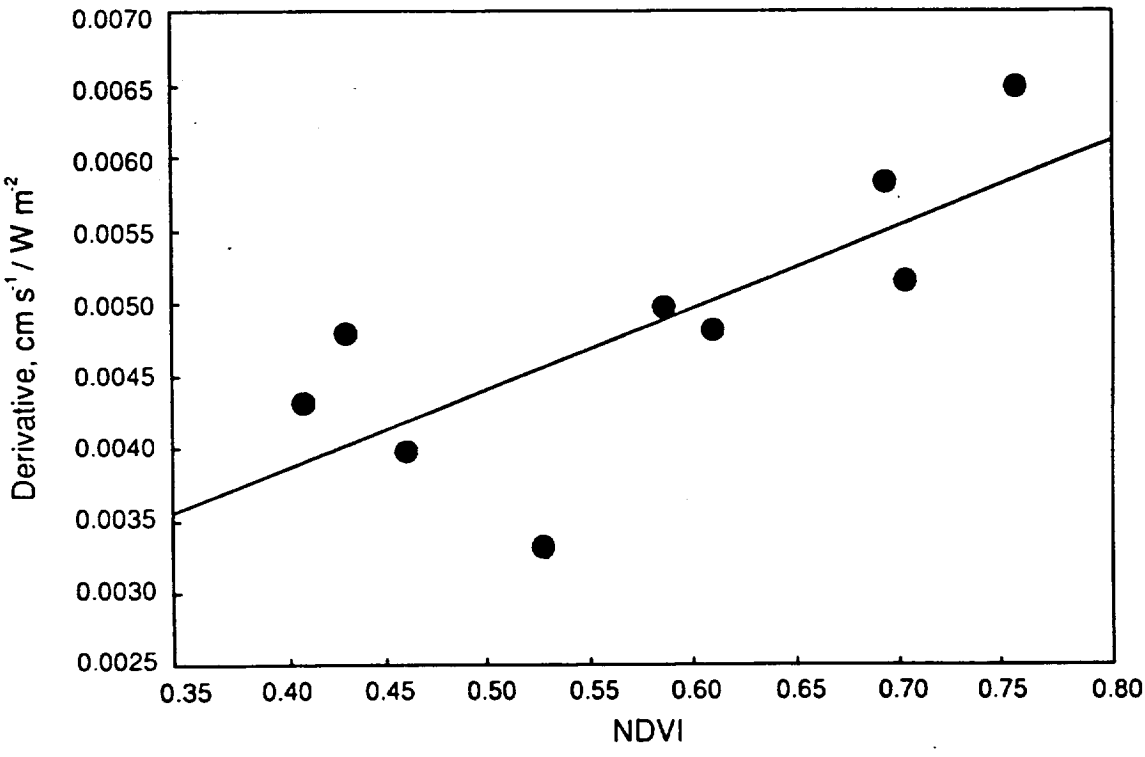

Figure 5.3: Relationship between the derivative of g^*_c with respect to K_{par} and the NDVI calculated using MMR data collected from a helicopter.

Although the available data set was limited, there is a reasonable agreement between the derivative and the NDVI, with one observation appearing to be an outlier. Fifty-seven percent of the variance in the derivative is attributable to the NDVI when all the data points are considered; this figure increases to 72% if the single outlier is removed. The regression of dg^*_c/dK_{par} on the NDVI produced the expression

$$D = 0.004991\ NDVI + 0.002121\ , \qquad (5.7)$$

where $D = dg^*_c/dK_{par}$ (cm s^{-1}/W m^{-2}).

Helicopter data used to determine the NDVI for Tergra-2 simulations were collected over the experimental flux measurement sites in 1987 and 1989 at least once during each study period. Approximately 30 observations were made at each station, and the mean NDVI from these observations was used to determine dg^*_c/dK_{par} (Equation 5.7). The incident photosynthetically active radiation used to convert the derivative to maximum canopy conductance and then r_{cm} was assumed to be a constant fraction (0.51) of the incident shortwave radiation.

Plant resistance (the sum of root epidermis resistance and plant hydraulic resistance) used in the Tergra simulations was determined using the procedure described by Soer (1977), whereas the rooting depth of the vegetation was assumed to be equal to the soil depth measured at each station. Data for determining the relationship between leaf conductance and leaf water potential for C_3 and C_4 prairie grasses were obtained from Barnes and Harrison (1982) and Polley et al. (1992) respectively. These data were used in a least squares fitting routine to determine the constants in Equation 5.5, which defines the stress factor for leaf water

potential. The values of d_2 and d_3 for C_3 plants were -2.8 MPa and 1.44 respectively while for C_4 plants, the respective values of d_2 and d_3 were -7.5 MPa and 4.8. The constant, d_4, required in Equation 5.6 to calculate the vapor pressure deficit stress factor, was given by Sellers et al. (1990) as 0.02645 kPa for the Konza prairie.

The relationship between soil water potential and soil water content in Tergra is described by a relationship developed by Laliberte et al. (1968). Soil water retention data for the Dwight and Tulley soil series were obtained from the FIS, and an algorithm presented by Huygen (1978) was used to determine the retention curve parameters. The data obtained from the FIS were based on soil samples collected at a depth of 10 cm. This was considered to be the appropriate depth for use in the model, since the roots of the Konza grasses concentrate near the soil surface (Reichman 1987). Wetzel and Chang (1987) also concluded that the top 10 cm of soils generally contains over 50% of the root mass of most natural vegetation. The heat conductivity of the soils was determined using the procedure described by De Vries (1975) and adopted by Soer (1977).

Model performance was evaluated using the root-mean-square error as a measure of agreement between observed and estimated LE for the period of simulation. Plots of observed and estimated LE over time were also examined visually to determine the nature of any disagreement between observed and modeled values.

5.3.4. Results

The root-mean-square (rms) errors for simulated LE during daylight hours for both Tergra-1 and Tergra-2 are listed in Table 5.4 for each station and study period, and the corresponding plots of observed versus estimated LE for Tergra-2 are given in Figures 5.4, 5.5 and 5.6.

Table 5.4: Root-mean-square error for Tergra-1 and Tergra-2 simulations for three periods during FIFE

	Station	Tergra-1	Tergra-2
June 1987	02 (1916-BRS)	100.38	40.84
	08 (3129-BRK)	85.87	37.45
	36 (2655-BRL)	85.77	46.37
	44 (2043-BRL)	79.23	43.19
August 1987	02 (1916-BRS)	166.36	63.01
	08 (3129-BRK)	141.82	48.31
	36 (2655-BRL)	145.58	43.70
	44 (2043-BRL)	120.03	56.23
August 1989	902 (1916-BRK)	68.82	67.98
	908 (2330-BRK)	79.46	107.36
	936 (2655-BRL)	108.68	62.82
	944 (1942-BRL)	75.41	98.42

Root-mean-square errors are given in watts per square meter.

In all but two cases, Tergra-2 simulations were more accurate than those of Tergra-1 (Table 5.4). The exceptions occurred in August 1989 at station 908 and 944. For one test in August 1989 at station 902 (1916-BRK), the two models had almost the same rms errors.

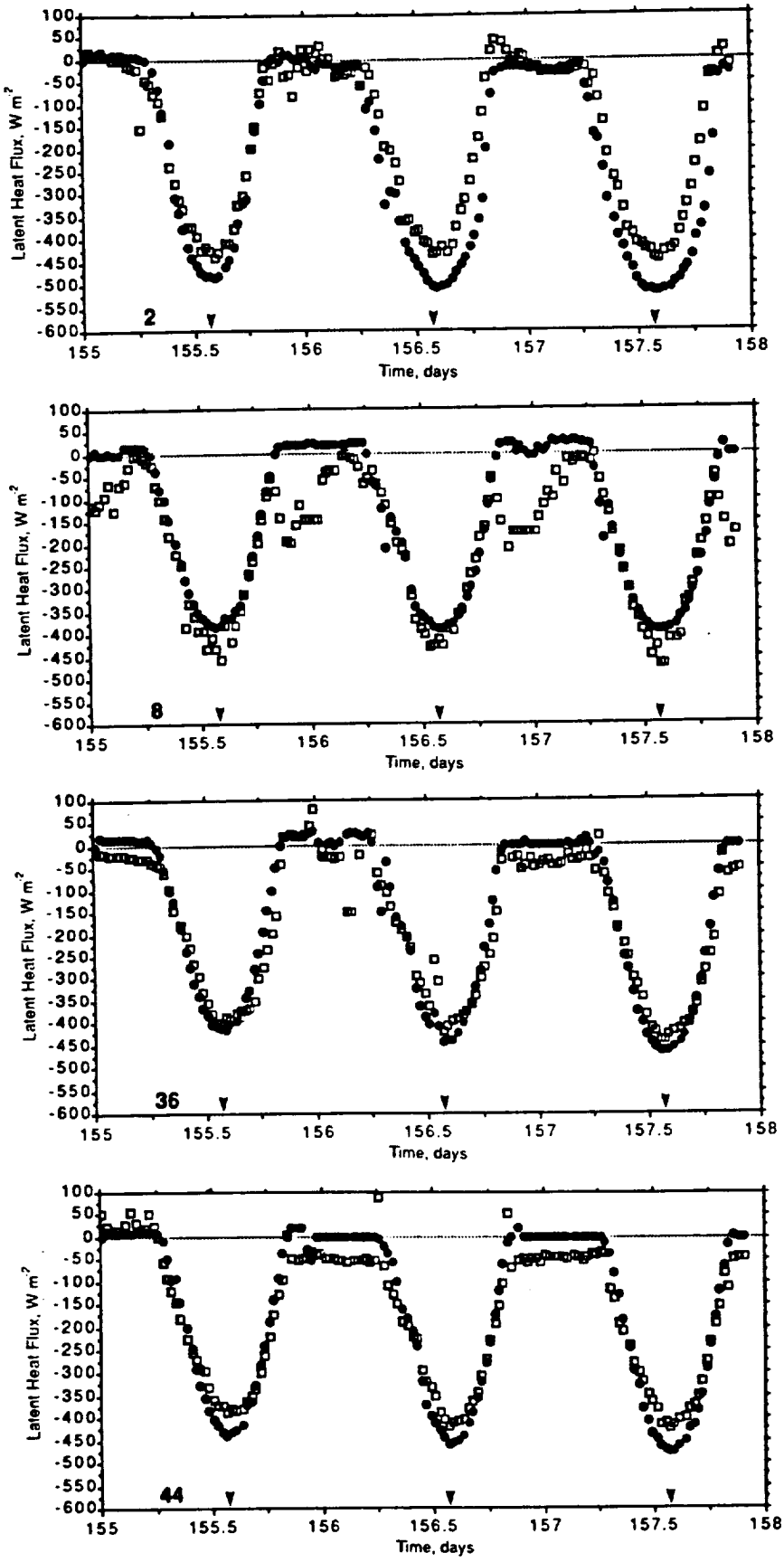

Figure 5.4: Observed LE (squares) and Tergra-2 estimated LE (circles) for the period June 4 - 6, 1987 (days 155 - 157).

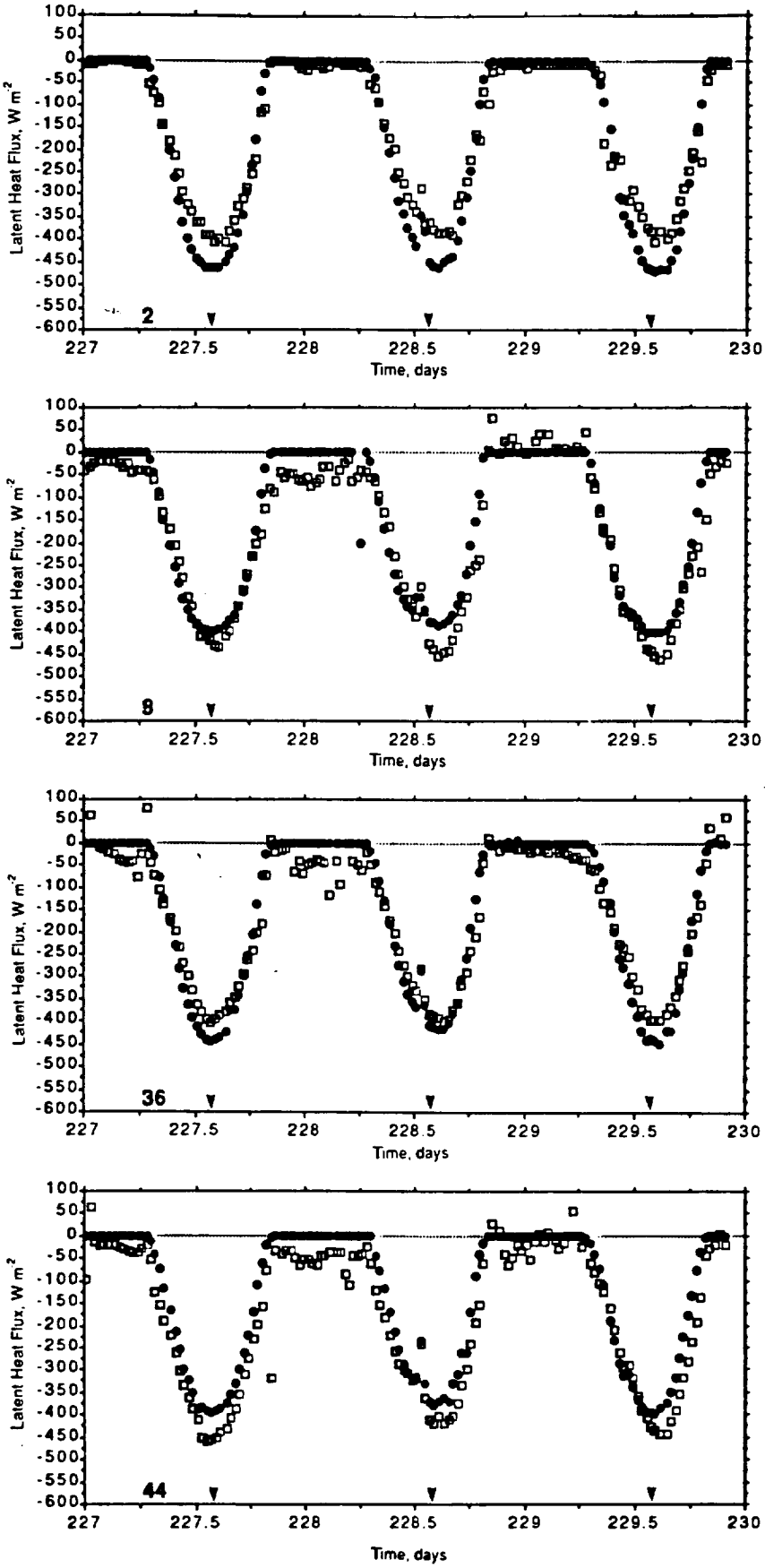

Figure 5.5: Observed LE (squares) and Tergra-2 estimated LE (circles) for the period August 15 - 17, 1987 (days 227 - 229).

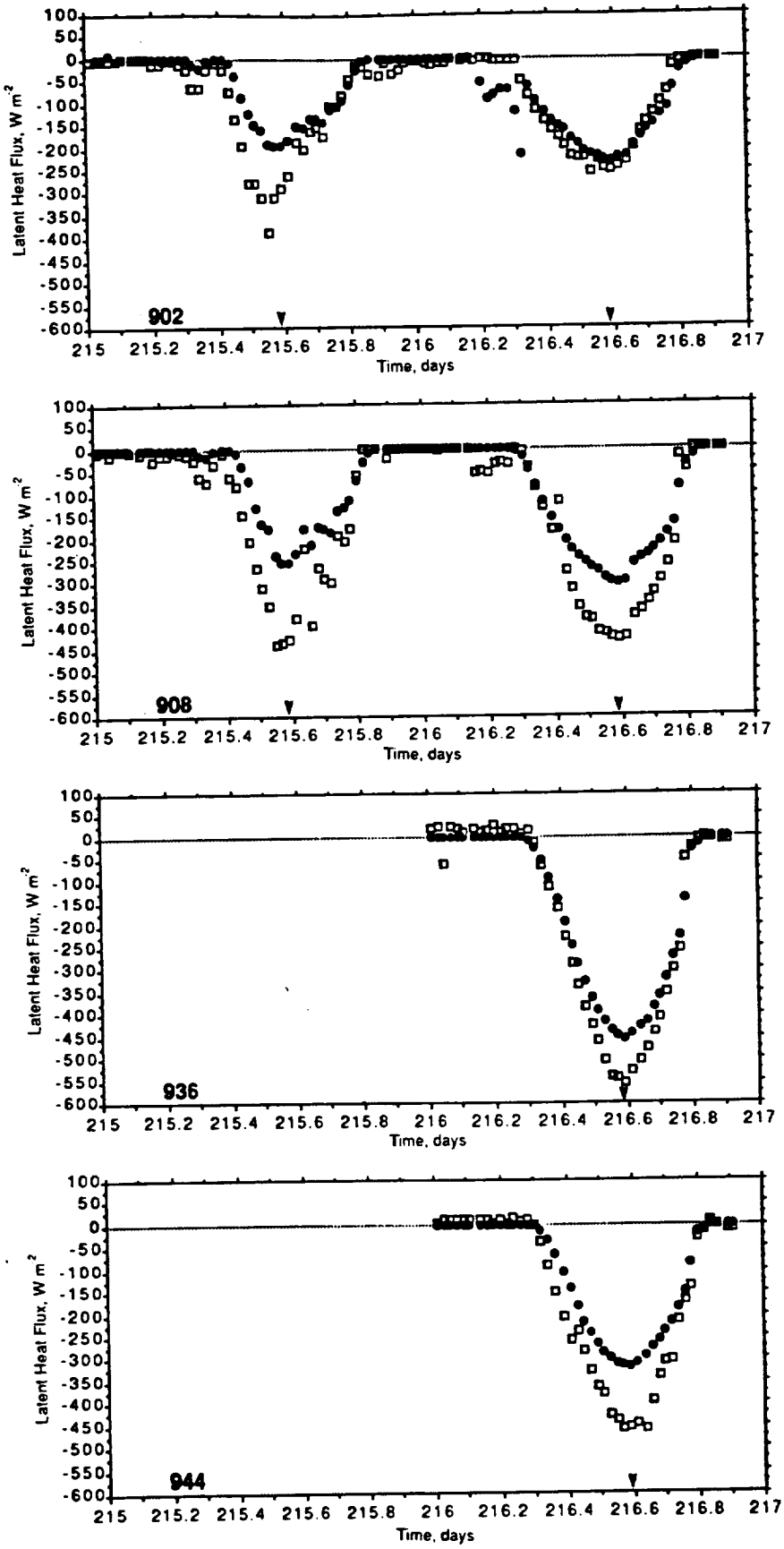

Figure 5.6: Observed LE (squares) and Tergra-2 estimated LE (circles) for the period August 3 - 4, 1989 (days 215 - 216). Data were available only for day 216 at sites 936 and 944.

C-2

Tergra-2 estimates of LE during the two 1987 periods were more accurate than those of the 1989 period at each flux station. Soil water potentials during 1989 were substantially lower than those observed in 1987 (Table 5.3). While the rms error ranged between 37 and 63 W m^{-2} for the two wetter periods, the rms error for the 1989 simulations ranged between 62 and 107 W m^{-2} (Table 5.4). Some of the smallest rms error values for Tergra-1 were observed using the 1989 data. As will be discussed later, this may not have reflected a superior representation of conditions at this time period by Tergra-1, but may be attributable to compensating errors.

An examination of the daily course of modeled and observed LE for the two 1987 periods (Figures 5.4 and 5.5) reveals that most of the Tergra-2 model error tended to be associated with simulations close to solar noon. A consistent overestimation/underestimation of LE at this time was not discernable in an intersite comparison of the model results. In contrast, Tergra-1 consistently overestimated LE and this overestimation was not confined to the midday period. This result could be expected, since Tergra-1 includes a leaf water potential adjustment of r_c that is specific only to C_3 plants. Stomatal closure of the Konza prairie C_4 plants and the associated reduction in transpiration would be initiated at a higher leaf water potential than the corresponding value defined in Tergra-1.

In the results presented in Figures 5.4 and 5.5 there was no evidence of a decrease in Tergra-2 accuracy as simulations progressed from the soil moisture conditions defined at the start of each simulation period. It would, however, be necessary to conduct tests of the model over more extensive time periods to establish whether the soil moisture budgeting and model accuracy were stable over time.

The diurnal patterns of estimated LE using Tergra-1 for sites 908 and 944 in 1989 are given in Figure 5.7.

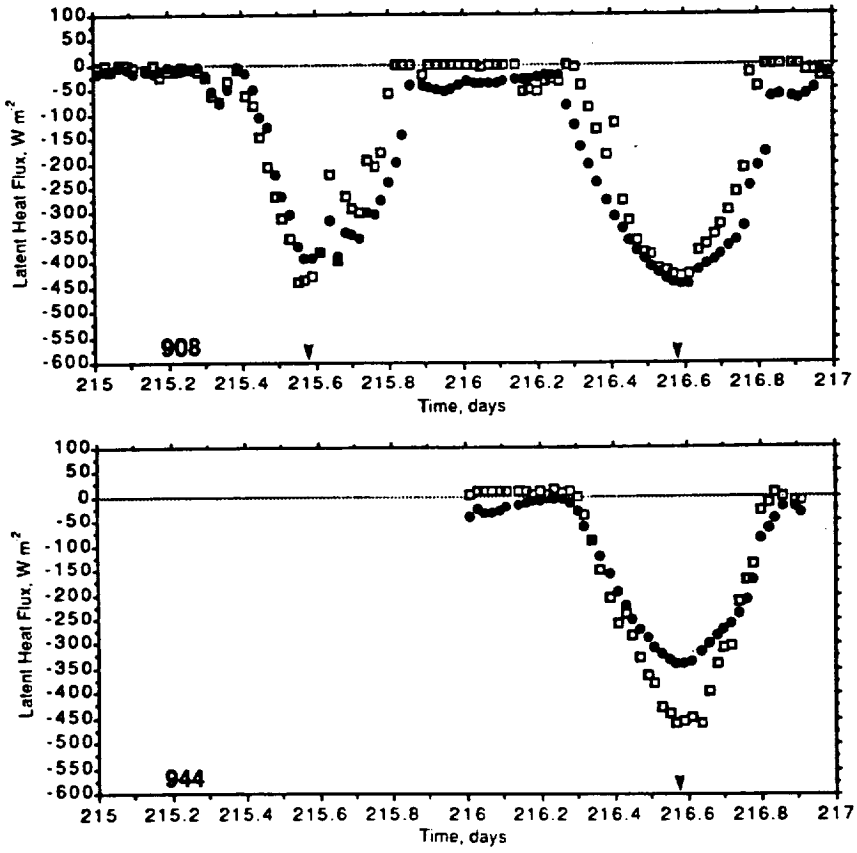

Figure 5.7: Observed LE (squares) and Tergra-1 estimated (circles) LE for sites 908 and 944 for the August 1989 simulation period.

Tergra-1 rms error values for these tests were notably smaller than those obtained using Tergra-2. Comparing the results for the corresponding sites using Tergra-2 (Figure 5.6), the most notable difference between the estimates from the two models occurred at station 908. Tergra-1 estimates of LE were close to the observed values on both simulation days

for periods close to solar noon. The characteristic overestimation of LE by Tergra-1 was still evident for simulated fluxes at times other than the midday period. Estimates of LE using Tergra-2 at station 908 were consistently less than the observed fluxes, except for the period up until mid-morning and the period after mid-afternoon on the second simulation day (day 216).

The location of sites 908 and 944 in 1989 were close to the locations of sites 8 and 44 in 1987. Comparing observed LE values in August 1987 with those observed in August 1989 at these sites, it is apparent that there were similar magnitudes of LE at both times despite large differences in soil water potential. The differences in fluxes at midday were less than 25 W m^{-2} for both locations. At station 8 (908) the soil water potential was -30 kPa in 1987 and -794 kPa in 1989 and at station 44 (944) the corresponding soil water potentials were -89 kPa and -698 kPa (Table 5.3). It would be expected that LE at the two sites for the August 1989 period would be substantially less than that which was observed. Since the soil moisture used in the model simulations was measured at a depth of 10 cm, it may be argued that the plants were responding to soil moisture conditions deeper in the soil profile. Jarvis (1989) concluded that as stress sets in close to the soil surface, the location of peak water uptake by plants shifts steadily down the soil profile. Alternatively, there may have been local sources of LE that were not responding to the average soil water content used in the model calculations.

If it is assumed that the soil water potential or the parameterization of the soils for this station was incorrect in the direction of greater soil water stress, then the exclusively C_3 parameterization of the leaf water

potential stress index in Tergra-1 would tend to compensate for the reduction in LE. It is notable that station 908 had the lowest ratio of C_3:C_4 plants (0.18:0.82) of any of the sites at any of the three time periods (Table 5.3). Thus, if soil water stress was greater than it should have been, Tergra-2 would have been particularly sensitive to this error, given the dominance of C_4 plants at this station.

The introduction of a vapor pressure deficit stress factor to determine actual canopy resistance did not have a major impact on the modeled LE. In most cases, the increase in modeled canopy resistance above its minimum value was caused by a reduction in leaf water potential.

5.3.5 Discussion

Modifications made to the canopy resistance component of the Tergra model resulted in a model that was better suited to the simulation of LE over the Konza prairie than the original model. Basing canopy resistance on the NDVI in Tergra-2 makes the model more compatible with remotely sensed data and more suitable for making estimates of spatial patterns of LE. An added advantage of including the NDVI in the model is that it provides a means for simulating the relationship between surface temperature and the NDVI.

The evaluation of Tergra-2 accuracy in these tests needs to be made in the context of the spatial variability of plant and soil variables that characterize the Konza prairie. Reichman (1987) points to the large species diversity that tends to occur on the shallow and rocky soils of the Konza prairie and the occurrence of "specialist" plants on these soils. Reichman also describes how forbs and shrubs are generally found in

patches. Wetzel and Chang (1987) allude to the great variability in soil characteristics commonly found in a single soil type, which can cause a wide disparity in water content within a relatively small area. In the Tergra model, variables such as soil water potential, rooting depth, canopy height, and soil depth are represented as average values, whereas a disproportionate contribution to the fluxes measured at a station may be originating from isolated sources not characterized by mean conditions. Attention should be given to structuring Tergra-2 to include measures of variance in some of the input variables and parameters. It is also recognized that the modified resistance component of Tergra-2 still may not be fully representative of the processes operating in the Konza prairie and additional modifications may be necessary.

While the modeled canopy resistance in Tergra-2 was generally affected by leaf water potential and not vapor pressure deficit, field studies conducted by Sellers et al. (1990) indicated that stomatal closure of the plants in the Konza prairie was under the control of vapor pressure deficit. These contrasting findings may be explained by considering the correlation between leaf water potential and vapor pressure deficit. A decrease in LE, caused by stomata closing in response to a reduction in leaf water potential, may have reduced the vapor pressure at the bottom of the atmospheric boundary layer (ABL) where measurements were made for the FIFE. This is a basic premise in the explanation given by Bouchet (1963) and others for the observed reciprocal relationship between actual and potential evaporation. Thus, the role of vapor pressure deficit in stomatal closure can not be regarded as independent of the leaf water potential. Jarvis and McNaughton (1986) concluded that when plants are grouped together, it can not be assumed that the vapor pressure deficit of

the air passing through the canopy is independent of a change in the average stomatal resistance of the assemblage of plants. The degree of coupling of the canopy with the atmosphere may also be a factor that determines the relative importance of vapor pressure deficit in stomatal closure. After reviewing many stomatal resistance formulations, Lynn and Carlson (1990) were unable to understand the basis for a direct effect of vapor pressure deficit on stomatal resistance. They concluded that it is necessary to further examine the relationship between stomatal resistance, transpiration, and leaf water potential, and there is a need to clarify the vapor pressure deficit effect. The simulation results using Tergra-2 support this conclusion.

The introduction of separate leaf water potential adjustments to canopy resistance for C_3 and C_4 plants in Tergra-2 avoided the consistent overestimation of LE evident for Tergra-1 simulations. The spatial and temporal distribution of these two plant types is likely to become a significant requirement when the modeling is extended to estimating the spatial patterns of LE. Barnes and Harrison (1982) found that the C_3:C_4 distribution in a Nebraska prairie was associated with soil type and topographic position. The use of remote sensing and geographic information system techniques may offer promise for mapping the C_3:C_4 mix in the Konza prairie.

The mix of C_3 and C_4 plants in the Konza prairie may also provide a partial explanation for the large LE observed at two sites under dry soil moisture conditions and the underestimation of these fluxes by Tergra-2. Jarvis and McNaughton (1986) suggested that when stomata start to close, the relative allocation of transpiration between individual plants or plant types (or leaves) should be considered, rather than the regulation of the

absolute amount from the stand as a whole. Thus, when C_4 plants start to close their stomata, the reduction in vapor pressure within the stand may induce greater transpiration from the C_3 plants (O'Toole and Tomar 1982). This feedback is not represented in Tergra-2.

The simulation of canopy temperature in the Tergra model allows for model calibration or verification over large areas when remotely sensed observations of this temperature are available (Soer 1980). Although Tergra-2 provided good estimates of LE at the sites used in this experiment, a preliminary comparison of observed and estimated canopy temperatures revealed overestimates of up to 6 K (Figure 5.8). The observed canopy temperature values were obtained from the same helicopter MMR data set that provided the reflected radiances used to calculate the NDVI. Hall et al. (1990) reported similar differences between observed radiometric temperatures and aerodynamic temperatures that were calculated from observed sensible heat flux, air temperature and wind speed data. Hall et al. suggested that the sensible heat flux is driven by the gradient between the air temperature above the canopy and the temperature within the canopy air space. The modeled canopy temperature approximates this aerodynamic temperature, whereas the temperature recorded by the radiometer may include thermal contributions from bare soil, rock and dead plant material. The directional properties of vegetation temperature (Kimes et al. 1980) and the concept of aerodynamic temperature need to be researched further to interpret modeled surface temperatures in terms of heat fluxes.

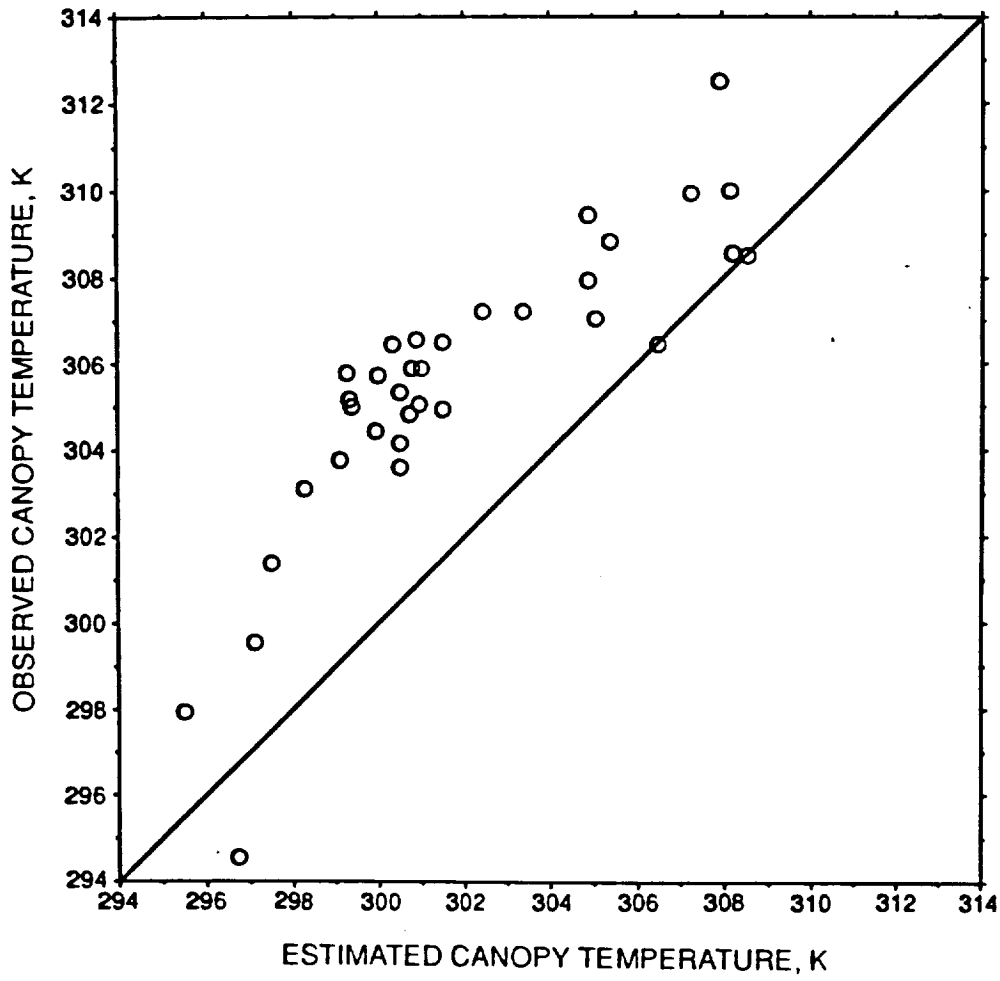

Figure 5.8: Observed canopy temperature using a helicopter-mounted MMR versus Tergra-2 estimates of canopy temperature.

5.3.6 Conclusions

Experimental tests of the Tergra-2 model were based on data collected under wet to moderately wet and very dry soil moisture conditions. Additional testing of the model under intermediate soil moisture conditions is necessary and further testing under very dry

conditions may lead to modifications that make the model more suitable to water-stressed conditions. Combining the Tergra model with a soil evaporation routine should improve the accuracy of the model and would allow it to be used in situations where vapor fluxes are not almost exclusively attributable to transpiration. There are also broader research questions that need to be addressed, such as developing techniques to represent the spatial variability of soil and plant variables in SPA models, the feedback between transpiration and stomatal functioning, the redistribution of transpiration when certain species (for example, C_4 plants) reduce their transpiration and the relationship between modeled and observed canopy temperatures.

The determination of canopy resistance from a spectral vegetation index and the stresses leading to stomatal closure need to be investigated further. The empirical canopy resistance-NDVI relationship used in Tergra-2 may only be suited to conditions observed during FIFE 1987 and FIFE 1989.

6. MODELING LARGE AREA LE FLUXES AND T_S

6.1 Background

During the development and testing of Tergra-2, efforts were also made to couple the model to a GIS so that the model could be used to simulate spatial patterns of LE and T_S over the entire FIFE site. The primary focus was on LE since modeled T_S was likely to differ substantially from radiometric temperatures. However, it was still anticipated that there would be a systematic agreement between the modeled and observed T_S across the FIFE site. This attempt to scale the modeling procedures to the scale of the FIFE site necessitated the use of satellite data and the Thematic Mapper (TM) and AVHRR systems were used in the analyses. Since a soil evaporation routine had not been included in the modeling scheme, tests were conducted on days when surface soil moisture content was minimal and soil evaporation could be assumed to be a minor contribution to total LE flux.

6.2 Study Objectives

A general goal of this project was to develop a procedure to estimate regional LE fluxes using thermal infrared and reflected shortwave radiation data from a system such as the AVHRR. The extension of the Tergra-2 model from a simulator of LE and T_S at a single location to a procedure for estimating the spatial patterns of these variables was in keeping with this goal. The spatially explicit Tergra-2 model (Tergra-2.GIS) was designed to simulate LE and T_S at the spatial resolution of the

AVHRR sensor. A key component of the study was obtaining, interpolating and estimating the spatially variable inputs and parameters for the model.

Once Tergra-2.GIS had been developed, the following research questions were addressed:

1) How accurately can Tergra-2.GIS replicate the observed area averaged LE and T_S of the FIFE site? The 15 x 15 km study site is treated as the spatial resolution of interest for the model simulations.

2) How accurately can Tergra-2.GIS replicate the spatial pattern of LE and T_S observed across the FIFE site?

3) Does the use of an area averaged SVI value at the AVHRR ground resolution and the failure to address spatial heterogeneities at finer spatial scales affect the accuracy of model predictions of LE and T_S? Over many landscapes, the large AVHRR pixels are likely to average reflected spectral radiances from a heterogeneous surface.

The averaging of land-surface characteristics (e.g., surface conductance estimated from a SVI) may give rise to errors in the estimation of LE. The latent heat flux process is acutely nonlinear so it is important to consider land surface heterogeneities in LE models (Dickenson et al. 1991). This process involves variables that can vary widely over short distances (Wetzel and Chang 1988). Avissar (1991) has demonstrated how mesoscale circulation models are sensitive to the parameterization of intra-patch variability. The use of average parameter values over large areas is often inappropriate and may lead to significant errors in the prediction of latent heat flux (Wetzel and Chang 1987; Wetzel and Chang 1988; Avissar 1991; Dickenson, Henderson-Sellers et al. 1991).

6.3 Methodology

Tergra-2.GIS was used to simulate the diurnal course of LE and T_s on three days in 1987, June 4-6. AVHRR data were available on June 6 so this became the primary day for evaluating model performance. Most of the comparisons between observed and estimated quantities were made at the time of the NOAA 10 satellite overpass. Spectral vegetation index values required to determine minimum canopy resistance (i.e., $r_{cm} = 1/g^*_c$) were obtained using AVHRR and TM data. The AVHRR data were used to determine the NDVI for each grid cell (1.3 x 1.3 km) covering the FIFE site. The TM data were used with Tergra-2.GIS in two modes, the first mode using the original 30 m resolution data to calculate LE and T_s for each 1.3 x 1.3 km grid cell. The histogram of SVI values for each grid cell was divided into 10 classes (equal width) and the simulations executed using the SVI from mid-points of each class. The average LE and T_s of each grid cell was determined by weighting the modeled class values by the relative frequency of TM pixels in each class. The second procedure ignored intra-cell heterogeneity and used the average SVI from TM data for each cell to calculate the two output variables.

An attempt was made to remove spatial auto-correlation from output variables (T_s and LE) used in statistical analyses. Semi-variogram analyses of the AVHRR thermal observations indicated that the lag in the data corresponded to approximately 3.07 pixels. Consequently, every third pixel was extracted from the 63 original grid cells to give a sample size of 21 for model comparisons.

6.3.1 Research data

Satellite data

Level 1a NOAA10 AVHRR data were acquired at 1536 (CDT) on June 6 over the FIFE site. The view angle for this location was 34.9∞ which produced pixel size of approximately 1.3 km. A 9 x 7 pixel sub-scene covering the FIFE site was extracted from the image and the NDVI and T_s determined for each pixel. The split window technique was used to derive apparent surface temperature while the dark object subtraction technique was used to correct the red and near infrared bands for atmospheric haze (cf. Section 2.3).

In order to address the third research question (effects of spatial heterogeneity), it was necessary to obtain satellite data with a finer spatial resolution than that of AVHRR. A Landsat TM image was acquired over the FIFE site a week before the AVHRR image (May 28, 1987). It was assumed that the change in SVI over this period was minimal. The Kauth-Thomas "greeness" SVI was calculated for the study site using the TM data and made available by the FIS. This image was co-registered to the AVHRR image and all non-grassland pixels were masked from the TM sub-scene.

Model inputs

The implementation of Tergra-2.GIS to estimate spatial patterns of LE and T_s at the AVHRR ground resolution required spatially variable soil, plant and atmosphere inputs. Soil parameters were estimated from the 1:18,000 general soil series map. Proportions of the various soil series in each grid cell were determined for the estimation of average parameters.

Soil moisture characteristic curves were obtained for each soil type from the FIS. Soil moisture characteristic curve parameters required for Tergra were derived using the scheme described by Huygen (1978). A summary of the Tergra-2.GIS soil parameters for the four major soil series in the FIFE site are given in Table 6.1

Table 6.1: Tergra-2.GIS parameters for the four major soil series.

	SOIL TYPE			
PARAMETER	BenFlor	Clime	Dwight	Tully
THETAS	0.425	0.400	0.410	0.400
BL	0.286	0.415	0.334	0.155
SR	0.320	0.370	0.180	0.000
D	1.178	1.230	1.280	1.300
DD	0.144	0.107	0.247	0.166
RD	9.028	12.150	5.263	7.831
SO	0.042	0.040	0.039	0.029
AKO	0.370	0.581	0.171	0.232
HCS	1.296	1.298	1.403	1.288
HCD	1.176	1.242	1.344	1.226
PSIA	-14.648	-15.108	-17.064	-13.445
PSIS	-4.236	-3.830	-3.129	-3.834

THETAS - saturated volumetric water content (-)
BL - pore size distribution factor (-)
SR - rest saturation (-)
D - density of soil ($kg.m^{-3}$)
DD - effective rooting depth (m)
RD - root density resistance factor (m)
SO - volume fraction of soil organic components (-)
AKO - saturated hydraulic conductivity ($m.s^{-1}$)
HCS - heat conductivity of saturated soil ($W.m^{-1}.K^{-1}$)
HCD - heat conductivity of dry soil ($W.m^{-1}.K^{-1}$)
PSIA - air entry value of soil (Pa)
PSIS - soil water pressure (Pa)

Spatial patterns of soil moisture content on June 4 were obtained for each grid cell using the maps developed by Peck (1993). These maps were constructed using airborne gamma radiation, gravimetric, neutron probe and microwave radiometer (PBMR) measurements (see Appendix 1). Soil density, organic matter fraction, saturated hydraulic conductivity and texture were obtained from the FIS.

Numerous vegetation parameters had to be interpolated from measurements made at the individual flux towers or other point locations (e.g., C_3:C_4 ratio, canopy height). Rooting depth was assumed to be equal to the soil depth. Maximum canopy conductance ($g^*_{c)}$ was estimated from a SVI. The relationship between g^*_c and the Kauth-Thomas GN is given by Sellers et al. (1990). A separate expression had to be developed for the NDVI based on AVHRR data. The red and near infrared radiances were interpolated for each flux station using the AVHRR pixel values and then used to calculate the NDVIs for these stations. In order to obtain an equation similar to Equation 5.7 to estimate g^*_c, the station values of dg^*_c/dK_{par} were regressed on these NDVI values to give the following expression:

$$dg^*_c/dK_{par} = 0.203\ NDVI - 0.073 \qquad (r^2 = 0.887) \qquad (6.1)$$

6.3.2 Modeling area averaged LE and T_s

The average LE for the FIFE site on each of the three study days (June 4, 5 and 6) was obtained by averaging observed values from all flux measurement stations. A comparison between the diurnal course of observed and estimated LE using Tergra-2.GIS and AVHRR NDVI, TM Kauth-

Thomas GN (GN1) and the average Kauth-Thomas GN (GN2) for each cell, is given in Figure 6.1. A summary of observed and estimated LE at three times on June 6 is given in Table 6.2.

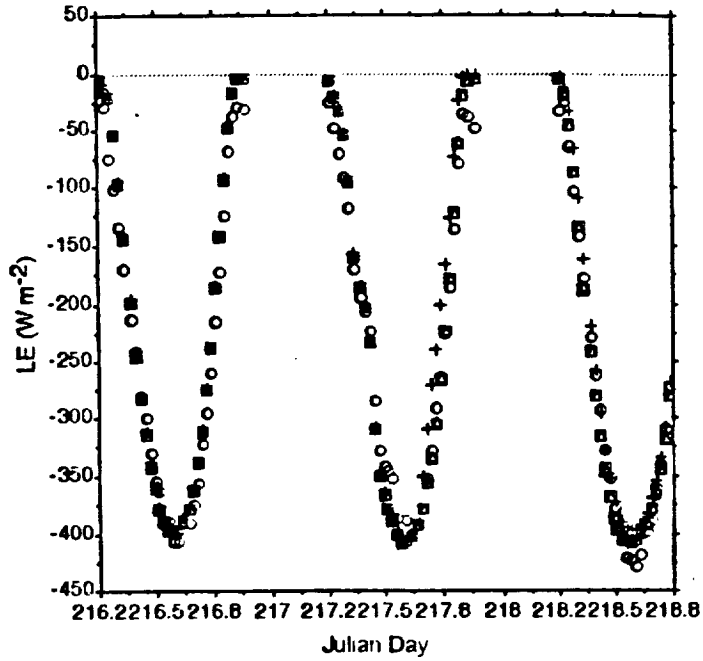

Figure 6.1: Comparison of observed (o) and modeled LE using the AVHRR NDVI (o), TM Kauth-Thomas GN (□) and the average Kauth-Thomas GN (+).

Table 6.2: Comparison at three times on June 6, 1987 of observed LE (Obs) and estimated LE using Tergra-2.GIS and AVHRR NDVI, TM Kauth-Thomas GN (GN1) and the average Kauth-Thomas GN (GN2) for each cell.

	TIME		
LE	10h45	13h45	16h45
Obs	-317.6	-424.7	-282.8
NDVI	-341.9	-405.3	-329.2
GN1	-333.8	-405.3	-329.2
GN2	-316.7	-387.9	-314.2

Estimates of area averaged site LE using Tergra-2.GIS were accurate throughout the simulation period, regardless of the SVI approach used in the model. The results given in Table 6.2 indicate that there may be a tendency for model predictions using the AVHRR NDVI to be slightly less accurate after mid-day with errors approaching 80 W m^{-2}. Clearly, the use of a mean Kauth-Thomas GN gives essentially the same results as the high spatial resolution approach (GN2) and the additional computational time was not justified.

Model estimates of area average site T_S on June 6 were less accurate than estimates of LE (Table 6.3). As expected, the model underestimated T_S as had been found in the original model evaluations at individual flux stations (Chapter 5). The Terga-2.GIS model also reduced the intra-site variability in T_S, with the coefficient of variation for modeled values being half that of the observed values (Table 6.3). The three different SVI approaches did not have a substantial effect on estimated T_S with mean values being within 0.8 K of each other.

Table 6.3: Mean and coefficient of variation for observed T_S and estimated T_S using Tergra-2.GIS and AVHRR NDVI, TM Kauth-Thomas GN (GN1) and the average Kauth-Thomas GN (GN2) for each cell.

	MEAN (K)	CV
Observed	305.3	0.4
T_S(NDVI)	302.6	0.2
T_S(GN2)	302.6	0.2
T_S(GN1)	301.8	0.2

6.3.3 Modeling spatial patterns of LE and T_S

The modeled LE at each of the flux measurement stations was estimated by interpolating values from the grid of modeled values. These interpolated LE values were, however, found to be substantially different from the modeled values regardless of the SVI approach that was used in Tergra-2.GIS. An example of the discrepancy between observed and estimated LE at the flux measurement stations is illustrated in Figures 6.2 and 6.3.

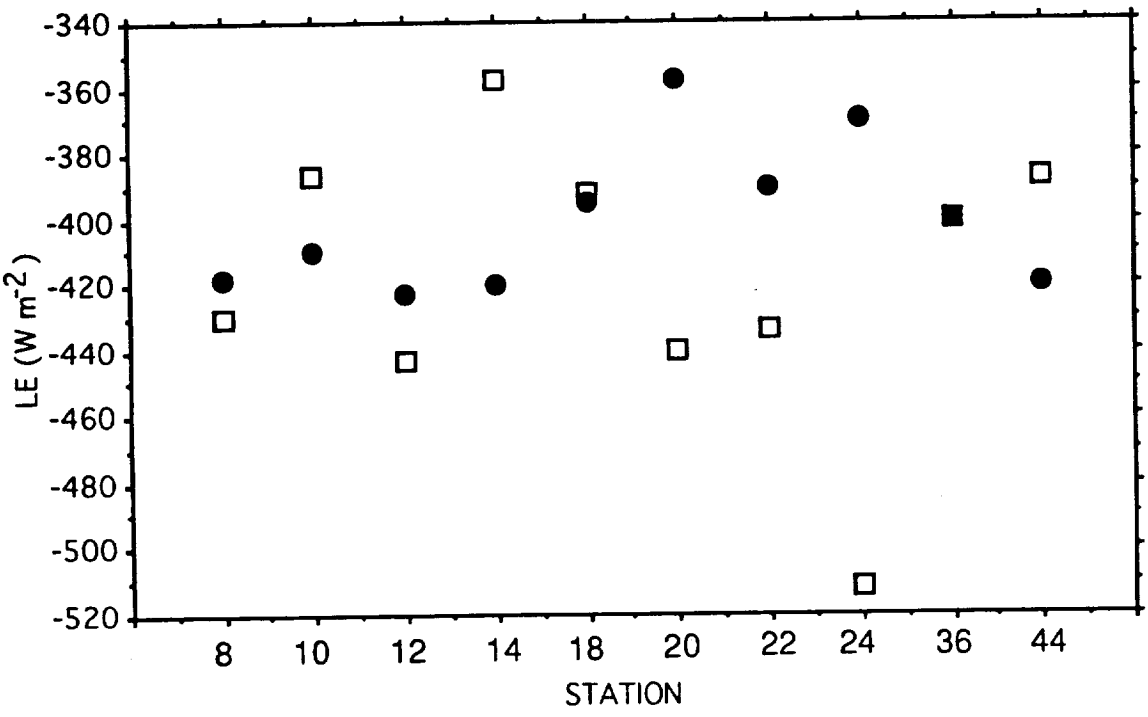

Figure 6.2: Observed (square) and estimated LE (circle) at 10 flux measurement stations on June 4, 1987. LE modeled using AVHRR NDVI.

While the model may not have captured the spatial dynamics in variables controlling LE, it is also likely that the interpolation approach for estimating point LE fluxes from the grid values was inappropriate. Fluxes observed at the measurement stations were local fluxes controlled by features within approximately 200 m of the flux towers (approximate fetch). The large grid cell size (1.3 x 1.3 km) and the averaging of model variables to simulate fluxes at this resolution, may also have suppressed spatial variability in LE. While the observed range in station-to-station LE approached 165 W m^{-2} at 1345 CST on June 4, the modeled cell-to-cell range was approximately 65 W m^{-2}. This reduction in variability with increase in modeled ground area would be expected since the modeled LE values would all approach a regional mean as the ground area increased.

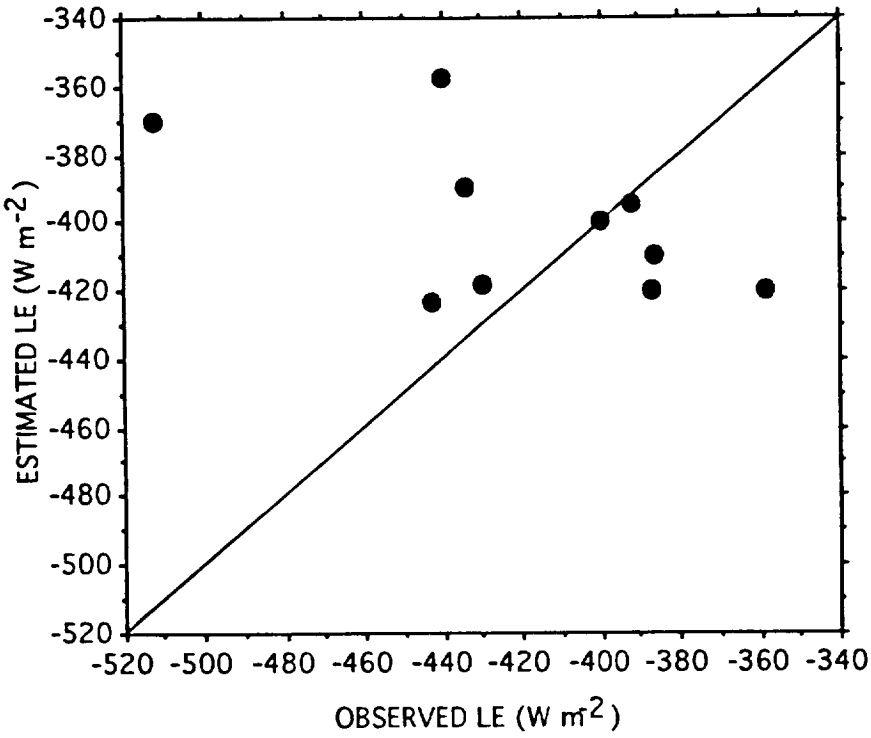

Figure 6.3: Observed versus estimated LE at the flux measurement stations on June 4, 1987. LE modeled using AVHRR NDVI.

More appropriate tests of the spatial patterns of simulated LE using Tergra-2.GIS may incorporate fluxes observed from aircraft. However, a more pressing need is to include a soil evaporation sub-routine.

The comparison between modeled T_S and values determined from the AVHRR data on June 6 revealed the expected systematic underprediction of T_S. The relationship between observed and estimated values using the three SVI approaches in the model are illustrated in Figure 6.4. The scatterplots were similar for the three approaches and the relative magnitude of underestimation of T_S appeared to increase with an increase in observed T_S.

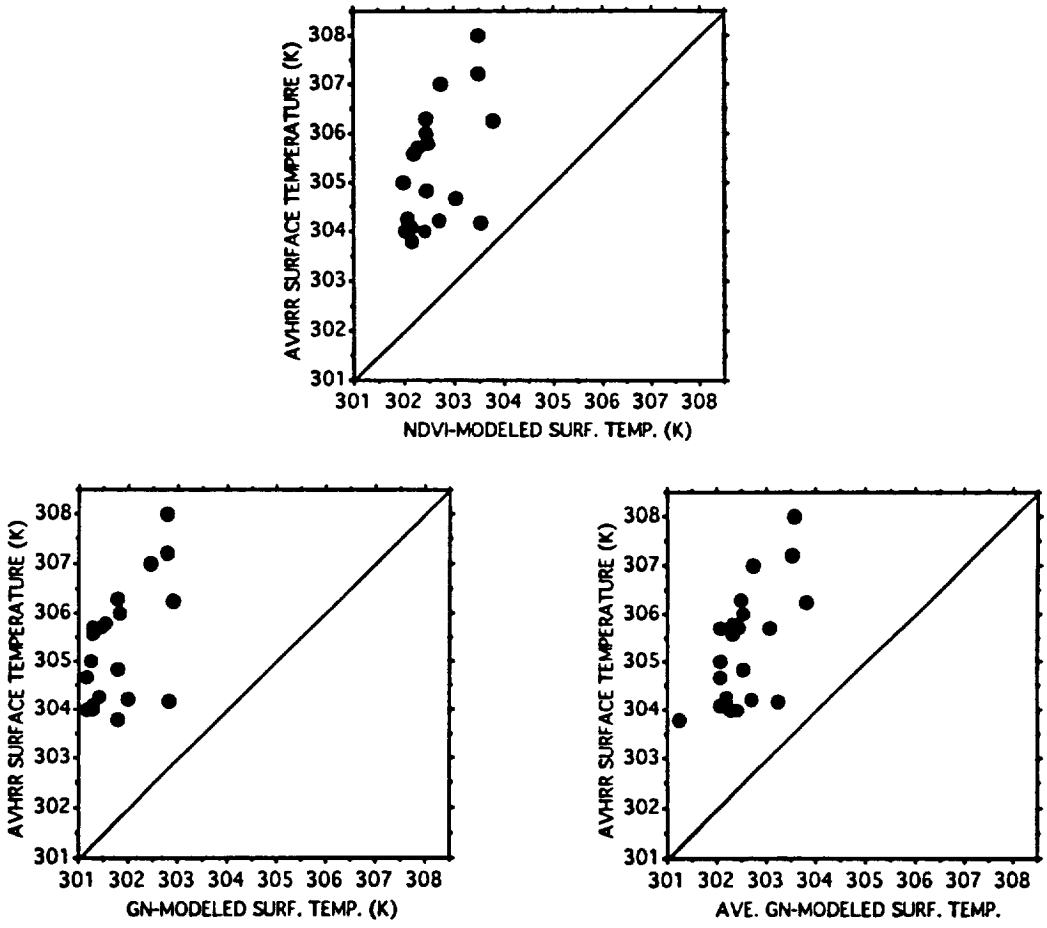

Figure 6.4: AVHRR derived surface temperature (June 6, 1987) versus surface temperature modeled using three different spectral vegetation index approaches in Tergra-2.GIS.

6.4 Conclusions

Modelling spatial patterns of LE at AVHRR ground resolution using remotely sensed SVI and soil moisture inputs was more accurate than the modeling of T_s. The inclusion of a soil evaporation sub-model should improve estimates of LE and make the model better suited to a wide range of cover and soil moisture conditions. The sub-grid cell spatial heterogeneity of the SVI, and hence r_{cm}, did not have a significant effect on the estimated LE or T_s.

7. CONCLUSIONS

A combination of empirical and modeling studies were conducted to develop an understanding of the T_S-NDVI relationship in terms of energy exchange processes. Procedures to estimate large area LE fluxes using these combined observations were investigated using data collected from a variety of sensors and platforms. While conclusions of the research have been summarized at the end of each section or chapter, the following general observations may benefit related studies that are conducted in the future:

1) Simple atmospheric correction routines, such as the split window technique Price (1984), darkest object subtraction technique (Chavez 1989) or the procedure described by Hall (1991), are valuable procedures for the operational use of satellite data for energy balance studies.

2) Fractional vegetation cover is a major determinant of the thermal response of grassland landscapes and this fraction is quantified by spectral vegetation indices. This is the underlying cause of the widely observed linear relationship between spectral vegetation indices and T_S. Consequently, the variations in the T_S-NDVI relationship at large NDVI values is more likely to be diagnostic of plant water stress than variations associated with small NDVI values where T_S is largely controlled by bare soil conditions.

3) It is unlikely that the slope (or intercept) of the T_S-NDVI regression line will be useful as a direct indicator of LE fluxes due to the large influence of terrain, surface cover conditions and management treatment on the relationship. However, a significant relationship between the regression slope and ground heat flux was observed.

4) Surface soil moisture conditions appear to be an important determinant of the relationship between T_S and the NDVI at the local scale (areas surrounding individual flux stations) or regional scale (AVHRR coverage of 1∞ latitude by 2∞ longitude).

5) Terrain-induced variations in insolation (at the time of the radiometric data collection) did not appear to affect the T_S-NDVI regression characteristics.

6) The use of thermal infrared data and spectral vegetation indices in soil-plant-atmosphere (SPA) models appears to be more promising for surface energy balance studies than the analysis of T_S-SVI relationships. However, the utility of remotely sensed surface temperatures over incomplete vegetation canopies is still uncertain given that sensible heat flux is controlled by aerodynamic temperature.

7) Techniques for estimating spatial patterns of soil moisture will be critical for advances to be made in predicting spatial patterns of energy fluxes using SPA models and remotely sensed data.

8) While the use of SVIs to estimate area averaged canopy conductances is valuable for applying SPA models over large areas, estimating evaporative contributions from the underlying soil is a source of considerable uncertainty in modeling LE fluxes.

9) Vegetation composition, particularly the C3:C4 ratio, can not be ignored in SPA models. Furthermore, landscape heterogeneity including soil moisture, may explain the observed discrepancies between observed and modeled area averaged LE fluxes.

The use of spectral vegetation indices to estimate minimum canopy resistance over large areas for SPA models is promising. The relationship between spectral indices and the resistance may vary with vegetation

type or season and these relationships need to be investigated further. The development of procedures to convert minimum canopy resistance to actual resistance needs to be a priority if this approach to modeling evaporation is to be pursued.

It is clear from the studies summarized in this report and numerous other investigations that radiative surface temperature deviate from the effective surface temperature (aerodynamic temperature) controlling sensible heat flux (Huband and Monteith 1986; Vining and Blad 1990; Lloyd et al. 1992). The grasses of the Konza Prairie do not provide complete canopy coverage so differential soil and vegetation heating will have to be considered if thermal emissions and the residual energy balance approach is to be used to estimate LE. Simple modifications to the bulk transfer equation may be possible so that estimates of sensible heat flux are made with acceptable accuracy (Stewart 1993). The observed difference between radiative and aerodynamic surface temperatures has generally been explained in terms of the differential heating of exposed soil and vegetation elements. Therefore, it may be expected that measures of fractional vegetation cover, such as the NDVI, would be useful for estimating empirical corrections to the bulk heat transfer equation.

Improved large area energy balance models will need to explicitly deal with landscape heterogeneity at a number of scales. Spatial variations in vegetation cover type and composition (particularly C3:C4 ratios), management treatment, soil moisture and terrain may control fluxes to a greater or lesser extent depending on the scale of observation. The use of high spatial resolution remotely sensed data (e.g., NS001, SPOT) should be included in future studies that address the problems of heterogeneity and scaling.

REFERENCES

Asrar, G., T. R. Harris and R. L. Lapitan. 1988. Radiative surface temperatures of burned and unburned areas in a tallgrass prairie. Remote Sensing of Environment 24: 447-457.

Asrar, G., R. B. Myneni, Y. Li and E. T. Kanemasu. 1989. Measuring and modeling spectral characteristics of tallgrass prairie. Remote Sensing of Environment 27: 143-155.

Asrar, G., R. L. Weiser, D. E. Johnson, E. T. Kanemasu and J. M. Killeen. 1986. Distinguishing among tallgrass prairie cover types from measurements of multispectral reflectance. Remote Sensing of Environment 19: 159-169.

Avissar, R. 1991. A statistical-dynamical approach to parameterize subgrid-scale land-surface heterogeneity in climate models. Surveys in Geophysics 12: 155-178.

Barnes, P. W. and A. T. Harrison. 1982. Species distribution and community organization in a Nebraska sandhills mixed prairie as influenced by plant/soil-water relationships. Oecologia 52: 192-201.

Bouchet, R. J. 1963. Evapotranspiration Reelle et Potentielle, Signification Climatique. Proceedings of the International Association of Scientific Hydrology 62: 134-142.

Carlson, T. B., E. M. Perry and T. J. Schmugge. 1990. Remote estimation of soil moisture availability and fractional vegetation cover for agricultural fields. Agriculture and Forest Meteorology 52: 45-69.

Carlson, T. N., J. K. Dodd, S. G. Benjamin and J. N. Cooper. 1981. Satellite Estimation of the Surface Energy Balance, Moisture Availability and Thermal Inertia. Journal of Applied Meteorology 20: 67-87.

Chavez, J., P.S. 1988. An improved dark-object subtraction technique for atmospheric scattering correction of multispectral data. Remote Sensing of Environment 24: 459-479.

Chavez, J., P.S. 1989. Radiometric calibration of Landsat Thematic Mapper multispectral images. Photogrammetric Engineering and Remote Sensing 55(9): 1285-1294.

Choudhury, B. J. and S. B. Idso. 1985. An Empirical Model for Stomatal Resistance of Field-Grown Wheat. Agriculture and Forest Meteorology 36: 65-82.

Choudhury, B. J. and S. B. Idso. 1985. Evaluating Plant and Canopy Resistance of Field Grown Wheat from Concurrent Diurnal Observations of Leaf Water Potential, Stomatal Resistance, Canopy Temperature, and Evapotranspiration Flux. Agriculture and Forest Meteorology 34: 67-76.

Choudhury, B. J., S. B. Idso and R. J. Reginato. 1986. Analysis of a Resistance-Energy Balance Model for Estimating Daily Evaporation from Wheat Plots Using One-Time-of-Day Infrared Temperature Observations. Remote Sensing of Environment 19: 253-268.

DeVries, D. A. (1975). Heat Transfer in Soils. *Heat and Mass Transfer in the Biosphere. Part 1: Transfer Processes in the Plant Environment.* Washington, D.C., Scripta. 5-28.

Dickenson, R. E., A. Henderson-Sellers, C. Rosenweig and P. J. Sellers. 1991. Evapotranspiration models with canopy resistance for use in climate models, a review. Agricultural and Forest Mteorology 54: 373-388.

Dubayah, R., J. Dozier and F. Davis. 1989. The distribution of clear-sky radiation over varying terrain. International Geoscience and Remote Sensing Symposium, Vancouver.

Feldman, D. S., J. Gagnon, R. Hofmann and J. Simpson (1987). *StatView II.* Berkeley, Abacus Concepts.

Fisher, M. J., D. A. Charles-Edwards and M. M. Ludlow. 1981. An analysis of the effects of repeated short-term w ater deficits on stomatal conductance to carbon dioxide and leaf photosynthesis by legume macroptilium stropurpureum cv. sirato. Autralian Journal of Plant Physiology 8: 347-357.

Goward, S. N., G. D. Cruickshanks and A. S. Hope. 1985. Observed Relation Between Thermal Emissions and Spectral Radiance from a Complex Vegetated Landscape. Remote Sensing of Environment 18: 137-146.

Goward, S. N. and A. S. Hope. 1986. Measurement of evapotranspiration with combined multispectral solar reflective and thermal infrared radiance observations. First ISLSCP Field Experiment (FIFE) proposal submitted to: National Aeronautics and Space Administration.

Goward, S. N. and A. S. Hope. 1989. Evapotranspiration from Combined Reflected Solar and Emitted Terrestrial Radiation: Preliminary FIFE Results from AVHRR Data. Advances in Space Research 9(7): 239-249.

Gurney, R. J., J. P. Ormsby and D. K. Hall. 1983. A Comparison of Remotely Sensed Surface Temperature and Biomass Estimates For Aiding Evapotranspiration Determination in Central Alaska. Permafrost: Fourth International Conference, Proceedings, National Academy Press, Washington, D. C.

Hall, F. G., D. E. Strebel, J. E. Nickeson and S. J. Goetz. 1991. Radiometric rectification: Toward a common radiometric response among multidate, multisensor images. Remote Sensing of Environment 35: 11-27.

Hall, F. G., P. J. Strebel, E. T. Kanemasu, R. D. Kelly, B. L. Blad, B. J. Markham, J. R. Wang and F. Huemmerich. 1990. FIFE, First ISLSCP Field Experiment: Results Overview. Symposium on FIFE, Anaheim, CA, American Meteorological Society, Boston, MA.

Holben, B. N. and C. O. Justice. 1980. The Topographic Effect on Spectral Response from Nadir-Pointing Sensing. Photogrammetric Engineering and Remote Sensing 46(9): 1191-1200.

Hope, A. S. 1992. Monitoring ecosystem response to global change: high spatial resolution data. Symposium on Anticipated Effects of a changing Global Environment on Mediterranean-Type Ecosystems, Valencia, Spain, (Proceedings in Review).

Hope, A. S., S. N. Goward and D. E. Petzold. 1988. Tersail: A Numerical Model for Combined Analysis of Canopy Bidirectional Reflectance and Thermal Emissions. Remote Sensing of Environment 26: 287-300.

Hope, A. S. and T. P. McDowell. 1990. The use of remotly sensed surface temperature and a spectral vegetation index for evaluating heat fluxes over the Konza prairie. Proceedings of Symposium on the First ISLSCP Field Experiment (FIFE), Anaheim, CA., American Meteorological Society.

Hope, A. S. and T. P. McDowell. 1992. The relationship between surface temperature and a spectral vegetation index of a tallgrass prairie: effects of burning and other landscape controls. International Journal of Remote Sensing 13(15): 2849-2863.

Hope, A. S., D. E. Petzold, S. N. Goward and R. M. Ragan. 1986. Simulated Relationships Between Spectral Reflectance, Thermal Emissions and Evapotranspiration of a Soybean Canopy. Water Resources Bulletin 22: 1011-1019.

Huband, N. D. S. and J. L. Monteith. 1986. Radiative surface temperature and energy balance of a wheat canopy. I. Comparison of radiative and aerodynamic canopy temperature. Boundary-Layer Meteorology 36: 1-17.

Huete, A. R., R. D. Jackson and D. F. Post. 1985. Spectral response of a plant canopy with different soil backgrounds. Remote Sensing of Environment 17: 37-53.

Hulbert, L. C. 1969. Fire and litter effects in undisturbed bluestem prairie in Kansas. Ecology 50: 874-877.

Huygen, J. 1978. An improved method for the definition of soil moisture parameters used in the Tegra model. Tellus Newsletter, 6. Ispra, Italy, Commmission of the European Communities, Joint Research Center. 3: 1-6.

Huygen, J. and P. Reiniger (1977). A sensitivity analysis of the Tegra model for the conditions of the grendon test site. Ispra, Italy, Commission of the European Communities, Joint Research Center.

Jarvis, N. J. 1989. A simple empirical model of root water uptake. Journal of Hydrology 107: 57-72.

Jarvis, P. G. 1976. The interpretation of the variation in leaf water potential and stomatal conductance found in canopies in the field. Phil. Transactions of the Royal Society, London, B. 273: 593-610.

Jarvis, P. G. and K. G. McNaughton. 1986. Stomatal control of transpiration: Scaling up from leaf to region. Advanced Ecological Research 15: 1-49.

Kidwell, K. B. 1986. NOAA Polar orbiter guide. Washington, D.C., National Oceanic and Atmospheric Administration , National Climate Center.

Kimes, D. S., S. B. Idso, J. Pinter P.J., R. J. Reginato and R. D. Jackson. 1980. View angle effects in the radiometric measurement of plant canopy temperatures. Remote Sensing of Environment 10: 273-284.

Knapp, A. K. 1984. Post-Burn Differences in Solar Radiation, Leaf Temperature and Water Stress Influencing Production in a Lowland Tallgrass Prairie. American Journal of Botony 71(2): 220-227.

Kondratyev, K. (1969). *Radiation in the Atmosphere.* New York, Academic Press.

Kustas, W. P., R. D. Jackson and G. Asrar (1989). Estimating surface energy-balance components from remotely sensed data. *Theory and Applications of Optical Remote Sensing.* New York, John Wiley and Sons. 604-627.

Laliberte, G. E., R. H. Broods and A. T. Corey. 1968. Permeability calculated from desaturation data. Journal of Irrigation and Drain Diversion, ASCE 94: 57-71.

Lloyd, C. R., J. H. C. Gash and M. V. K. Sivakumar. 1992. Derivation of the aerodynamic roughness parameters for a Sahelian sanannah site using the eddy correlation technique. Boundary-Layer Meteorology 58: 261-271.

Ludwig, J. A. and J. F. Reynolds (1988). *Statistical Ecology.* New York, John Wiley and Sons.

Lynn, B. H. and T. N. Carlson. 1990. A stomatal resistance model illustrating plant vs. external control of transpiration. Agriculture and Forest Meteorology 52: 5-43.

Nemani, R. R. and S. W. Running. 1989. Estimation of Regional Surface Resistance to Evapotranspiration from NDVI and Thermal-IR AVHRR Data. Journal of Applied Meteorology 28(4): 276-284.

Nieuwenhuis, G. J. A., E. H. Smidt and H. A. M. Thunnissen. 1985. Estimation of Regional Evapotranspiration of Arable Crops from Thermal Infrared Images. International Journal of Remote Sensing 6: 1319-1334.

Nieuwnhuis, G. J. A. and W. Klaasen (1978). Estimation of Regional Evapotranspiration from Remotely Sensed Crop Surface Temperature. Ispra, Italy, Commission of the European Communities, Joint Research Center.

O'Toole, J. C. and V. S. Tomar. 1982. Transpiration, leaf temperature and water potential of rice and barnyard grass in flooded fields. Agricultural and Forest Meteorology 26: 285-296.

Pallaconi, F. 1988. Jet Propulsion Laboratory, Pasadena, CA.

Peck, E. L. and A. S. Hope. 1993. Spatial patterns of soil moisture for the FIFE study area derived from remotely sensed and ground data. Journal of Geophysical Research. Submitted:

Polley, H. W., J. M. Norman, T. J. Arkebauer, E. A. Walter-Shea, D. H. Greegor Jr. and B. Bramer. 1992. Leaf gas exchange of *Andropogon gerardii* Vitman, *Sorghastrum nutans* (L.) Nash in a tallgrass prairie. Jornal of Geophysical Research 97(D17): 18,837-18,844.

Price, J. C. 1984. Land surface temperature measurements from the split window channels of the NOAA-7 advanced very high resolution radiometer. Journal of Geophysical Research 89(D5): 7231-7237.

Price, J. C. 1990. Using spatial context in satellite data to infer regional scale evapotranspiration. IEEE Transactions on Geoscience and Remote Sensing 28(5): 940-948.

Reichman, P. E. (1987). *Konza Prairie: A Tallgrass Natural History.* Lawrence, KS, University Press of Kansas.

Ritjema, P. E. (1965). An Analysis of Actual Evaportanspiration. Agricultural Research Report, Wageningen, The Netherlands, Pudoc. 107.

Roscoe, J. T. (1975). *Fundamental Research Statistics for Behavioral Sciences.* New York, Holt, Rinehart and Winston.

Saunders, R. U. and K. T. Kriebel. 1988. An improved method for detecting clear sky and cloudy radiances from AVHRR data. International Journal of Remote Sensing 89: 7231-7237.

Schmugge, T. J., E. T. Kanemasu and G. Asrar. 1987. Airborne multispectral observations over burned and unburned prairies. IGARSS'87 Symposium, Ann Arbor, MI, Institute of Electrical and Electronic Engineers.

Sellers, P., M. Heiser, C. W. Walthall, F. Huemmerich, D. E. Strebel and F. G. Hall. 1990. A Comparison of surface biophysical properties and remotely sensed variables from FIFE. Symposium on FIFE, Anaheim, CA, American Meteorological Society, Boston, MA.

Sellers, P. J. 1985. Canopy reflectance, photosynthesis and transpiration. International Journal of Remote Sensing 8(6): 1335-1372.

Shawcroft, R. W., E. R. Lemon and D. W. Stewart. 1973. Estimation of Plant Internal Crop Water Status from Meteorological and Plant Parameters. Proceedings Uppsala Symposium, Plant Response to Cimatic Factors, 449-459.

Sirkov, S. I. 1971. *Computation of Solar Radiation Characteristics.* Jerusalem, Keter Press.

Soer, J. G. R. 1977. The Tegra model, a mathematical model for the simulation of the daily behaviour of crop surface temperature and actual evapotranspiration. Delft, The Netherlands, Netherlands Interdepartmantal Working Community for the Application of Remote Sensing Techniques. Publication 46: 44.

Soer, J. G. R. 1980. Estimation of regional evapotranspiation and soil moisture conditions using remotely sensed crop surface temperatures. Remote Sensing of Environment 9: 27-45.

Stewart, J. B. 1993. Radiative surface temperature derived sensible heat flux for sparse prairie grass. American Geophysical Union Spring Meeting, May 24-28, Baltimore, Maryland.

Vining, R. C. and B. L. Blad. 1990. Relationship Between Radiometric, Aerodynamic and Kinetic Canopy Temperatures of Prairie Vegetation. AMS Symposium on the First ISLSCP Field Experiment, Anaheim, CA.

Weiser, R. L., G. Asrar, G. P. Miller and E. T. Kanemasu. 1986. Assessing grassland biophysical characteristics from spectral measurements. Remote Sensing of Environment 20: 141-152.

Wetzel, P. J. and J. T. Chang. 1987. Concerning the relationship between evapotranspiration and soil moisture. Journal of Climate and Applied Meteorology 26: 18-27.

Wetzel, P. J. and J. T. Chang. 1988. Evapotranspiration from non-uniform surfaces: a first approach for short term numerical weather prediction. Monthly Weather Review 116: 600-621.

Whitehead, V. S., W. R. Johnson and J. A. Boatright. 1986. Vegetation assessment using a combination of visible, near-IR, and thermal-IR AVHRR data. IEEE Transactions on Geoscience and Remote Sensing GE-24(1): 107-112.

Wilson, W. H. 1980. Solar ephemeris algorithm. Scripps Institute of Oceanography, Visibility Laboratory, University of California.

APPENDICES

APPENDIX 1

SPATIAL PATTERNS OF SOIL MOISTURE FOR THE FIFE STUDY AREA DERIVED FROM REMOTELY SENSED AND GROUND DATA

EUGENE L. PECK

Hydex Corporation, Vienna, Virginia

ALLEN S. HOPE

San Diego State University, San Diego, California

Paper Submitted To: Journal Of Geophysical Research

SPATIAL PATTERNS OF SOIL MOISTURE FOR THE FIFE STUDY AREA DERIVED FROM REMOTELY SENSED AND GROUND DATA

EUGENE L. PECK

Hydex Corporation, Vienna, Virginia

ALLEN S. HOPE

San Diego University, San Diego, California

Soil moisture observations were made over the FIFE study area in 1987 and 1989 using a variety of ground and airborne techniques. A procedure is described for deriving spatial patterns of soil moisture by combining these different data types. The spatial patterns of soil moisture are represented as both contour and grid values so that they can be readily incorporated in other FIFE studies. Two examples are given that illustrate the utility of these soil moisture maps for remote sensing and hydrometeorological studies over the FIFE study area.

INTRODUCTION

The First ISLSCP (International Satellite Land Surface Climatology Project) Field Experiment (FIFE) was conducted during the summer months of 1987 and 1989 near Manhattan, Kansas, in support of an inter-disciplinary experiment sponsored by the National Aeronautics Space Administration (NASA). A major objective of FIFE is to develop methodologies for deriving quantitative information concerning land-surface climatological variables from satellite observations of radiation reflected and emitted by the earth. Information on the FIFE experiment and on analyses and results of many of the scientific investigations are presented in the special FIFE issue of the Journal of Geophysical Research [AGU 1992].

Knowledge of the temporal and spatial variations in soil moisture is required for many FIFE investigations. To provide information for this need, seven ground based and remote sensing soil moisture data collection experiments were conducted. Three of these soil moisture investigations provided daily estimates for large portions of the FIFE research area (15 by 15 km). These are the Pushbroom microwave radiometer (PBMR) system operated by NASA [Wang et al., 1990], the airborne gamma radiation system of the National Weather Service [Carroll et al., 1988], and the application of a hydrologic model to Kings Creek basin [Famiglietti et al., 1992]. In addition, in situ measurements (gravimetric) were made daily by the FIFE staff at a network of field experiment sites. The soil moisture values obtained using the different measurement procedures can not be compared directly. To be of most value to other investigators, a method of combining the information content of the varies soil moisture estimates and measurements is required.

The purpose of this study is to derive the spatial patterns of daily soil moisture over the FIFE study area during the principle experimental periods using data collected from a variety of ground and airborne sources (gravimetric, neutron probe, microwave and gamma ray). The utility of the soil moisture maps developed in this project is illustrated using selected examples.

DATA SOURCES

CORE In Situ Ground Measurements

Ground soil moisture samples were collected daily by the FIFE staff [Sellers and Hall, 1987; Sellers and Hall, 1989] at CORE sites (located at flux and automatic meteorological measuring stations). Soil moisture samples were obtained daily from five points at the CORE stations, one at the center of the site and four at short distances along cardinal directions from the center. Soil samples for 0 to 5 cm and 5 cm to 10 cm soil depths were obtained at each of the five locations . The soil moisture values for the samples were determined by the gravimetric method (percent per dry weight). Average values of soil moisture for the 0 to 10 cm depth were computed.

Airborne Gamma Radiation Measurements

The National Weather Service airborne gamma radiation system [Carroll et al., 1988] was used to

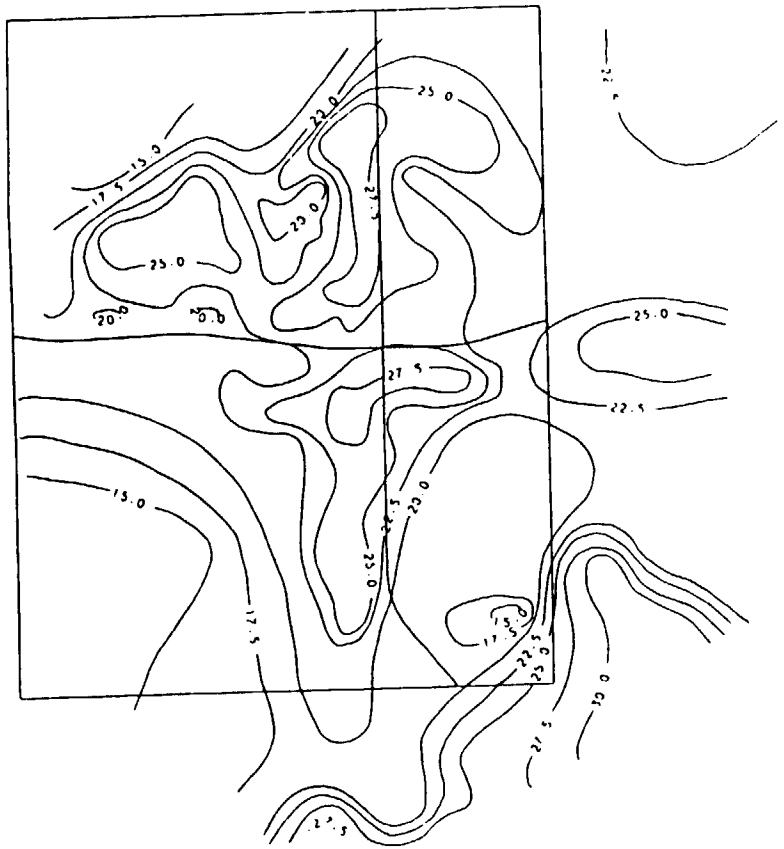

Fig. 1a

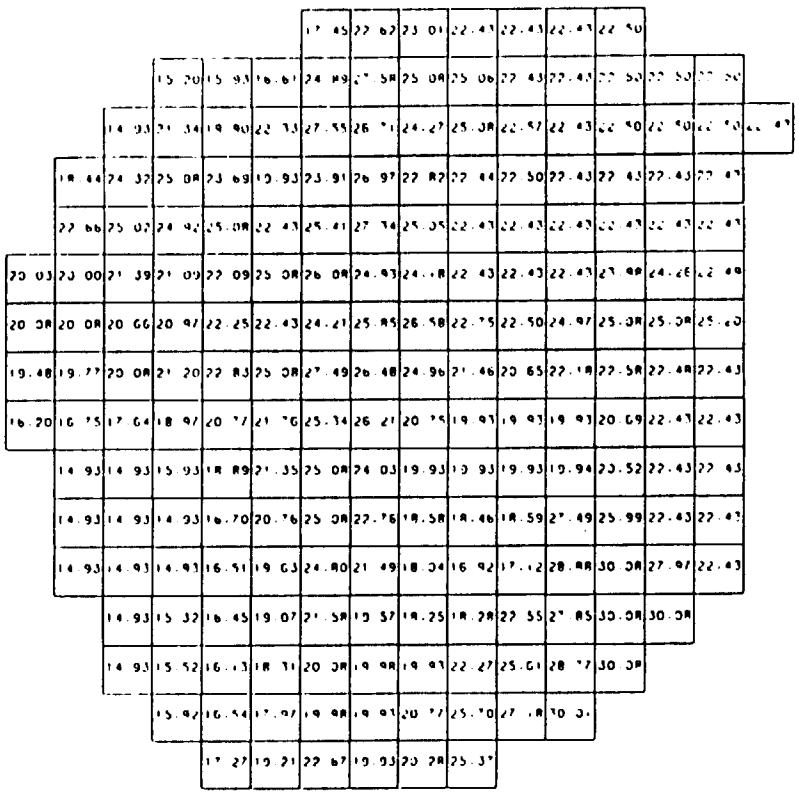

Coverage 890808*
Data L Peck, HYDEX Corp

CESAR-San Diego State University

Fig. 1b

Fig. 1. 1a) An example of an isoline map with values representing the average soil moisture for a 0.5 km^2 area, and 1b), isoline values of 0.5 km^2 average soil moisture shown on a 1.0 km by 1.0 km grid.

measure soil moisture during FIFE 1987 and FIFE 1989. Information on the locations of the 24 gamma radiation flight lines established and flown during FIFE field experiments (19 flight lines in 1987 and 24 flight lines in 1989) and on the flight line sections established (portions of the flight lines) was presented by Peck et al. [1992]. Detailed information is available in the FIFE Information System (FIS) located at the NASA, Goddard Space Flight Center, Greenbelt, Md.

Measurements obtained by the airborne gamma radiation system along a flight line are measurements of the average soil moisture over an area rather than along a single line. The airborne measurement of a flight line is assumed to measure a width of approximately 305 meters across the line. The average length of the 142 flight line sections established for the FIFE 24 flight lines is 1230 m. The area represented by an average section measurement of a flight line is 0.38 km^2 (1.23 km times 0.305 km).

The method for determining soil moisture estimates for sections of the flight lines from the radiation data collected by the airborne gamma flights was presented by Peck, et al. [1990]. Soil moisture estimates for flight lines and for flight line sections, and 800 individual in situ soil moisture measurements (gravimetric method) obtained for calibration of the airborne gamma radiation flight lines are available in the FIS.

Neutron Probe Measurements

In situ measurements of soil moisture were obtained by Ungar et al. [1992] during FIFE 1987 using neutron probes. Data from some of the access tubes were averaged to represent the soil moisture along line transects (e.g., hillslope) and others were used to determine the average soil moisture at individual sites. Information on the neutron probe measurements is given in the FIS.

Microwave Radiometer (PBMR) Measurements

PBMR measurements were obtained prior to, during, and following the FIFE experiments by Wang et al. [1990]. Information on the PBMR flights and soil moisture measurements is described in the FIS. The PBMR flight lines had an west-east orientation during the 1987 experiment and a north-south orientation during the 1989 experiment. Detailed information on biomass and the spatial distribution of vegetation were used in a model for computing soil moisture estimates for 1987 [Wang et al., 1990]. A simple method, using only ground soil moisture records, was used to compute soil moisture estimates from the PBMR measurements in 1989 [private communication].

Files of estimated soil moisture values, computed from the PBMR data, were provided by FIS for all days flights were flown during 1987 and 1989. These files consisted of percent average soil moisture values for pixels approximately 15 m by 15 m.

Hydrologic Model Values

A hydrologic model has been applied by Famiglietti et al. [1992] to the Kings Creek Basin for the summer season of 1987. The Kings Creek Basin is located in the center of the Konza research area (a research area operated by the Kansas State University and an important part of the FIFE study area). Daily soil moisture estimates for the Kings Creek Basin from the model study were provided in a digital format by Eric Wood for the periods June 3-4 and July 6-9, 1987 (personal communication). Each pixel of the file has a resolution of 30 by 30 meters.

EVALUATIONS OF SOIL MOISTURE ESTIMATES

All available measurements of soil moisture were considered for use in the analyses to produce soil moisture maps. The largest number of soil moisture measurements for the Konza research area where most of the FIFE studies were conducted, were from the airborne gamma system. These remote estimates were for flight lines, flight line sections, or combination of sections. The flight line sections estimates in the Konza research area represent areal measurements of 0.30 km^2 to 0.67 km^2. The second largest number of soil moisture estimates available for this area were those from the PBMR study. Areal values for any size area may be computed from the PBMR data. Because of the greatest availability of airborne gamma and PBMR data, an appropriate spatial resolution for deriving spatial patterns of soil moisture was considered to be 0.5 km^2, about the average of the airborne gamma flight line sections in the Konza research area.

Evaluations of the accuracy of the measurements of soil moisture over the FIFE research area have been reported by several FIFE investigators [Wang et al., 1990; Peck, et al. 1990; Peck and Carroll,1991]. Most of these studies have used the in situ ground soil moisture (CORE) measurements for the evaluations since these data are considered to be most accurate and are available for all days.

The various measurements and estimates of the soil moisture have different, and variable, relationships with the average soil moisture for a 0.5 km^2 area. These relationships are discussed in the following sections.

Microwave Versus Airborne Gamma and CORE Data

Peck and Carroll [1991] made a comparison study of the soil moisture estimates by the airborne gamma technique with 1987 soil moisture estimates (and a few 1989 estimates) obtained with the PBMR system. The results of this study found that the airborne gamma estimates correlated well with the CORE data (average error 3.1 percent and a bias of 0.1 percent). The PBMR 1987 estimates were found to have an average error of 6.3 percent and a bias of 6.5 percent. Most of the average error and bias of the PBMR estimates were a result of a high bias (8 to 9 percent) when the volumetric soil moisture content was less than 25 percent. The bias was found to vary in relation to ground conditions (e. g., little or no vegetation to high vegetation and grazed area versus non-grazed area). No apparent bias was found for the few microwave estimates available at that time for 1989 .

Model Estimates Versus Gamma and CORE

Peck and Carroll [1992] compared average soil moisture estimates derived from the hydrologic model implemented by Famiglietti et al. [1992] with CORE measurements and with airborne gamma estimates. Average daily soil moisture values were computed for the area measured by each section of the airborne gamma flight lines over the Kings Creek basin by averaging pixel values from the hydrologic model (using the average of 11 data points across the flight line section).

The study found that the CORE and airborne measurements during June and July 1987 were well related and followed the same temporal soil moisture pattern during the period. The soil moisture values for the CORE and airborne gamma system decreased during the field days in June 1987 and increased approximately 6 percent by early July. The values from the hydrologic model output continued to decrease from early June through July and did not properly account for the rainfall that occurred during the time between the June and July experimental periods.

Neutron Probe Versus CORE Data

The neutron probe soil moisture estimates were limited in number but were in agreement with the CORE measurements as reported by Ungar et al. [1992].

ANALYSES OF DATA

The results of the previous comparison studies were used as a basis for examining relationships among the soil moisture estimates from the various sources and determining the relationships of the in situ soil moisture measurements with the average soil moisture for a 0.5 km^2. The method for handling each of the different sets of data is presented below:

Microwave PBMR Measurements

Average values for each 0.5 km^2 area were computed from the digitized information furnished by the FIS for the total area covered by the PBMR measurements for three days in 1987 and three days in 1989. The number of 0.5 km^2 area values computed for each day are given in Table 1 and depended on the height that the PBMR sensors was flown and on the area covered by the flights.

TABLE 1. Number of 0.5 km^2 areas from PBMR measurement system.

1987	Number of areas	1989	Number of areas
June 4	282	August 4	190
July 7	356	August 7	640
July 9	360	August 10	192

The computed average 0.5 km^2 values were compared with the daily measurements at CORE stations located within the same 0.5 km^2 areas. Comparison for eight areas in 1987 revealed that the PBMR values averaged 5.47 percent soil moisture less than the corresponding CORE values. A similar bias (-6.2 percent) was reported by the Peck and Carroll [1991] comparison study for the 1987 field period.

The bias for the 1989 PBMR data furnished by the FIS as compared with in situ CORE data was found to vary over the FIFE area. Comparison of the average 1989 PBMR 0.5 km^2 values for 16 areas, when the microwave estimates were less than 25 percent, was positive 4.4 percent. For four other areas, with 1989 PBMR microwave estimates greater than 25 percent, a minus bias of 4.8 percent was observed. The bias seemed to be correlated with the vegetation cover of the areas.

CORE Measurements

The CORE values have been considered to be the most reliable and most consistent set of soil moisture measurements for the FIFE research area. As such, they have been used for comparison with other measurements. However, CORE measurements do not necessarily represent the average soil moisture for the surrounding 0.5 km^2 area.

Most CORE measurement locations are in open, well exposed sites, and except for very wet periods, the CORE measurements are lower than the average of soil moisture for the area surrounding the location. This was shown by Peck [1992] in the final report on the activities and results of the FIFE airborne gamma radiation studies.

Peck [1992] compared the measurements for a CORE station (site 906) located in an open site in the Konza research area with measurements along a north-south flight line. He found that the CORE value for August 5, 1989, was 6.5 percent lower than the average of 37 measurements along the flight line. The values for three points with similar exposure near the station had average soil moisture values within 1.0 percent of the value at the station. The average value for nine points, including the three with exposures similar to the CORE site, along the flight line nearest the station was 3.0 percent higher. For CORE locations that have open exposures, and the soil moisture values are less than 30 percent, the average value for the 0.5 km^2 area centered at a CORE station has been assumed to be 2.0 to 3.0 percent greater than that of the CORE station. For those few CORE sites in protected locations, the reported soil moisture are believed to be more representative of the average over a 0.5 km2 area.

Neutron Probe Measurements

For those locations in the Konza Research area where neutron probe measurements were made along specific transects, the average of these measurements were used in preparing the maps.

Hydrologic Model Estimates

Since the hydrologic model application during 1987 did not adequately reflect temporal soil moisture changes as indicated by CORE and airborne gamma radiation measurements these estimates were not used in the soil moisture map analyses.

MAPS PREPARED

Soil moisture maps were analyzed for the 15 days in 1987 and 1989 as shown in Table 2.

The CORE, airborne gamma radiation flight line sections, and the neutron probe soil moisture values for each day were plotted on a base map (scale 1 to 24,000) using the ARC/INFO geographic information system (GIS) at San Diego State University, San Diego, California. The average values for the 0.5 km^2 areas, as computed from the digitized files of the PBMR measurements, were also plotted on these base maps.

Using the plotted information, the differences between the airborne gamma and PBMR soil moisture estimates could be easily observed. Having a personal knowledge of the entire FIFE research area was of value in considering these average differences and relating the variation of the differences to vegetative cover and land use. The differences between the airborne gamma soil moisture estimates and the computed PBMR were considerably different for 1987 than for 1989.

TABLE 2. Days soil moisture maps wereprepared.

1987	1989
June 3	August 2
June 4	August 4
July 6	August 5
July 7	August 6
July 8	August 7
July 9	August 8
July 10	August 9
	August 10

The computed soil moisture estimates from the PBMR digital files were extremely valuable for defining the isolines for specific days, especially for areas where there were little or no other information. The six days of PBMR values provided great enhancement of the areal extent of information. PBMR values were available within one day, for each day maps were prepared.

The PBMR estimates were also valuable as a check on a few of the gamma radiation values for those locations where access to the flight line was limited or not permitted (e. g. flight lines KS110 and KS113 in the southwest portion of the FIFE research area). For these lines, even though the values for the entire flight lines appeared to be reliable, the ground soil moisture values were apparently not adequate to properly calibrate the variation in soil moisture for all sections along the flight lines. For these flight lines, soil moisture values for some sections were found to be consistently low, or high, whenever the measured soil moisture for the flight line deviated considerably from the value of the soil moisture for the day the flight line was calibrated . On these same days, the values for other sections of that flight line were found vary the opposite direction.

Isolines of equal 0.5 km^2 soil moisture values were analyzed taking into account the results of the comparison studies of the various soil moisture estimates and comparing the plotted values by sub areas where the vegetative cover and or land use was known.

DIGITIZED MAP DATA

The soil moisture isolines for the 16 maps were digitized by the Geography Department of San Diego State University. Files of the digitized isolines and corresponding files of 0.5 km^2 grid interpolated values for each day were prepared and have been submitted for inclusion in the FIS. An example of a isoline map and of 0.5 km^2 values on a 1.0 km grid are shown in Figure 1a and Figure 1b, respectively.

UTILITY OF SOIL MOISTURE MAPS

The isoline and gridded soil moisture values provide other scientists with daily soil moisture values that have been developed using data from many sources but specific information of potential errors or uncertainty is not provided. The primary advantage of the map and grid values is having a single value for a location rather than a large number of values over the surrounding area that are difficult to evaluate. Validation studies need to be continued. The following two examples illustrate how the gridded soil moisture values can be used to investigate soil moisture dynamics over the Konza study area or to assist with the interpretation of other data sets.

A preliminary examination of the soil moisture grid values has indicated their potential utility for explaining spatial variations in observed surface temperature. Hope and McDowell [1992] have demonstrated that most of the variance in remotely sensed surface temperatures over the Konza study site can be accounted for by variations in the normalized difference vegetation index (NDVI). These authors also found soil moisture measured at a depth of 25 mm, affected the relationship between these two variables. Reflected red and near infrared radiances and emitted thermal radiances were collected using the NS001 Thematic Mapper simulator on board the NASA C-130 aircraft that was flown over the Konza study site on August 4, 1989. The spatial resolution of these data (12 m at nadir) were degraded to correspond to the soil moisture grid illustrated in Figure 1b. Thermal counts obtained from this sensor were regressed on the normalized difference vegetation index (NDVI) that was calculated using the red and near infrared radiances. This regression produced a coefficient of determination of 0.678 which increased to 0.778 when soil moisture was included in the analysis (n= 84). Figure 2a illustrates the observed relationship between surface temperature and the NDVI while Figure 2b indicates the relationship between the regression residuals and the corresponding grid soil moisture values.

The soil moisture maps also may be valuable for examining soil moisture dynamics along transects

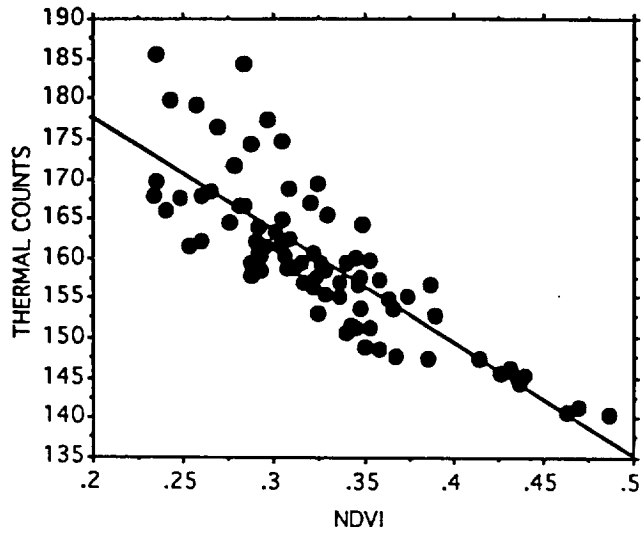

Fig. 2a

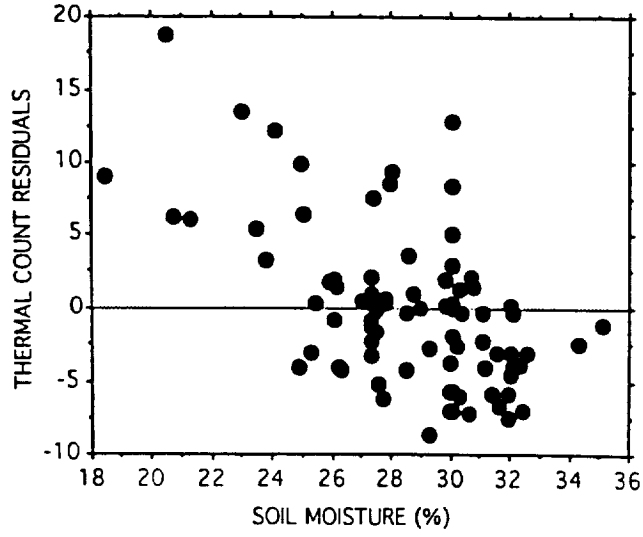

Fig. 2b

Fig. 2. 2a) Relationship between NS001 surface temperature and NDVI on August 4, 1989 and, 2b) the relationship between surface temperature residuals and corresponding grid soil moisture values.

corresponding to environmental or landscape gradients. Changes in soil moisture were examined along a north-south transect over a five-day dry-down period (August 5-9, 1989). This transect was located just west of highway R-177. The changes in soil moisture during the five day period are illustrated in Figure 3. While the drying trend is evident in Figure 3, it is also apparent that the day-to-day pattern of soil moisture content varies. The causes of this variability need to be investigated further.

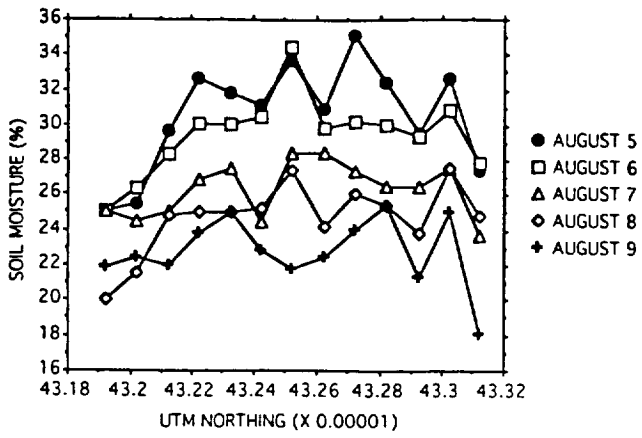

Fig. 3. Soil moisture content along a north-south gradient during a five day dry-down period (5-9 August, 1989).

Soil moisture is a major determinant of the magnitude of latent heat fluxes once the moisture status in the rooting zone falls below a critical threshold. The relationship between the mapped soil moisture and observed latent heat fluxes was examined over the same five-day period as the previous analysis. The ratio of daily latent heat flux to net radiation (evaporative fraction) was determined for sites 902, 908 and 910. The average evaporative fraction for each day was then plotted against the average soil moisture obtained from the 16 grid cells that covered the flux sites (Figure 4). As expected, the decrease in evaporative fraction over this five day period appeared to relate directly to the observed soil moisture status.

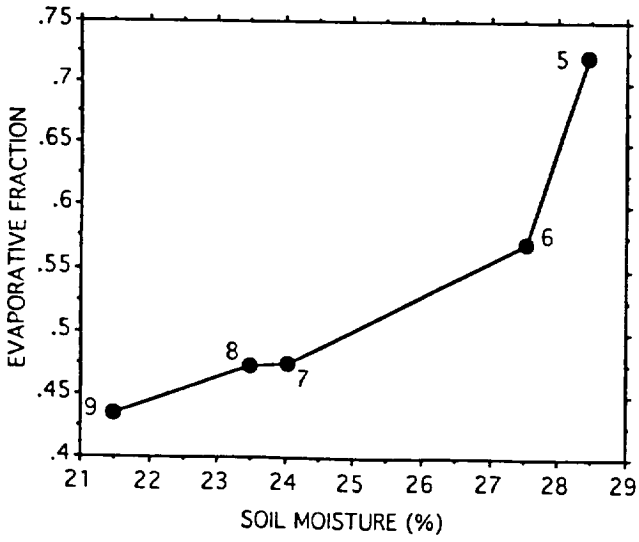

Figure 4. Relationship between the mean evaporative fraction from three flux sites (902, 908 and 910) and the mean soil moisture from the 16 km^2 area containing the sites (August 5-9, 1989)

CONCLUSION

Soil moisture data collected from a number of different ground and airborne techniques can be combined to produce spatial patterns of soil moisture for use in hydrologic and hydrometeorological studies. The interpolation of soil moisture from contour to grid values is particularly useful for analyses that include remotely sensed data in a raster format or for studies along transects or gradients. Further research is required to quantify the accuracy of these spatial patterns of soil moisture.

ACKNOWLEDGEMENTS

Thanks are extended to Eric Wood, Princeton University, and to James Wang, NASA, for help with their soil moisture data. Our thanks also to the FIS staff at NASA Goddard Space Flight Center, Fred Huemmrich and Jeff Newcomer, for providing data and information. Special thanks are extended to Derren Duburquet and Scott Augustine, Geography Department, San Diego State University, for their assistance with digitizing the soil moisture maps and computing the grid soil moisture values.

REFERENCES

AGU, 1992. First ISLSCP Field Experiment (FIFE), Jour. of Geophys. Res., Vol. 97. D17, Pages 18,345-18,371, November 30.

Carroll, T. R., E. L. Peck and D. M. Lipinski, 1988, Airborne Time-series Measurements of Soil Moisture Using Terrestrial Gamma Radiation. Proc. Annual Conf. American Soc. for Photogrammetry and Remote Sensing, St. Louis, MO, March 13-18. pp. 141-151.

Famiglietti, J. S., E. F. Wood, M. Sivapalan, and D. J. Thongs, 1992, A Catchment Scale Water Balance Model for FIFE. Jour. of Geophys. Res., Vol. 97. D17, pp. 18,997-19,007, November 30.

Hope, A. S. and T. P. McDowell,1992. The Relationship Between Surface Temperature and a Spectral Vegetation Index of a Tallgrass Prairie: Effects of Burning and Other Landscape Controls. Int. J. Remote Sensing, Vol. 13, No. 15, pp. 2849-2863.

Peck, E. L. 1992. Airborne Gamma Radiation Measurements of Soil Moisture during FIFE; Activities and Results. Final Contractor Report in FIS, NASA Contract NAS5-30959, Goddard Space Flight Center, Greenbelt, MD, April.

Peck, E. L. and T. R. Carroll, 1991, Comparison of Airborne Soil Moisture Measurements by Microwave and Gamma Radiation Techniques, Contract Report, Hydex Corp., NASA/GFSC. Greenbelt, Md. 21 p.

Peck, E. L. and T. R. Carroll, 1992. Comparison of Airborne Gamma Radiation Soil Moisture Measurements with Hydrologic Model Output. Contractor Report in FIS, NASA Contract NAS5-30135, Goddard Space Flight Center, Greenbelt, MD. Dec., 1991, Revised Jan.

Peck, E. L., T. R. Carroll, and D. M. Lipinski, 1990, Airborne Gamma Radiation Soil Moisture Measurements over Short Flight Lines. Preprint, Sym. on the First ISLSCP Field Experiment, Anaheim, CA, Amer. Meteorol. Soc., Boston, MA, Feb. 7-9. pp. 79-84.

Peck, E. L., T. R. Carroll and L. P. Lipinski, 1992. Airborne Soil Moisture Measurements for First International Satellite Land Surface Climatology Program Field Experiment. FIFE Special Issue of American Geophysical Union, Jour. of Geophys. Res., Vol. 97. D17, pp. 18,961-18,967. Nov.,1992.

Seller, P. J. and F. G. Hall, 1987, FIFE Experiment Plan. NASA Internal Doc., 623, NASA/GSFC, Greenbelt, MD. p. 394.

Seller, P. J. and F. G. Hall, 1989, FIFE-89 Experiment Plan. NASA Internal Doc., 623, NASA/GSFC, Greenbelt, MD. p. 223.

Ungar, S. G., R. Layman, J. E. Campbell, John Walsh and Harlan J. McKim, 1992, Determination of Soil Moisture Distribution From Impedance and Gravimetric Measurements. Jour. of Geophys. Res., Vol. 97. D17, pp. 18,969-18,978, November 30.

Wang, J. R., Shiue, J. C., Schmugge, T. J., and Engman, E. T. 1990. The L-Band Radiometer Measurements of FIFE Test Site in 1987-1989. Preprints, Sym. on the First ISLSCP Field Experiment (FIFE), Anaheim, CA, Amer. Meteorol. Soc., Boston, MA, Feb 7-9. pp. 85-87.

APPENDIX 2

A MODEL FOR COMPUTING IN-BAND REFLECTANCE DATA SETS FROM DIGITAL SATELLITE IMAGE DATA

FREDERICK C. MERTZ AND SALLY J. WESTMORELAND

Photon Research Associates, San Diego, California

DOUGLAS A. STOW AND ALLEN S. HOPE

San Diego State University, San Diego, California

Proceedings, Workshop on Atmospheric Correction of Landsat Imagery, Torrance, CA, June 29-July 1. In Press

A MODEL FOR COMPUTING IN-BAND REFLECTANCE DATA SETS FROM DIGITAL SATELLITE IMAGE DATA

Frederick C. Mertz and Sally J. Westmoreland

Photon Research Associates, Inc.
10350 North Torrey Pines Court, Suite 300
La Jolla, CA 92037-1020

Douglas A. Stow and Allen Hope

Department of Geography
San Diego State University
San Diego, CA 92182

1. INTRODUCTION

Measurement of objects or phenomena based on remotely sensed data are affected by illumination geometry, viewing geometry, sensor characteristics, and intervening atmosphere. Direct comparisons of remotely sensed data across time and space require that collection dependent variations be minimized among observations. To minimize this variation, a robust model that reduces environmental and sensor dependent artifacts must be developed. In this paper, we present a deterministic model that computes in-band reflectance data from digital imagery by compensating for key environmental and sensor dependent variables.

The model is currently applicable to satellite and aircraft imaging sensors in the visible and short wave infrared region of the spectrum when the spectral response function, sensor calibration coefficients, and the illumination and viewing geometries are known. The model has been designed to provide rigorous and flexible atmospheric correction capability coupled with ease-of-use. The model is robust in that it: performs detailed atmospheric radiative transfer calculations for any atmospheric state, spectral band, and sensor viewing geometry, rather than using a pre-computed data base; models the atmosphere based on the base altitude of the site, and uses background material reflectances extracted from a global data base to estimate the reflected earthshine; supports a user defined spectral response function as well as providing a library of spectral filters for commonly modeled instruments; allows input of user calibrated imagery in byte, short integer, and real data formats, as well as supporting simple gain and offset calibration coefficients; models atmospheric variations in atmospheric path length across the scene due to changes in solar and sensor zenith angles, and changes in surface altitude; compensates for changes in surface illumination effects due to variations in the orientation of a pixel by calculating the vector between the sun and the surface normal vector; and treats the image as a flat plane at user specified altitude, ignoring atmospheric path length and surface orientation corrections when the user determines that the digital elevation data are of questionable quality, or when the data are not available for a site.

2. THE MODEL

The model utilizes several separate computer programs integrated into a user-friendly shell, RHO_DRIVER. The user interfaces with the model via a single input file that contains the following parameters: date and time of image acquisition; scene

center latitude and longitude; sensor latitude, longitude, and altitude; climatological definition of the atmospheric state; sensor spectral response function; image calibration coefficients; and file names for the geo-referenced image, a registered digital elevation file, and a custom model atmosphere file. For each of the separate programs used in the model, RHO_DRIVER constructs an input file using the appropriate parameters and submits a batch process. Figure 1 is a representation of the data and processing flow incorporated in the RHO_DRIVER program.

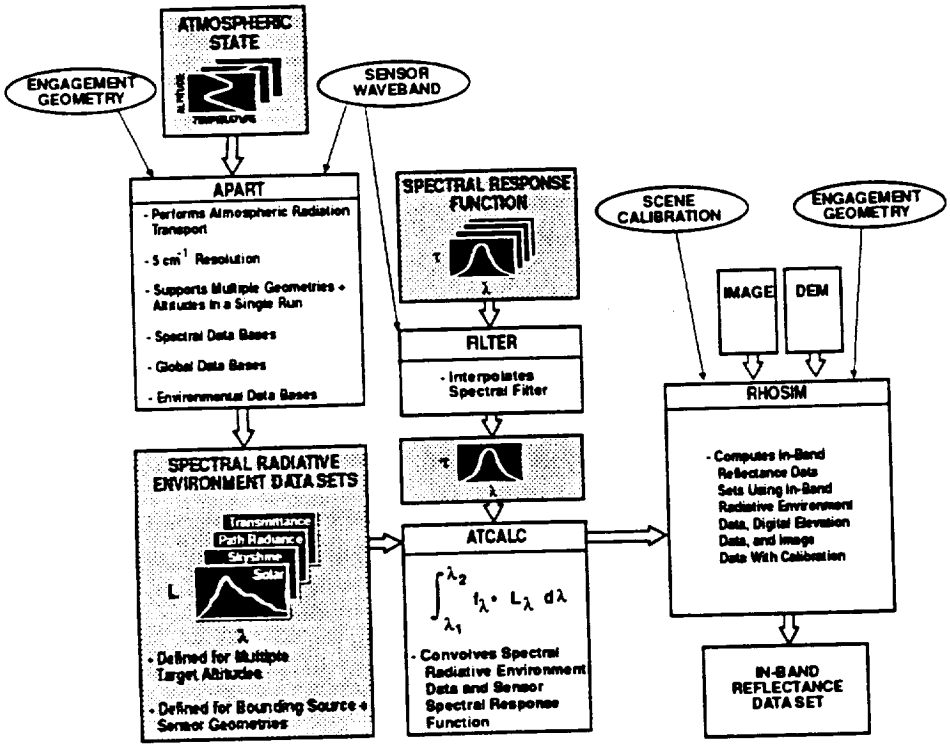

Figure 1. RHO_DRIVER Data and Processing Flow.

The atmospheric radiative environment is modeled by the Atmospheric Propagation and Radiative Transport (APART) code, developed by Photon Research Associates (PRA) to calculate all atmospheric radiative environment data required for calculating reflectance data sets. The ATCALC and FILTER programs perform intermediate processing to produce sensor-specific in-band atmospheric radiative environment data, from spectral data computed by APART. In-band reflectances are then calculated by the RHOSIM program.

APART is based on the Phillips Laboratory LOWTRAN band model at 20 cm^{-1} resolution and the Naval Weapons Center LOWTRAN band model at 5 cm^{-1} resolution. Although these codes have provided the basis for the APART code, extensive modifications have been made to support various atmospheric radiation transfer applications, including scene modeling. The APART architecture permits a complete definition of the radiative environment at any point in the atmosphere, and includes the following components: path transmittance, scattered and emitted path radiance, direct solar irradiance, diffuse solar scattered irradiance, reflected and emitted earthshine, and scattered and emitted skyshine. Each of these components is computed at 5 cm^{-1} resolution, for each user requested geometry (solar-surface-sensor) and surface altitude. Output from a single APART run can be the equivalent of 100 LOWTRAN runs. APART supports the spectral range .2 - 50 μm.

An algorithmic improvement incorporated into APART is the calculation of a "fully correlated" radiative environment for multiple segment atmospheric paths. APART applies the Curtis-Godson approximation for inhomogeneous paths over the multiple segment path from the source (sun), to the earth/cloud, and back to the viewer or sensor. Thus, for a given simulation, all relevant atmospheric radiative environment terms (direct solar, reflected skyshine, reflected earthshine) are provided for a two-way path (source to surface to sensor).

Like the MOSART code currently under development, and discussed in these proceedings (Cornette et al., 1993), the APART code includes a number of global data bases. These data bases provide global maps of surface altitude, material reflectance, and temperature; cloud cover type, percentage, and altitude; and snow and ice cover.

The FILTER program (see Figure 1) converts a user supplied spectral response function at variable resolution to a defined format of transmission-wavenumber pairs at 5 cm^{-1} resolution, and provides a mechanism for including user-specific instruments.

The ATCALC program (see Figure 1) converts spectral atmospheric radiative environment data calculated by APART to in-band atmospheric radiative environment data. All APART spectral radiative environment data are weighted by the spectral filter integrated over spectral limits supplied by the user. The output from ATCALC contains in-band quantities defined at specific surface altitudes, and solar and sensor zenith angles. The in-band radiative environment values included in the file are: one-way path transmittance for the path surface-sensor, scattered and emitted path radiance for the path surface-sensor, reflected solar/lunar irradiance for the path source-surface-sensor, and reflected skyshine irradiance for the path source-surface-sensor.

The RHOSIM code (see Figure 1) is the core of the in-band reflectance model. It models changes in radiative environment variables (e.g., transmittance, source intensity, path radiance, and skyshine), due to variations in atmospheric path length, surface altitude, and pixel orientation. It converts image data into at-sensor radiance (L_{sensor}) provided gain and offset values are provided. As stated above, the solar position is defined by the image acquisition date and time. The sensor position is defined by the latitude, longitude and altitude of the instrument; including aircraft. A geo-referenced digital image is used by the geometry routine to calculate the vector to the sun, the vector to the sensor, and the azimuth angle between them for each pixel in the image. When a digital elevation data set is included the geometry routine also calculates the angle between the surface normal and the sun (z'), the surface normal and the viewer, and the azimuth angle between them.

At each pixel in the data set, the geometry and altitude data are used drive interpolations in radiance-angle space given the bounding conditions in the in-band radiative environment data set calculated by ATCALC. Interpolated values of path radiance (L_{path}), solar irradiance (L_{sol}) and skyshine irradiance (L_{sky}) are then used to calculate in-band reflectance at a pixel using following equation:

$$\rho = \frac{\left(L_{sensor} - L_{path}\right)}{\cos(z') * \frac{\left(L_{sol} + L_{sky}\right)}{\pi}}$$

It should be noted that both the skyshine and direct solar terms are computed for the path source-surface-sensor, assuming a surface reflectance of 1.0.

3. DISCUSSION

The RHO_DRIVER and RHOSIM codes have recently been developed and have not been extensively test or validated. Preliminary test cases, discussed below, indicate that the codes are predicting reasonable results, however, detailed comparisons with ground-based measurements are required before statements of model accuracy or precision can be made. These codes, however, are an inversion of PRA scene simulation models, and many of the algorithms employed in the programs were retained to ensure the integrity and continuity of this experience base. Presented in Reeves et al. (1988) and Mertz et al. (1991) are direct comparisons of measured and modeled scene radiances that serve to validate our deterministic approach to scene simulation. It should also be noted that the RHO_DRIVER and RHOSIM codes calculate surface reflectance using LOWTRAN-based approaches similar to those implemented by Moran et al. (1990), and Richter (1990).

In preliminary test cases the model was used to convert two full-frame Landsat Thematic Mapper (TM) scenes to in-band reflectance data sets. For the first case, on the Iraq/Syria border, material reflectances computed by the model appeared to agree with reflectances for materials having similar properties calculated by Davis et al., (1989) using the regression-intersection method. In this case, hot oil processing facilities and oil well fires produced computed reflectances with values greater than 1.0 in TM bands 4, 5 and 7. For the second test case, North Central Iran, ground truth was not available. In this scene the elevation of the surface ranged from 100 to 4000 meters above sea level. Computed reflectance values for this scene were in the range 0 to 1.0 except for locations where the model placed satellite illuminated pixels on shadowed ridges due to an inaccurate digital elevation data set. Other artifacts related to elevation data set errors included shifts in reflectance due to abrupt shifts in surface altitude along quad boundaries, and visual contour lines present across gently sloping playa. The magnitude of these errors, however, was quite low, and is dependent on illumination conditions and spectral band.

To compare model computed reflectances with measured surface reflectance data the model was run using TM imagery acquired on August 15, 1987 during the First International Satellite Land Surface Climatology Project (ISLSCP) Field Experiment FIFE. A user-defined model atmosphere was developed by combining measured atmospheric profiles of water vapor, temperature, and pressure acquired near the site at the approximate time of the overpass. These data were combined with the Mid-Latitude Summer model atmosphere to customize the atmospheric information. Preliminary results indicated that the RHOSIM corrected TM reflectances agreed well with concurrent helicopter and ground-based Barnes multiband modular radiometer (MMR) reflectances for the red and two mid-infrared bands (3,5,7). In the near-infrared band (4), model computed reflectances agreed well with ground MMR reflectance data, but were higher than the helicopter measurements acquired at the same time. In the blue and green bands (1,2) the model corrected TM reflectances were higher than most helicopter and ground MMR reflectance values. Further testing and analysis is required to determine the source of the differences. However, it should be noted that other investigators have reported similar results between corrected satellite data and ground reflectances over well-vegetated targets with low reflectances in visible wavelength bands (Pinter et al., 1990; Moran et al., 1990).

4. FUTURE DIRECTIONS

We intend to continue testing the model using image data sets collected with adequate atmospheric and ground truth. Candidate data sets include: multi-date FIFE data sets acquired by Landsat TM, SPOT HRV, and NOAA AVHRR; and multi-date data sets collected over the USDA Maricopa Agricultural Center, as discussed in Moran, et al., (1992).

Several upgrades are planned for the model, including: development of an interface to the new atmospheric radiative transfer code, MOSART (Cornette et al, 1993); enhancement of the codes to model within-scene sun-surface-sensor azimuth angle changes; development of an atmospheric correction approach for thermal imagery; modeling of adjacency effects; and modeling of projected shadows. These upgrades will further enhance the flexibility and broaden the applications for which this model can be employed for rigorous correction of atmospheric effects.

REFERENCES

Cornette, W.M., D.C. Robertson, G.P. Anderson, 1993. The moderate spectral atmospheric radiance and transmittance (MOSART) program. Presented at the Workshop on Atmospheric Correction of Landsat Imagery, June 29-July 1, 1993, Torrance, CA.

Davis, P.A., K.F. Mullins, G.L. Berlin, A.M. Al-Farasani, and S.M. Dini, 1989. Phosphorite exploration in the Thaniyat and Sanam districts, Kingdom of Saudi Arabia, Using Landsat Thematic Mapper data. 7th Thematic Conf. on Remote Sensing for Exploration Geology. Calgary, Alberta, Canada, pp. 1205-1221.

Mertz, F.C., C.B. Blasband, L.W. Hendricks, R.J. Francis, and D.C. Anding, 1991. Validation of a cloud scene simulation model using NOAA multi-spectral imagery. Proc. of the Cloud Impacts on DoD Operations and Systems 1991 Conference (CIDOS-91), Los Angeles, CA, pp. 261-267.

Moran, M.S., 1990. A satellite-based approach for evaluation of the spatial distribution of evapotranspiration from agricultural lands, Ph.D. Dissertation, University of Arizona, Tucson, 223 pp.

Moran, M.S., R.D. Jackson, G.F. Hart, P.N. Slater, R.J. Bartell, S.F. Biggar, D.I. Gellman, and R.P. Santer, 1990. Obtaining surface reflectance factors from atmospheric and view angle corrected SPOT-1 HRV data. Remote Sensing of Environment, 32: 203-214.

Moran, M.S., R.D. Jackson, P.N. Slater, P.M. Teillet, 1992. Evaluation of simplified procedures for retrieval of land surface reflectance factors from satellite sensor output. Remote Sensing of Environment, 41: 169-184.

Pinter, P.J., R.D. Jackson, and M.S. Moran, 1990. Bidirectional reflectance factors of agricultural targets: A comparison of ground-, aircraft-, and satellite-based observations. Remote Sensing of Environment, 32: 215-228.

Reeves, R., D. Anding, and F. Mertz, 1988. First-principles deterministic simulation of IR and visible imagery. Proc. of the SPIE Conference, Orlando, FL.

Richter, R., 1990. A fast atmospheric correction algorithm applied to Landsat TM images. International Journal of Remote Sensing, 11: 159-166.

APPENDIX 3

RESEARCH PUBLICATIONS

Mertz, F.C., S.J. Westmoreland, D.A. Stow and A.S. Hope. 1993. A model for computing in-band reflectance data sets from digital satellite image data. Proceedings, Workshop on Atmospheric Correction of Landsat Imagery, Torrance, June 29-July 1. In Press.

Peck, E.L. and A.S. Hope 1993. FIFE level 3 example grided soil moisture data. In: Strebel, D.E., J.A. Newcomer, D.R. Landis, J.E. Nickeson, S.J. Goetz, B.W. Meeson, P.A. Agbu and J.M.P. McManus; Collected Data of the First ISLSCP Field Experiment, Vol. 5: Images Derived from Satellite, Aircraft and Geographic Data. Published on CD-ROM by NASA Goddard Space Flight Center, Greenbelt, MD, 1993.

Peck, E.L. and A.S. Hope 1993. Spatial patterns of soil moisture for the FIFE study area derived from remotely sensed and ground data. Journal of Geophysical Research. Submitted.

Hope, A.S. 1992. Estimating the daily course of Konza Prairie latent heat fluxes using a modified Tergra model. Journal of Geophysical Research. 97(D17), 19,023-19,031.

Hope, A.S. and T.P. McDowell. 1992. The relationship between surface temperature and a spectral vegetation index of a tallgrass prairie: Effects of burning and other landscape controls. International Journal of Remote Sensing, 13(15), 2849-2863.

Goward, S.N. and A.S. Hope. 1989. Evapotranspiration from combined reflected solar and emitted terrestrial radiation. Advances in Space Research. 9: 239-249.

Hope, A.S. and T.P. McDowell. 1990. The use of remotely sensed surface temperature and a spectral vegetation index for evaluating heat fluxes over the Konza prairie. Proceedings, Symposium on FIFE, American Meteorological Society, Anaheim, CA, 106-111.

McDowell, T.P. and A.S. Hope. 1989. Estimating energy balance components of a grassland using remotely sensed data. Paper presented at: Association of American Geographers Conference, Baltimore, MD.

Hope, A.S. 1989. The relationship between thermal emissions and spectral vegetation indices in the context of evapotranspiration. Presentation at at: California Space Institute, University of California, San Diego, CA.

Hope, A.S. 1988. Simulated relationship between spectral reflectance, thermal emissions and evapotranspiration of canopies. Seminar presented at: Centre National De La Recherche Scientifique, Montpellier, France.

Hope, A.S. 1988. Surface moisture availability and evapotranspiration estimates using a spectral vegetation index and canopy temperature. Paper presented at: 26th Congress of the International Geographical Union, Sydney, Australia.

Goward, S.N., A.S. Hope and T.E. Eck. 1988. Evapotranspiration from combined reflected solar and emitted terrestrial radiation. Paper presented at: 27th Plenary Meeting, COSPAR, ESPOO, Finland.

Hope, A.S. 1988. The effects of sensor spatial resolution on the relationship between remotely sensed surface temperature and a spectral vegetation index. Paper presented at: Third Annual Landscape Ecology Symposium, Albuquerque, NM.

Hope, A.S.. and T.P. McDowell. 1988. Relating surface temperature and the normalized difference vegetation index to surface heat fluxes in the Konza prairie. Paper presented at: Association of Pacific Geographers Conference, San Diego, CA.